ORMOCER (inorganic-organic hybrid polymer)-zeolite Nanocomposites: Advanced Membrane Materials for Gas Separation

Dissertation

Zur Erlangung des akademischen Grades
eines Doktors der Naturwissenschaften (Dr. rer. nat.)
im Fach Chemie der Fakultät Für Biologie, Chemie und Geowissenschaften
der Universität Bayreuth

Vorgelegt von
Suresh M Kumbar
Fraunhofer-Institut für Silicatforschung ISC

Bayreuth, 2010

Die vorliegende Arbeit wurde im Zeitraum von November 2006 bis April 2010 am Lehrstuhl für Anorganische Chemie I der Universität Bayreuth und am Fraunhofer-Institut für Silicatforschung ISC, Würzburg.

Vollständiger Abdruck der Fakultät für Biologie, Chemie und Geowissenschaften der Universität Bayreuth genehmigten Dissertation zur Erlangung des akademischen Grades Docktor der Naturwissenschaften (Dr. rer. nat.).

Promotionsgesuch eingereicht am: 20.04.10

Tag des wissenschaftlichen Kolloquiums: 14.09.10

Prüfungsausschuss:

Professor Dr. Josef Breu
Professor Dr. Gerhard Sextl (Zweiter Gutachter)
Professor Dr. Hans Keppler
Professor Dr. Jürgen Senker (Erster Gutachter)

_____

<u>Declaration by the Research Scholar</u>

I hereby declare that dissertation entitled

ORMOCER® (inorganic-organic hybrid polymer)-zeolite

Nanocomposites: Advanced Membrane Materials for Gas Separation

submitted for the Degree of Doctor of Philosophy to the faculty of Biology, Chemistry and Geosciences, University of Bayreuth has been carried out by me at the Fraunhofer Institute for Silicate Research (ISC) and the Department of Inorganic Chemistry-I, University of Bayreuth, under the supervision of Professor Dr. Gerhard Sextl and Professor Dr. Josef Breu. The work is original and has not been submitted in partial or full by me for any other degree (diploma) to this or to any other university

Suresh M Kumbar

_____

<u>Acknowledgements</u>

Contents

_____

Summary

This work represents a comprehensive study on the applicability of novel ORMOCER® (inorganic-organic hybrid polymer) resins for the fabrication of free-standing mixed matrix membranes. Such mixed matrix membranes comprise molecular sieve entities integrated in ORMOCER® matrix. Mixed matrix membranes have the potential to combine the processability of ORMOCER® materials with the superior transport and ion exchange properties of molecular sieves. The versatility of ORMOCER® materials is a decisive factor in achieving the desired separation properties of a novel mixed matrix membrane material. The glycerine-1,3-dimethacrylateurethanetriethoxysilane (GUS)-based ORMOCER® and dimethylsiloxane modified GUS-ORMOCER® resins were used for the fabrication of free-standing mixed matrix membranes. The zeolite Beta was used as a dispersed phase and its amount was varied between 10 to 40 wt.%. The effect of different type of zeolites was also studied using zeolite 3Å, 4Å, and 5Å. The membranes were prepared by conventional solution casting method followed by UV-curing. The ORMOCER® resins and cured membranes were analysed using FT-IR, liquid-state ^{29}Si NMR, TG, DSC, SEM, N_2 sorption and single-gas permeation measurements. The permeation performance of the membranes was examined using H_2, He, CO_2, O_2 and N_2 as a test gases at room temperature, the upstream pressure was varied between 1.3 to 2.5 atm. The effect of the amount of dimethylsiloxane moiety, zeolite content, different zeolite type and annealing temperature were systematically investigated in relation to the gas permeation performance of the membranes. The addition of dimethylsiloxane moiety in GUS-based ORMOCER® membrane appears to result in a significant increase in gas permeability, with a correspondingly large decrease in selectivity. The mixed matrix membranes show improved gas permeation performance in comparison to pure ORMOCER® membranes. This study was shown important role of zeolite particles in inorganic-organic hybrid (ORMOCER®) system. The potential usefulness of ORMOCER®-zeolite mixed matrix membranes as gas separation membranes is discussed.

_____

_____

<u>Zusammenfassung</u>

Die vorliegende Arbeit beschreibt erstmals die erfolgreiche Verwendung neuartiger ORMOCER®-Harze (anorganisch-organische Hybridpolymere) für die Herstellung freistehender Membranen, dadurch dass in einer Matrix aus ORMOCER® Partikel von Molekularsieben dispergiert werden. So wird es möglich, die gute Verarbeitbarkeit von ORMOCER®en mit den hervorragenden Transporteigenschaften von Molekularsieben zu kombinieren.

Die Vielseitigkeit der ORMOCER®e spielt eine entscheidende Rolle für das Einstellen bestimmter Trenneigenschaften in diesen neuartigen Membranmaterialien. Glycerin-dimethacrylat-urethan-triethoxysilan (GUS) basierte und mit Dimethyl-diethoxysilan modifizierte GUS-ORMOCER®e wurden eingesetzt zur Herstellung freistehender Membranen. Als dispergierte Phase diente Zeolith β mit variiertem Mengenanteil von 10 bis 40 Masse-%. Die Wirksamkeit der Zeolith-Typen 3Å, 4Å und 5Å wurde ebenfalls untersucht. Die Membranen wurden konventionell aus einer Gießlösung hergestellt und anschließend UV gehärtet.

ORMOCER®-Harze und Membranen wurden mittels FT-IR, ^{29}Si NMR-Spektroskopie in Lösung, TG, DSC, SEM, N_2-Adsorptionsmessungen sowie Einzelgaspermeation (H_2, He, CO_2, O_2, N_2) bei Raumtemperatur charakterisiert. Der Anströmdruck wurde zwischen 1,3 und 2,5 atm variiert.

Systematisch untersucht wurden ferner die Einflüsse variierender Dimethylsiloxan- und Zeolithgehalte, verschiedener Aufarbeitungstemperaturen sowie der Verwendung unterschiedlicher Zeolith-Typen auf die Permeationsleistungen der Membranen. Die Zugabe von Dimethylsiloxan-Anteilen in GUS-basierten ORMOCER®-Membranen führt zu einem signifikanten Anstieg der Gaspermeation, gekoppelt mit einer entsprechend sinkenden Selektivität.

Membranen mit Zeolithen zeigen im Vergleich zu reinen ORMOCER®-Membranen eine verbesserte Gas permeations. Die vorliegende Arbeit dokumentiert damit die Bedeutung von Zeolith-Partikeln in hybrid-polymeren ORMOCER®-Systemen. Eine erfolgversprechende Entwicklung zu einer Gastrennmembran auf der Basis von Zeolithen in ORMOCER®-Matrix wird anhand der experimentellen Ergebnisse diskutiert.

_____

_____

Chapter 1. General Background

1.1 Introduction to membranes and membrane processes

Membranes are permselective barriers that allow the preferential transport of certain penetrants, thereby enabling the separation of mixtures of such components.Membranes and membrane-based separation processes, over the last four decades, have played an important role in the separation industry. They are often more energy efficient and compact than conventional separation processes and hence they find a wide range of application in various industries such as chemical, food, petrochemical, pharmaceutical and biotechnology to separate or concentrate liquid solutions, cellular suspensions or gaseous mixtures [1]. In principle, membrane separation methods include microfiltration, ultrafiltration, nanofiltration, reverse osmosis, electrolysis, dialysis, electrodialysis, gas separation, vapor permeation, pervaporation and membrane distillation [2]. In recent times, the use of membranes in gas separation is gaining popularity and is considered to be the most prominent emerging technology in gas separation. This is because of its advantages in separation, low capital cost, low energy consumption, ease of operation, cost effectiveness even at low gas volumes and good weight and space efficiency [3-5].

The performance and efficiency of the membrane can be characterized by two key process parameters: the permeability and permselectivity. The permeability or the permeability coefficient is defined as the thickness and pressure-normalized flux of the gas molecules through the membrane [6]. The permeability of the membranes is described by the Equation 1.1:

$$P_A = \frac{N_A \times \ell}{\Delta p_A} \qquad (1.1)$$

where P_A is the permeability of the gas A, N_A is the steady state flux of the penetrating gas A at standard temperature and pressure [cm^3(STP)/s cm^2], ℓ is the thickness of the

_____

_____

membrane (cm) and Δp_A is the pressure difference across the membranes (cm Hg). Permeability of dense film materials is commonly expressed in Barrers, where

$$1\ \text{Barrer} = 1 \times 10^{-10}\ \frac{cm^3(STP) \times cm}{s \times cm^2 \times cm\ Hg} \qquad (1.2)$$

The permselectivity (which is also known as separation factor or ideal selectivity) is the ability of the membrane to reject or to prevent the passage of one or more species in the feed suspension. The permselectivity is governed by the intrinsic nature of the membrane material and is defined as the ratio of the permeability of gases. For example, a gas mixture containing A and B components, the permselectivity ($\alpha_{A/B}$) is given by:

$$\alpha_{A/B} = \frac{P_A}{P_B} \qquad (1.3)$$

where P_A is the permeability of the more permeable gas component A and P_B is the permeability of the less permeable gas component B, across the membrane.

Criteria for selecting membranes for a given application are complex; nonetheless, durability and the mechanical integrity at operating conditions, flux and selectivity are the most important requirements that must be balanced against the cost in all cases [7-8]. The relative importance of each of these requirements varies with the application. In principle, however, it can be stated that the higher the selectivity, the more efficient the process will be and the lower the partial pressure required to achieve separation which, in turn, lowers the operating cost of the membrane system. The higher the flux, the smaller the required membrane area will be which again lowers the cost of the membrane system. In the absence of defects, the selectivity is a function of the material at operating conditions. The flux is a function of material properties as well as the membrane thickness, and the smaller the thickness, the higher the flux will be.

_____

_____

1.2 Membrane types

Synthetic membranes can be classified according to various properties such as the material base (e. g. polymer, inorganic and inorganic-organic) and according to their structure (porous and non-porous) [9]. The porous membranes enable transport through their pores, whereas non-porous membranes allow transport through the bulk of the material. The membrane transport theory will be discussed in detail in chapter 2.

1.2.1 Polymeric membranes

Polymers are the most widely used membrane materials. They are attractive because they offer low materials and processing cost, and they can be processed into hollow fibers with high surface areas. Moreover, they possess adequate mechanical andthermal stability for the membrane separation process [10].Generally, polymeric membranes are non-porous, and gas permeation through them is described by the solution-diffusion mechanism [11]. Despite their various advantages, standard polymeric membranesshow low productivity and selectivity resulting in economic viability only in small to medium scale processes or in specialized applications. Ideally, membranes should exhibit high selectivity and high permeability. For most membranes, however, the selectivity increases with decreasing permeability and vice versa. In 1991, Robeson analyzed the separation performance of a large number of polymer membranes known from the literature data and discussed their performance in terms of so-called "upper-bound" curves or trade-off lines [12]. These curves show the traditional trade-off line between permeability and selectivity for polymeric membranes. This has motivated materials scientists to develop new concepts to overcome the trade-off line. One concept is the integration of highly selective inorganic particles such as zeolites, or carbon molecular sieves into a continuous polymer matrix [11]

_____

_____

1.2.2 Inorganic membranes

Inorganic membranes refer to membranes made of materials such as ceramics (Al_2O_3, ZrO_2, TiO_2, and SiO_2), carbon, metals and zeolites [13-16]. Among others, molecular sieve (zeolite) membranes show promising properties due to their well defined pore structures that preferentially allow the smaller molecules to penetrate through the membrane faster, while mainly restricting the larger gas molecules from penetrating [16]. They possess excellent chemical, mechanical and thermal stability. They can separate molecules based on size, shape and polarity. The separation performance of these membranes can surpass that of polymeric membranes, including higher separation rates. However, such membranes are quite expensive due to their multilayered composition and not easy to handle and process. Because of these drawbacks, their application is restricted to only a small scale. In order to overcome this obstacle the use of hybrid materials has been proposed as an alternative solution [17-18]

1.2.3 Mixed matrix membranes (MMMs)

Mixed matrix membranes have been developed as a material alternative to overcome the conventional limitations of polymer and inorganic materials. They are composed of a dispersed inorganic phase in a continuous polymer matrix. The dispersed inorganic phase can be zeolite, carbon molecular sieves or other nanosized particles. The most commonly used dispersed inorganic phases are zeolites and carbon molecular sieves. They have interesting separation properties for desired molecules (i.e. by molecular sieving mechanism). Based on the precise molecular sieving ability of molecular sieves and flexibility and processibility of polymers, the performance of such mixed matrix membranes can be thought to be above the limiting tradeoff curve as shown in Fig 1.1. W. J. Koros and T. S. Chung and their coworkers have made a major contribution to the development and understanding of these materials [19-21]. Although these mixed matrix materials have shown some promising results, there are a few challenges involved in their formation. The most common challenge is the formation of defect free mixed matrix membrane. Usually, defects are generated at the interface due to the week

_____

_____

interaction between polymer and molecular sieve particles. These defects could lead to the formation of interfacial voids through which non-selective gas transport can take place [22].
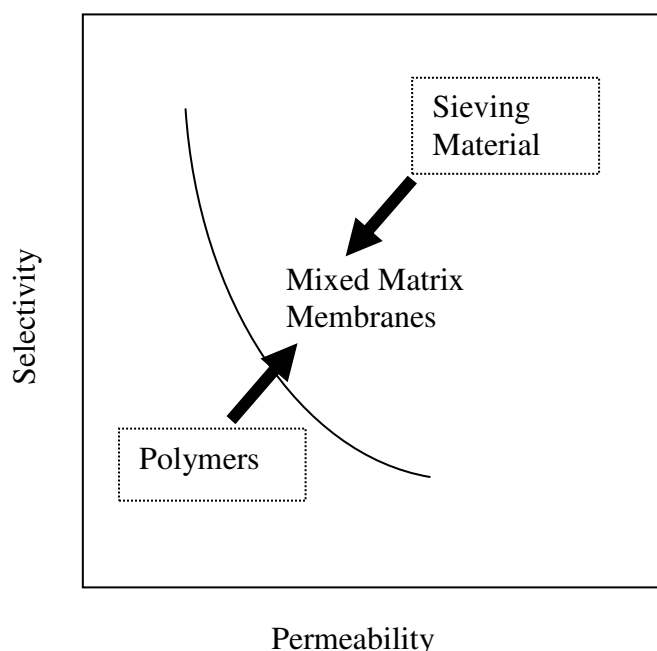
Figure 1.1: Relative positions of sieving materials and mixed matrix membrane with respect to permeability and selectivity trade-off curve for polymer.

This phenomenon is called "sieve-in-a-cage" morphology, and is shown in Fig.1.2. This morphology is undesirable since the void is much more permeable than the zeolite and the penetrants will bypass the zeolite. The formation of interfacial voids leads to higher permeability and lower selectivity. This and other processing challenges have hindered the commercial production of mixed matrix membranes. Current research focuses on overcoming these obstacles by developing new materials which will eliminate the causes. The surface modification of the molecular sieving phase and changes in the membrane casting conditions have been suggested to overcome the formation of interfacial voids in large scale mixed matrix membranes. However, these materials have not yet yielded the desired simultaneous increase in both permeability and selectivity, with the exception of a few reported cases. Therefore, this project is focused on the development of a new material for the fabrication of mixed matrix membranes.

_____

_____
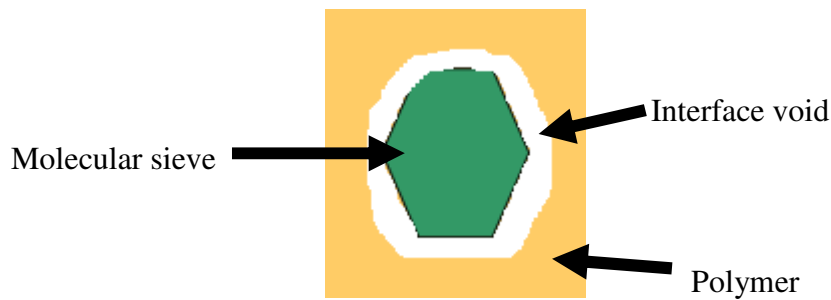
Figure 1.2: Formation of a sieve-in-a-cage morphology in mixed matrix membranes

1.3 ORMOCER®s (Inorganic-organic hybrid polymers)

ORMOCER®s are inorganic-organic hybrid polymers created on basis of chemical nanotechnology, whose property profile can be varied almost at liberty. The synthesis of this material is based on a modified sol-gel process, i.e. they are manufactured from a molecular dispersion. First, inorganic structures are developed via controlled hydrolysis and condensation of organically modified Si alkoxides. Further, in a subsequent step, the polymerizable groups attached to the inorganic parts are interconnected via thermal or UV-cross linking. Moreover, theorganically modified Si alkoxides which are not susceptible for organic polymerization can be used for the organic functionalization of inorganic network. They contain structural elements of
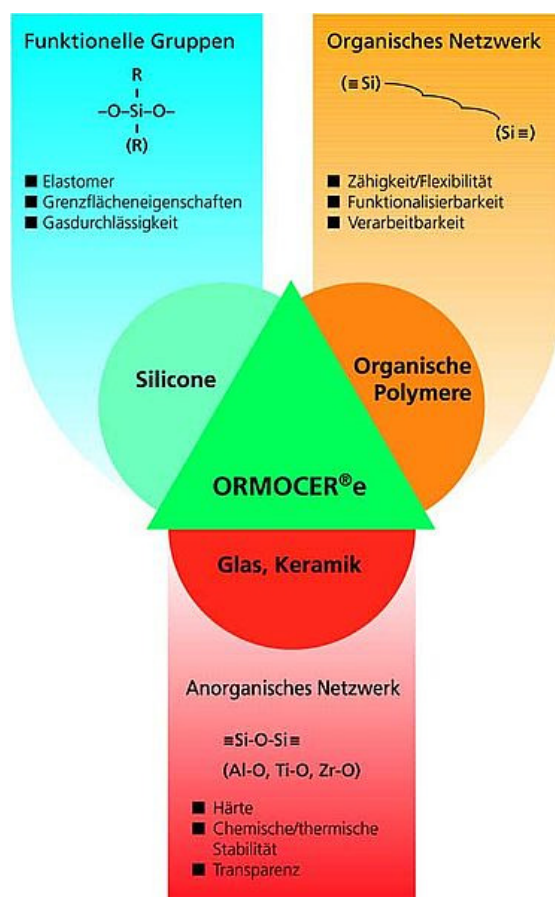
Figure 1.3 Basic structural elements and possible properties of ORMOCER®s

_____

glass and ceramics, organic polymers and silicons. The basic structural elements and the possible properties of ORMOCER®s are shown in Fig. 1.3. They are highly cross-linked, transparent materials that are derived from more than one species of monomer, each having a different role [glass-like (transparency, chemical, mechanical and thermal) and polymer-like (toughness, functionalization and low processing temperature)]. These characteristic features enable their use as functional coatings (scratch/abrasion resistant, antireflective, easy-to-clean, corrosion protection and barrier), dental composites and optical/photonic/micro-electronic (phot-opatternable dielectric and optical wave guide) devices. Due to the incorporation of special types of organic functional groups, the target properties can be accomplished for the intended application. The versatile nature of ORMOCER® materials can be further explored for their use as membrane matrix material.

1.4 Research Objectives

The overall objective of this thesis was to develop a new kind of mixed matrix membrane by combining promising ORMOCER® systems (inorganic-organic hybrid polymers) with molecular sieving materials and evaluate their gas permeation performance. The concept was to realize gas permeable hybrid membranes by filling a hybrid polymer matrix with porous particles. Throughout the thesis much attention was given to the preparation and in-depth characterization of mixed matrix membrane materials highlighted to understand the role of zeolite particles and to explore the molecular sieving properties in the ORMOCER® matrix. In order to work towardsthese goals the following objectives were developed:

Objective 1: To fabricate free-standing mixed matrix membranes by combining the glycerine-1,3-dimethacrylateurethanetriethoxysilane   (GUS)-based   ORMOCER® (inorganic-organic hybrid polymer) and zeolite Beta (BEA) via solution casting followed by UV-curing. The zeolite Beta was chosen for its large pore size (0.55 - 0.76 nm) which was expected to positively influence the overall flux of the GUS-based ORMOCER® membranes.

The basic aim was to improve the flux of pure GUS-based ORMOCER® membranes.

The mixed matrix membrane concept is investigated, zeolite Beta is chosen as a molecular sieve because it possesses a large pore diameter which should positively

_____

influence the overall flux of the GUS-based ORMOCER® membranes.   As observed from first measurements, these mixed matrix membranes have an enhanced gas permeation performance only for small gas molecules such as He, H_2. The insight provided by these results was then used to develop a new mixed matrix membrane with a modified GUS-based OMROCER® matrix, thereby defining the second objective of research.

Objective 2: To enhance the performance of mixed matrix membranes, the work defined in objective 1 was further extended to using modified GUS-based ORMOCER® systems to tailor the mixed matrix membranes.

Dimethyldiethoxysilane was used as a siloxane network modifier in ORMOCER®s.The zeolite Beta and LTA (zeolite 3Å, zeolite 4Å and zeolite 5Å) type zeolites are chosen, since these zeolites differ in pore size. The effects of zeolite loading and pore size on the gas separation performance are investigated. The single gas permeabilities for CO_2, N_2 and O_2 are evaluated at various pressures.

In addition, the effects of processing parameters on the material properties of glycerinedimethacrylateurethanetriethoxysilane (GUS)-based ORMOCER® systems are systematically evaluated.

1.5 Overview of the thesis

The thesis is organized in the following manner. Chapter 1 presents a general introduction on membranes and membrane processes and membrane types. The scope and objective of the present work has also been outlined at the end of this chapter.

Chapter 2 provides the fundamentals of the transport of gases in polymers   and molecular sieves along with some models describing the same. Chapter 3 includes the synthesis and characterization of glycerine-1,3-dimethacrylateurethanetriethoxysilane (GUS)-based ORMOCER® (Inorganic-organic hybrid polymer) resin and its applicability for the fabrication of free-standing ORMOCER®-zeolite Beta (BEA) mixed matrix membranes for gas separation. The resin sample was characterized by FT-IR, ^{29}Si NMR, and the mixed membranes were characterized by SEM, TG and DTG, N_2

_____

adsorption and desorption measurements. The gas permeation performance of these membranes was investigated in detail. Chapter 4 describes the tailoring of GUS-based ORMOCER® systems using dimethyldiethoxysilane (DMDES) as silicone component and the preparation and characterization of their corresponding mixed matrix membranes. The samples were characterized by FT-IR, ^{29}Si-NMR, SEM, TG and single gas permeation measurements. The detail study on the transport properties and their correlation towards the membrane structure is the main topic of this chapter. Chapter 5 describes the influence of technological processing parameters on the material properties of glycerinedimethacrylateurethanetriethoxysilane (GUS)-based ORMOCER® systems. The samples are characterized by ^{29}Si NMR and FT-IR spectroscopy, the optical properties are determined using a prism coupling method. The influence of the photoinitiator concentration on the degree of photopolymerization of novel GUS-based ORMOCER® system is systematically discussed in detail.

Chapters 3 to 5 are based on the following publications:

Chapter 3:

S. M. Kumbar, T. Selvam, C. Gellermann, W. Storch, T. Ballweg, J. Breu, G. Sextl, ORMOCER®s (organic-inorganic hybrid copolymers)-zeolite Beta (BEA) nanocomposite membranes for gas separation applications, J. Membr. Sci. 347 (2010) 132.

Chapter 4:

S. M. Kumbar, T. Selvam, C. Gellermann, W. Storch, T. Ballweg, J. Breu, G. Sextl, Fabrication of ORMOCER®-zeolite Beta mixed matrix membranes using dimethyldiethoxysilane (DMDES) as a siloxane modifier of networks, J. Membr. Sci. (submitted)

Chapter 5:

S. M. Kumbar, C. Gellermann, T. Ballweg, H. Wolter. G. Sextl, The influence of technological processing parameters on the material properties of glycerine-1,3-dimethacrylateurethanetriethoxysilane (GUS)-based ORMOCER® systems.

_____

J. Sol-Gel Sci. &Techn. (to be submitted)

References

[1] S. P. Nunes and K. V. Peinemann, Membrane technology in the chemical industry, Wiley-VCH Verlag GmbH, (2001).

[2] I. Pinnau and B. D. Freeman, Membrane Formation and Modification, ACS, (1999).

[3] R. W. Spillman, Economics of Gas Separation Membranes, Chem. Eng. Prog., 85 (1989) 41.

[4] M. Freemantle, Membranes for gas separation, Chem. Eng. News, 83 (2005) 49.

[5] R. W. Baker, Future directions of membrane gas separation technology, Ind. Eng. Chem. Res., 41 (2002) 1393.

[6] W. J. Koros, Y. Ma, and T. Shimidzu, Terminology for membranes and membrane processes, J. Membr. Sci., 120 (1996) 149.

[7] W. J. Koros and I. Pinnau, Membrane formation for gas separation processes, Polymeric gas separation membranes: in D. R. Paul and Paul and Y. P. Yamplo'skii (Eds.), CRC Press, Boca Raton, FL, (1994) 209.

[8] W.J. Koros and R. Mahajan, J. Membr. Sci., Pushing the limits on possibilities for large scale gas separation: which strategies? 175 (2000) 181.

[9] M. Mulder, Basic Principles of Membrane Technology. 2nd edition ed. (2003), Boston: Kluwer Academic Publishers.

[10] D. Paul and Y. P. Yampol'skii, Polymeric gas separation membranes, Baton Rouge: CRC Press (1994).

[11] N. Plate and Y. P. Yampol'skii, Relationship between structure and transport properties for high free volume polymeric materials, in: Polymeric Gas Separation Membranes. Baton Rouge: CRC Press (1994); 155.

[12] L. M. Robeson, Correlation of separation factor versus permeability for polymeric membranes, J. Membr. Sci., 62 (1991) 165.

[13] F. Hauler, T. V. Gestel, W. A. Meulenberg, M. Bram and H. P. Buchkremer, Characterisation and performance of novel TiO_2-ZrO_2 membranes for gas separation, E-MRS Fall Meeting (2009).

_____

_____

[14] T.A. Centeno and A. B. Fuertes, Carbon molecular sieve gas separation membranes based on poly(vinylidene chloride-co-vinylchloride), Carbon, 38 (2000) 1067.

[15] A. Tavolaro and E. Drioli, Zeolite membranes, Adv. Mater., 11 (1999) 975.

[16] J. Caro, M. Noack; P. Kolsch and R. Schafer, Zeolite membranes state of their development and perspective. Microporous Mesoporous Mater., 38 (2000) 3.

[17] T. T. Moore, R. Mahajan, D. Q. Vu, and W. J. Koros, Hybrid membrane materials comprising organic polymers with rigid dispersed phases. AIChE J., 50 (2004) 311.

[18] R. Mahajan, Formation, Characterization, and Modeling of Mixed Matrix Membrane Materials. PhD dissertation, The University of Texas at Austin, (2000).

[19] T. S. Chung, L. Y. Jiang, Y. Li and S. Kulprathipanja, Mixed matrix membranes (MMMs) comprising organic polymers with dispersed inorganic fillers for gas separation, Prog. Polym. Sci., 32 (2007) 483.

[20] De. Q. Vu, W. J. Koros and S. J. Miller, Mixed matrix membranes using carbon molecular sieves I. Preparation and experimental results, J. Membr. Sci., 211 (2003) 311.

[21] De. Q. Vu, W. J. Koros and S. J. Miller, Mixed matrix membranes using carbon molecular sieves II. Modeling permeation behavior, J. Membr. Sci., 211 (2003) 335.

[22] R. Mahajan, R. Burns, M. Schaffer and W: J. Koros, Challenges in forming a successful mixed matrix membranes with rigid polymeric materials, J. App. Polym. Sci., 86 (2002) 881.

_____

Chapter 2. Membrane Transport Theory

2.1 General gas transport theory

The ability of the penetrant to move in a polymeric membrane is determined by its transport properties, namely permeability and selectivity. As described in chapter 1, gas transport for a penetrant A in membrane materials is characterized by the permeability (the thickness and pressure normalized flux). If the transport mechanism is by solution-diffusion then the permeability coefficient, P_A, of penetrant A can be quantified as the product of the average diffusion coefficient, D_A, (cm^2), and the solubility coefficient, S_A, [cm^3(STP)/cm^3(polymer) cmHg] [1]

$$P_A = D_A \times S_A \tag{2.1}$$

The permeability (P_A) of the penetrant A can be increased by either increasing the sorption coefficient (S_A) or diffusion coefficient (D_A) through the membrane.

The ideal selectivity reflects the efficiency of a membrane to separate one component from another. For a gas separation, where the condition of negligible downstream pressure exists for an A, B gas pair, the ideal selectivity ($\alpha_{A/B}$) using equation 2.1 can be written as the product of diffusivity selectivity and solubility selectivity of the gas pair is given as:

$$\alpha_{A/B} = \frac{P_A}{P_B} = \frac{D_A \times S_A}{D_B \times S_B} \tag{2.2}$$

In order to increase the permselectivity of the membrane, it is required to adjust the diffusivity and the solubility of the penetrants. The solubility selectivity is dependent on the relative condensability of the gas penetrant and penetrant-membrane medium

interaction, whereas diffusivity selectivity is dependent on the relative difference on the diffusion coefficients of penetrants through the membrane materials [2].

2.2 Gas transport in polymeric and molecular sieve membranes

Gas transport through polymers and molecular sieves is commonly described by the solution-diffusion principle. However, diffusion in each material takes place via different mechanisms. Each mechanism is discussed below.

2.2.1 Diffusion in polymers and molecular sieves

The diffusion coefficient is defined as a quantity that measures the mobility of the penetrants in the membrane. For a polymer, the penetrants initially are sorbed into the polymer matrix and diffuse across the membranes. The penetrant moves through the thickness of the membrane by making jumps within the polymer. In order to do this, the gap between the polymer chains must be greater than the kinetic diameter of the penetrant molecules. Thermally induced motion of the polymer chains is responsible for the generation and destruction of the transient "gaps" within the polymer matrix through which diffusive jumps of the penetrant can occur followed by subsequent collapse of the sorbed cage that was previously occupied by the penetrant [2-3]. As shown in Fig. 2.1, the diffusive jumps of the penetrants in polymer can occur only when the gaps are greater than penetrant size, whereas diffusion of penetrants in molecular sieves occurs through the fixed pores of determined size [2]. Therefore, in polymers, the rate of diffusion depends on the concentration of the gaps that are sufficiently large to accept the diffusing molecules [4]. Separation of gas through the molecular sieves mainly depends on the molecular size of the penetrants as described in the preceding section. These materials are believed to possess large cavities with rigid narrow interconnections. Penetrant molecules sorb in the cavities at equilibrium and diffuse from one sorption cavity to another by activated jumps through the narrow cavity (Fig.2.1). These narrow cavities are interconnected to each other; hence a large permeability can also be realized from the molecular sieving process. The primary

barrier to diffusion is the repulsive forces between the penetrant and the constricted pores [5]. These materials can show infinity selectivity for a certain gas pairs if the size difference is such that one of the penetrant can enter the narrow cavity and other cannot.

Sorbed penetrant

Creation of a gap in polymeric material and jump of the penetrant

Collapse of the gap

Narrow constrictions

Molecular sieving material

Cavities
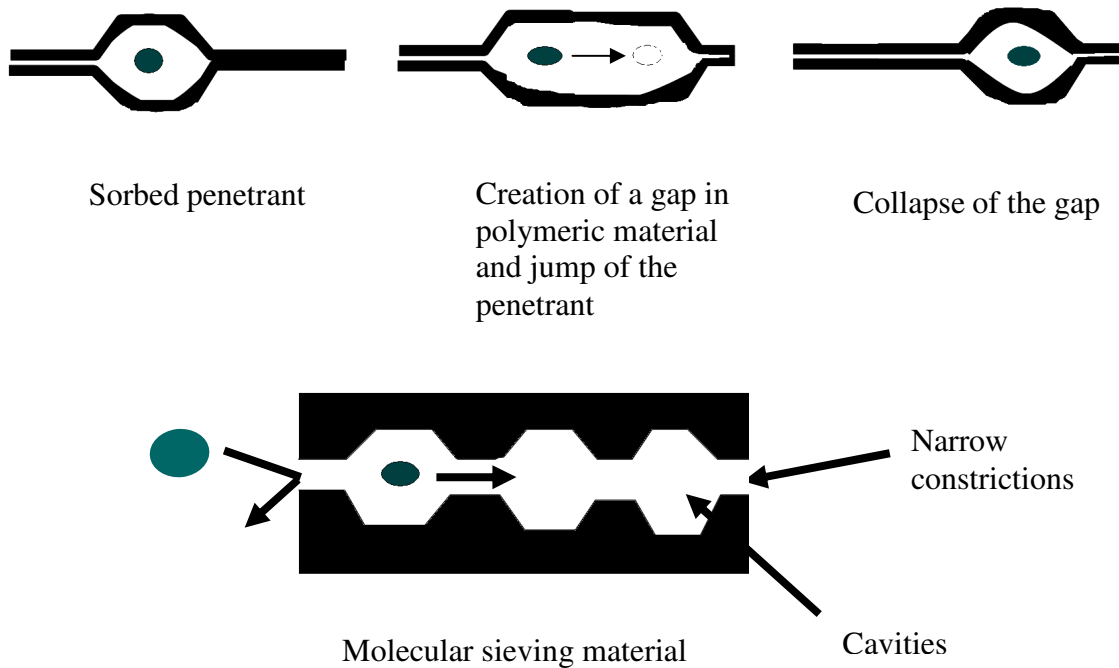
Figure 2.1: Transport of penetrant in polymer and molecular sieve materials [4].

It is believed that a major contribution to selectivity is made by entropic factors in molecular sieves, which is known as entropic selectivity. This results from the molecular sieving materials' ability to limit the degree of rotational freedom for one penetrant as compared to another.

Diffusion in these materials is a thermally activated process, thus, the temperature dependence of the diffusion coefficient (D_A) can be represented as:

$$D_A = D_0 \left[\exp \left\{ - \frac{E_d}{RT} \right\} \right] \tag{2.3}$$

where D_0 is the pre-exponential factor, E_d is the activation energy for the diffusion, R is the universal gas constant and T is the absolute temperature. Since E_d is positive, the

diffusion coefficient increases with temperature. In rigid molecular sieves, the diffusivity largely depends on both the penetrant size and pore size [5]. In the polymeric materials, the diffusivity is largely dependent on the size and shape of the penetrant and also on the thermal motion of the polymer chains [3].

The thermodynamic sorption coefficient (S_A) decreases with temperature according to the Van't Hoff equation:

$$S_A = S_0 \exp\left(\frac{-H_s}{RT}\right) \tag{2.4}$$

Where S_A is the sorption coefficient of the component A, S_0 is the pre-exponential factor, H_s is the apparent heat of sorption of the penetrant, R is the universal gas constant and T is the absolute temperature. H_s is negative for most materials; thus, the sorption decreases with increasing temperature. For gas mixtures, sorption selectivity depends on the condensability of the two penetrants.

The temperature has a stronger influence on the diffusion coefficient than on the sorption coefficient. The increase in diffusion coefficient with temperature is more than the decrease in the sorption coefficient. Thus, the overall permeability increases with increasing temperature. The equation 2.1 can be written as:

$$P_A = P_0 \exp\left(\frac{-E_p}{RT}\right) \tag{2.5}$$

where

$P_0 = D_0 \times S_0$ and $E_p = E_d + H_s$

2.2.2 Sorption in polymers and molecular sieves

The sorption coefficient is defined as the amount of penetrant sorbed at a given external partial pressure. The sorption coefficient of the penetrant in a polymer is described in Equation 2.6.

$$S = \frac{C}{p} \tag{2.6}$$

Where S is the sorption coefficient, C is the concentration of the dissolved penetrant in the polymer and p is the pressure of the penetrant in the continuous penetrant phase.

The sorption of the penetrant through the rubbery polymer follows the Henry's law at low concentration, while for higher concentrations a more complex explanation is needed. Sorption that follows the Henry's law is characterized by Equation 2.7;

$$C_{DA} = k_{DA} \times p_A \tag{2.7}$$

Where C_{DA} is the concentration of the dissolved penetrant A in the polymer, k_{DA} and p_A represent the Henry's sorption coefficient and partial pressure of the penetrant A respectively.

For glassy polymers, this quantity is modelled by the so-called dual-mode sorption model. It can be written analytically for a penetrant indicated by the subscript A, in terms of the sum of a Henry's laws of expression for C_{DA} and Langmuir expression for $C`_{HA}$;

$$C_A = C_{DA} + C`_{HA} = k_{DA}\, p_A + \frac{C`_{HA}\, b_A\, p_A}{1 + bAp} \tag{2.8}$$

Where k_{DA} (cm^3 (STP)/ cm^3 (polymer) atm) is the Henry's law of coefficient sorption of the penetrant into the densified equilibrium matrix of the glassy polymer, $C`_{HA}$ is the Langmuir sorption capacity, which characterizes the sorption into the non-equilibrium

_____

excess volume associated with the glassy state, and b (1/atm) is the Langmuir affinity parameter and p_A is the partial pressure of the penetrant A.

Sorption in molecular sieving materials is similar to that of rigid pores in glassy polymers. During the sorption process, the penetrant enters through the narrow cavities and is sorbed in the large cavities. The sorption in molecular sieves can be modelled by the dual-mode sorption with only a Langmuir sorption term, and with Henry's law of coefficient equal to zero for these systems since they do not possess a "dissolved" mode [6]. Most zeolites will behave according to strict Langmuir sorption term, although some instances can induce multi-layer sorption, where different sorption sites have different energies of adsorption. In this situation, more complex characterizations are needed such as the BET characterization method [7].

2.3 Model for performance prediction of mixed matrix membranes

Several theoretical models have been used to predict the permeation performance of mixed matrix membranes as a function of the permeabilities of the continuous and disperse phase [8-9]. The most useful and widely employed model is the Maxwell model which was derived from the J. C. Maxwell in 1867 to analyze the steady-state dielectric properties in a conducting dilute suspension of identical spheres [10]. The equations used by Maxwell governing the electrical potential of spheres in solution and the principles governing flux through a mixed matrix membrane are analogous, so Maxwell's work can be applied to this field [11-12]. The two phase equation is shown below, which predicts the permeability of the polymer matrix embedded spherical particles:

$$P_{MMM} = P_M \left[\frac{P_D + 2P_M - 2\Phi_D (P_M - P_D)}{P_D + 2P_M + \Phi_D (P_M - P_D)} \right] \qquad (2.9)$$

_____

In this equation, P is the permeability, Φ is the volume fraction of each component, the subscript MMM refers to the mixed matrix membranes, M refers to continuous matrix and the D refers to dispersed sieving phase.

Several other models have been studied for permeability prediction in mixed matrix membranes and give reasonable results [13-15]. These models are more complicated in nature and do not present significant improvement over the Maxwell Model, so the basic Maxwell Model is used as the theoretical basis for predicting crosslinked mixed matrix permeation properties.

References

[1] J. Crank, The Mathematics of Diffusion, Clanderon Press, Oxford, (1975).

[2] D. Q. Vu, Formation and Characterization of Asymmetric Carbon Molecular Sieve and Mixed Matrix Membranes for Natural Gas Purification. The University of Texas at Austin: Ph.D. Thesis, (2001).

[3] R. M. Barrer, Nature of diffusion process in rubber, Nature, 140 (1937) 106.

[4] R. Mahajan, Formation, Characterization and Modeling of Mixed Matrix Membrane Materials., University of Texas Austin: Ph.D. Thesis, (2000).

[5] J. Kärger, and D. M. Ruthven, Diffusion in Zeolites and Other Microporous Solids., New York: Wiley-Interscience, Inc. (1992).

[6] M. M. Dubinin "Fundamentals of the Theory of the Adsorption in Micropores of Carbon Adsorbents – Characteristics of Their Adsorption and Microporous Structures", Pure Appl. Chem., 61 (1989) 1841.

[7] S. Brunauer, P. H. Emmett, and E. Teller, Adsorption of gases in multimolecular layers, J. Am. Chem. Soc., 60 (1938) 309.

[8] H. T. Davis, The effective medium theory of diffusion in composite media. J. Am.Ceram. Soc., 60 (1977) 499.

[9] A. Erdem-Senatalar, M. Tatlier, and S. B. Tantekin-Ersolmaz, Questioning the validity of present models for estimating the performances of zeolite-polymer mixed matrix membranes, Chem. Eng. Commun., 190 (2003) 677.

[10] J. C. Maxwell, A treatise on electricity and magnetism. Vol. 1. (1873). Oxford Clarendon press.

[11] J. H. Petropoulos, A comparative study of approaches applied to the

permeability of binary composite polymeric materials. J. Polym. Sci., Polym. Phys. Ed., 23 (1985) 1309.

[12] R. H. B. Bouma, Permeation through a heterogeneous membrane: the effect of the dispersed phase. J. Membr. Sci., 128 (1997) 141.

[13] C. M. Zimmerman, A. Singh and W. J. Koros, Tailoring mixed matrix composite membranes for gas separations, J. Membr. Sci., 137 (1997) 145.

[14] D. A. G. Bruggemann, Berechnung verschiedener physikalischer Konstanten von heterogenen Substanzen. I. Dielektrizitatskonstanten und Leitfahigkeiten der Mischkorper aus isotropen Substanzen (The calculation of various physical constants of hetereogeneous substances. I. The dielectric constants and conductivities of mixtures composed of isotropic substances). Annalen der Physik V, 24 (1935) 636.

[15] R. Mahajan, and W .J. Koros, Mixed matrix membrane materials with glassy polymers, Part 1. Polym. Eng. Sc., 42 (2002) 1420.

Execute summary

The work presented in this thesis focuses on the preparation and characterization of a new kind of mixed matrix membrane (MMM) combining inorganic-organic hybrid polymer ORMOCER® resins with porous particles. Briefly, after an introductory part, this thesis includes three publications/manuscripts, which are presented in individual chapters.

In the first manuscript (chapter 3), the applicability of glycerine-1,3-dimethacrylateurethanetriethoxysilane(GUS)-based ORMOCER® resin was explored for the fabrication of free-standing MMMs. The basic aim was to improve the permeation performance of GUS-based ORMOCER® membranes by incorporating zeolite Beta particles. Since zeolite Beta has a large pore size (0.55 - 0.76 nm) which was expected to positively influence the overall flux of the GUS-based ORMOCER® membranes.

In order to prove the above concept, a series of GUS-based ORMOCER®-zeolite Beta mixed matrix membranes (MMMs) with different zeolite loadings (20 to 40 wt.-%) were prepared by solution casting followed by UV curing and characterized by SEM, TG-DSC, N_2 sorption and single gas permeation measurements. MMMs with a zoelite loading higher than 40 wt.-% were prepared but they are of a very fragile nature and not easy to handle for gas permeation measurements. Therefore, these membranes could not be used for gas permeation measurements.

SEM images reveal that GUS-based ORMOCER®-zeolite Beta MMMs are free of visual defects or interfacial voids. The zeolite Beta particles are homogeneously distributed within the GUS-based ORMOCER® matrix. This is suggested to be due to a strong interaction between the zeolite Beta particles and the GUS-based ORMOCER® matrix through hydrogen bonding. The effect of zeolite Beta particles on the thermal degradation of GUS-based ORMOCER® was studied under N_2 atmosphere resulting in a significant increase in the thermal stability of MMMs.

_____

The gas (H_2, He and N_2) permeabilites of MMMs were systematically investigated as a function of the zeolites Beta content. It was found that the gas (H_2, He and N_2) permeabilites of MMMs increase with increasing zeolite Beta loading within the studied range of 20 - 40wt.-%. Especially, the MMMs with 40 wt.-% of zeolites Beta exhibited a nearly 16 times increase in H_2 and He permeabilities in comparison to the pure ORMOCER® membrane. However, all the membranes showed negligible N_2 permeability, proving the highly condensed and/or cross-linked nature of the GUS-based ORMOCER® matrix. These results indicate that GUS-based ORMOCER®-zeolite Beta MMMs could be useful in the separation of H_2 and He from H_2/He/N_2 gas mixtues.

In the second manuscript (chapter 4), the work defined in the previous section was further extended to the use of modified GUS-ORMOCER® systems in order to enhance the performance of the MMMs, especially for large gas molecules (kinetic diameter > 0.289 nm), such as e.g. N_2, O_2, and CO_2.

The dimethyldiethoxysilane (DMDES) was used to incorporate silicone moieties into the inorganic network of the GUS-based ORMOCER® membranes. As a result, the DMDES modified GUS-based ORMOCER® (denoted as S-ORMOCER®) membranes showed a significant increase in gas permeability, with a correspondingly large decrease in selectivity.

In order to prove the concept, MMMs were prepared by combining the S-ORMOCER® with zeolite Beta (10 - 40 wt.-%) under similar conditions as described in the previous section. The fabricated MMMs were characterized by SEM and single gas permeation measurements.

Cross-sectional SEM images of the S-ORMOCER®-zeolite Beta (10 - 40 wt.%) MMMs showed that the zeolite Beta crystallites are homogeneously distributed throughout the S-ORMOCER® matrix, and the MMMs are completely free from visible voids.

The O_2, N_2 and CO_2 permeabilities of S-ORMOCER®-zeolite Beta MMMs decreased as the loading of zeolite Beta increased (from 10 - 30 wt-%). Moreover, the O_2/N_2 and CO_2/N_2 permselectivities of S-ORMOCER®-zeolite Beta (10 - 30 wt.-%) MMMs were found to be relatively higher than that of the S-ORMOCER® membrane. Notably,

_____

_____

S-ORMOCER$^®$-zeolite Beta (30 wt.-%) exhibits two-times higher permselectivities (O_2/N_2 = 4.8 and CO_2/N_2 = 29.8) than the S-ORMOCER$^®$ membrane (O_2/N_2 = 2.5 and CO_2/N_2 = 15.9). Such an enhancement of permselectivity could be either due to the intrinsic molecular sieving effect of zeolite Beta or to the polymer chain rigidification followed by pore blockage within the S-ORMOCER$^®$-zeolite Beta MMMs. The O_2, N_2 and CO_2 permeabilities of the S-ORMOCER$^®$-zeolite Beta (40 wt.-%) MMM are significantly higher than for the S-ORMOCER$^®$ membrane, albeit with lower O_2/N_2 (3.6) and CO_2/N_2 (17.7) permselectivities. This is most probably due to the fact that the percolation threshold is reached for the S-ORMOCER$^®$-zeolite Beta (40 wt.%) MMM.

In addition, the effect of different zeolite pore sizes on the gas permeation performance of the S-ORMOCER$^®$-zeolite A (3 Å, 4 Å and 5 Å; 30 wt.-%) MMMs was studied. The gas (O_2, N_2 and CO_2) permeabilities of S-ORMOCER$^®$-zeolite A (3 Å, 4 Å and 5 Å; 30 wt.-%) increased as the pore size of zeolite A increased (from 3 Å to 5 Å). However, S-ORMOCER$^®$-zeolite A (3 Å, 4 Å and 5 Å; 30 wt.-%) MMMs exhibit an overall decrease in O_2, N_2 and CO_2 permeabilities and O_2/N_2 and CO_2/N_2 permselectivities in comparison with S-ORMOCER$^®$-zeolite Beta (30 wt.-%) MMMs.

In the last part of the thesis (chapter 5), the effect of technological processing parameters on the cross linking and material properties of GUS-based ORMOCER$^®$ systems was investigated. The samples were characterized by ^{29}Si NMR and FT-IR spectroscopy, the optical properties were determined using a prism coupling method. The influence of the photoinitiator concentration on the degree of conversion of C=C bonds and its correlation towards the optical properties of the novel GUS-based ORMOCER$^®$ system was investigated in detail. It was found that the maximum conversion of C=C bonds is obtained at a photoinitiator concentration of 2.0 wt.-%, whereas further increase in the photoinitiator concentration does not result in any significant change in the C=C bond conversion any more. The observed refractive indices of GUS-based ORMOCER$^®$ materials are in agreement with the degree of conversion of C=C bonds. These results provide a better understanding of the influences of technological processing parameters on the GUS-based ORMOCER$^®$ material properties.

_____

All in all, a new kind of mixed matrix membrane (MMM) was successfully prepared and characterized. These MMMs have shown improved gas permeation performance in comparison to pure ORMOCER® membranes. This study has also demonstrated the essential effect of zeolite particles on the inorganic-organic hybrid (ORMOCER®) system. The results represent a first step towards the applicability in gas separation technology. However, further research will have to be done to increase the gas flux.

_____

Individual contribution to publications/manuscripts

The publications/manuscripts that form part of this thesis, were completed in cooperation with co-workers at the Fraunhofer ISC and at the University of Bayreuth. My contribution to each publication/manuscript is specified below.

Manuscript 1 – Chapter 3:

This work has been published under the title "**ORMOCER®s (organic-inorganic hybrid copolymers)-zeolite Beta (BEA) nanocomposite membranes for gas separation applications**". Listed authors are S. M. Kumbar, T. Selvam, C. Gellermann, W. Storch, T. Ballweg, J. Breu and G. Sextl. It was published in J. Membr. Sci. 347 (2010) 132.

> ➢ I have performed all the composite synthesis experiments and characterization.
> ➢ ORMOCER® (inorganic-organic hybrid polymer) was obtained from Fraunhofer ISC.
> ➢ T. Selvam, C. Gellermann, T Ballweg, W. Storch, J. Breu, and G. Sextl have contributed to the discussion.

Manuscript 2 – Chapter 4:

This work was submitted under title "**Fabrication of ORMOCER®-zeolite Beta mixed matrix membranes using dimethyldiethoxysilane (DMDES) as ORMOCER® siloxane network modifier**" to Journal of Membrane Science. Listed authors are S. M. Kumbar, T. Selvam, C. Gellermann, W. Storch, T. Ballweg, J. Breu, and G. Sextl.

> ➢ I have performed all the composite synthesis experiments and characterization.
> ➢ ORMOCER® (inorganic-organic hybrid polymer) was obtained from Fraunhofer ISC.

_____

> ➢ T. Selvam, C. Gellermann, T Ballweg, W. Storch, J. Breu, and G. Sextl have contributed to the discussion.

Manuscript 3 – Chapter 5:

This work titled "**The influence of technological processing parameters on the material properties of glycerine-1,3-dimethacrylateurethanetriethoxysilane (GUS)-based ORMOCER® systems**" is to be submitted to J. Sol-Gel Sci. &Techn by S. M. Kumbar, T. Selvam, C. Gellermann, T. Ballweg, H. Wolter and G. Sextl.

> ➢ I have performed all the sample preparations and characterization.
> ➢ ORMOCER® (inorganic-organic hybrid polymer) was obtained from Fraunhofer ISC.
> ➢ H Wolter, C. Gellermann, T Ballweg and G. Sextl have contributed to the discussion.

Chapter 3

ORMOCERs (inorganic-organic hybrid polymer)-zeolite Beta (BEA) nanocomposite membranes for gas separation applications

3.1 Abstract

The applicability of glycerinedimethacrylaturethanetriethoxysilane (GUS)-based ORMOCER (organic-inorganic hybrid copolymers) resin for the fabrication of free-standing ORMOCER-zeolite Beta (BEA) nanocomposite membrane was studied in detail. A series of ORMOCER/zeolite Beta nanocomposite membranes having different zeolite loadings (20 to 40 wt.%) were prepared by solution casting method followed by UV curing, and characterized by thermal analysis (TG/DSC), scanning electron microscopy (SEM) and N_2 sorption and single-gas (H_2, He and N_2) permeation measurements. The SEM studies revealed that zeolite Beta crystallites were homogeneously distributed within the ORMOCER matrix. There were no visible voids or defects between the ORMOCER matrix and the zeolite Beta crystallites, even at a very high zeolite loading (40 wt.%), as revealed by the high resolution SEM images. The ORMOCER-zeolite Beta nanocomposite membrane with 40 wt.% zeolite loading showed a nearly 16-times increase in H_2 and He permeabilities in comparison to the pure ORMOCER membrane.

3.2 Introduction

The past decade has witnessed an intense research effort on hybrid organic-inorganic membranes (Mixed Matrix Membranes; MMMs) owing to their wide range of potential applications such as gas separation [1-5], pervaporation [6-8], polymer

electrolyte membrane fuel cells (PEMFC) [9, 10] and direct methanol fuel cells (DMFC) [11, 12] applications. In particular, zeolite-based MMMs have become an important class of hybrid membranes given that they combine the inherent characteristics of both zeolites (molecular sieving capabilities and hydrophobicity/hydrophilicity etc.) and polymers (low capital investment and easy processing capabilities). Although, the fabrication of MMMs using various combinations of zeolites and polymers is well documented in the literature, the scientific community still faces ongoing challenges such as processibility, flux, selective gas separation and durability of the MMMs [13]. The reduction or elimination of voids within MMMs could be achieved through (a) chemical modification of the surface of zeolite crystals using desired silanes [14, 15] and polymers [16, 17]; or (b) introduction of a combatibilizer (2-4-6-triaminopyrimidine) [18, 19]. Recently, layered silicates with nanoporous layers such as MCM-22 (P) [20] and AMH-3 [21, 22], which are showing excellent intercalation and delamination/exfoliation properties, have also been used as precursors for the fabrication of nanocomposite membranes. This approach especially leads to MMMs with excellent H_2/CO_2 separation performance [21, 22] owing to their unique combination of mechanical strength (polymer-layered silicate) and molecular sieving (zeolite-like) properties. Indeed, zeolite-filled microporous mixed matrix (ZeoTIPS) membranes [23], in which zeolite particles are supported in a microporous polymer matrix by thermally induced phase separation (TIPS) process, offer significant benefits for the separation of gas (O_2/N_2) mixtures in comparison to dense MMMs.

The use of hollow fiber MMMs has seen tremendous growth in gas and vapour separation processes because of their excellent performances (high permeation area per volume ratio). An enhancement in the selectivity for gas separation (He/N_2 and O_2/N_2 etc) by hollow fiber membranes incorporated with zeolites such as zeolite Beta [24, 25] and SSZ-13 [26] is known. Li et al [24] suggested that high processing temperature close to glass transition temperature (Tg) of the polymeric materials allows the fabrication of void-free hollow fiber MMMs. During the last two decades, ORMOCERs [27-29], which are a class of highly cross-linked, transparent and hybrid inorganic-organic copolymers that are derived from more than one species of monomer, each having a different role [glass-like (transparency, chemical, mechanical and thermal) and polymer-

like (toughness, functionalization and low processing temperature)], have been extensively studied in the Fraunhofer ISC (Institut für Silicatforschung). The versatility of ORMOCER is evident from their widespread use as functional coatings (scratch/abrasion resistant, antireflective, easy-to-clean, corrosion protection and barrier), dental composites and optical/photonic/microelectronic (photopatternable dielectric and optical wave guide) devices.

Recently, a new class of proton-conducting polymer electrolyte membranes based on ORMOCERs exhibiting high thermal stability (~180 °C) has also been developed [30, 31]. In addition, the unique properties of ORMOCERs have been exploited for the fabrication of non-porous hollow fibers [32] having good mechanical properties (tensile strength: ~ 110 MPa and Young's modulus: ~2 GPa) and desired oxygen permeation characteristics (20 to 130 000 cm^3/m^2 d bar) [29, 33]. Furthermore, microporous inorganic hollow fiber membranes are novel composites that have been fabricated by pyrolysis of ORMOCER-based hollow fibers [34, 35]. While the incorporation of zeolites such as KNaA (LTA) and NaX (FAU) into ORMOCER matrices is known [36, 37], however, the fabrication of a zeolite incorporated free-standing ORMOCER-based nanocomposite membrane for gas separation applications has not been attempted so far. We present herein, the synthesis and characterization of glycerinedimethacrylaturethanetriethoxysilane (GUS)-based ORMOCER resin and the fabrication of free-standing ORMOCER-zeolite Beta (BEA) nanocomposite membranes. The aim of the present work is to investigate the effect of zeolite Beta loadings on the structural and textural properties of the ORMOCER-zeolite Beta (BEA) nanocomposites by various characterization techniques and the applicability of the resulting membranes for gas separation applications.

3.3 Experimental

3.3.1 Materials

Glycerine-1,3-dimethacrylate (98%) and 3-isocyanatopropyltriethoxysilane (IPTES, 99%) were obtained from Momentive Performance Materials. Dibutyl tin dilaurate (DBTDL, 95%) and ethyl

acetate (97%) were purchased from Aldrich. Dodecanediol-1,12-dimethacrylate (97%) and irgacure-184 (1-Hydroxy-cyclohexyl-phenyl-ketone) were purchased from Rohm & Haas and CIBA Specialty Chemicals, respectively. All chemicals were used as received without further purification. High-silica zeolite Beta ($SiO_2/Al_2O_3 = 350$) was obtained from Zeolyst International. The particle sizes of zeolite beta were in the range of 200 nm to 1 μm as revealed by scanning electron microscopy (SEM).

3.3.2 Synthesis of glycerinedimethacrylaturethanetri-ethoxysilane (GUS) based ORMOCER resin

The GUS-based ORMOCER resin was synthesized according to the previous literature [38]. The synthesis scheme of GUS-based ORMOCER resin is shown in Fig. 3.1. In a typical synthesis procedure, the addition reaction between glycerol-1,3-dimethacrylate ($C_{11}H_{16}O_5$) and 3-isocyanatopropyltriethoxysilane ($C_{10}H_{21}NO_4Si$) was carried out at room temperature in the presence of a catalyst (dibutyl tin dilaurate; $(C_4H_9)_2Sn(OOC(CH_2)_{10}CH_3)_2$, 95%, Aldrich), then the resultant silane was subjected to hydrolysis and polycondensation to construct the inorganic network. The molar composition of GUS-based ORMOCER resin used in the present study was $C_{10}H_{21}NO_4Si$: $C_{11}H_{16}O_5$: 0.2 $C_{20}H_{34}O_4$: 0.0016 $(C_4H_9)_2Sn(OOC(CH_2)_{10}CH_3)_2$. Note that no attempt has been made to remove the homogeneous catalyst (dibutyl tin dilaurate,) from the GUS-based resin since the amount of catalyst employed was very negligible.

3.3.3 Fabrication of GUS-based ORMOCER-zeolite Beta nanocomposite membranes

A schematic representation of the preparation of ORMOCER-zeolite Beta (BEA) nanocomposite membranes is shown in Fig. 3.2. In a typical method, 2 g of ORMOCER resin was added into the solvent (0.5 g of ethyl acetate) in a 10 ml glass vial. Then, 0.02 g of Irgacure-184 was added into the above mixture and then the resulting mixture was mixed

thoroughly until a clear solution appeared. Finally, a known weight of vacuum dried (moisture free) zeolite Beta (BEA) was added into the above solution and mixed thoroughly by ultrasonication (~30 min) at room temperature. The free-standing thin films of ORMOCER-zeolite Beta (BEA) nanocomposite membranes were prepared by solution casting method followed by UV-curing for 180 sec. The membranes had a thickness of 100 µm and a diameter of 0.65 cm. The ORMOCER-zeolite Beta nanocomposite membranes containing different amounts (20, 30 and 40 wt.%) of zeolite Beta were prepared using the optimised conditions described above. In addition, pristine zeolite-free ORMOCER membranes were also prepared under similar conditions for comparison purposes. Prior to the permeation measurements, these membranes were dried at 120 °C for 24 h under vacuum, cooled to room temperature and stored under moisture free conditions.

3.3.4 Characterization

FT-IR spectra of the resin and its precursors were recorded using a Nicolet Magna-IR 760 FT-IR spectrometer in the frequency range of 400 to 4000 cm^{-1}. An ORMOCER resin sample, coated on a KBr pellet and cured under UV light, was removed from the UV oven sequentially over a period of time, and analyzed immediately by FT-IR. The chemical conversion of the methacrylate groups of the ORMOCER resin was determined by monitoring the disappearance of C=C bonds. Liquid ^{29}Si-NMR measurements of the pristine ORMOCER resin were carried out on a Bruker Avance DPX 400 NMR spectrometer with a 9.4 T magnetic field and equipped with a quaternary nuclear probe head. All spectra were obtained with CDCl$_3$ as solvent and tetramethylsilane as the internal standard. Simultaneous thermogravimetry and differential scanning calorimetry (TG/DSC) measurements were performed on a SETARAM thermal analyzer TAG 24 S. The measurements were conducted from ambient temperature to 900 °C at a heating rate of 10 °C min^{-1} under synthetic air atmosphere. The BET surface areas of the samples were determined by an automated nitrogen adsorption analyzer (Quantachrome Autosorb). The samples were vacuum dried at 110 °C for 16 h prior to N$_2$ adsorption measurements. Scanning electron microscopy (SEM) images of nanocomposite membranes were acquired using a Zeiss-supra model 25 variable pressure field emission scanning electron microscope at an acceleration voltage of 10 kV.

_____

3.3.5 Permeation measurements

Single gas permeation measurements of the membranes were carried out at room temperature using a home-made constant volume-variable pressure system. Flat O-rings (Viton) were used for sealing the membranes in the stainless-steel permeation cell. High purity gases (H_2, He and N_2) were used in the present permeation study. Prior to each measurement, the entire system was degassed (pressure: 1×10^{-8} mbar) using a turbomolecular vacuum pump. Respective gases were dosed using mass flow controllers and argon was used as a sweep gas in the permeate side. The gas pressure in the feed side was varied from 0.5 to 2.0 bar, respectively, for all the experiments. The pressures at both sides (feed and permeate) could be monitored by pressure transducers (MKS Instruments Deutschland GmbH) which were linked to a computer. The PC program was set in such a way to collect permeation data for 3 minute at each pressure. The permeability and permselectivity of the membranes were calculated according to the literature procedures [39]. Each membrane was analyzed 4-times and the average permeability results are reported in Barrer. It was also verified that the results were reproducible over a long period of time.

3.4 Results and discussion

Figure 3.3 shows the FT-IR spectra of glycerine-1,3dimethylacrylate (curve 'a')   3-isocyanatopropyltriethoxysilane (curve 'b'), glycerinedimethacrylaturethane- triethoxysilane (curve 'c') and pure ORMOCER resin (curve 'd'). The broad peak at 3570 cm^{-1} is attributed to O-H stretching mode; and the peaks at 2950 and 2860 cm^{-1} are due to the C-H stretching of methyl and methylene groups respectively [38, 40]. The sharp peak of C=O carbonyl group at 1720 cm^{-1} and C=C of acrylate groups at 1638 cm^{-1} are also detected [41, 42]. The peak at 2270 cm^{-1} is a characteristic peak of N=C=O group of 3-isocyanatopropyltriethoxysilane (curve 'b'). Indeed, the peaks disappeared at 3570 cm^{-1} and 2270 cm^{-1} (curve 'c'), and the new peak at 3370 cm^{-1} is also observed (curve 'c'), which clearly shows that the reaction of

_____

glycerine-1,3-dimethacrylate with 3-isocynatopropyltriethoxysilane is nearly completed. The characteristic peak at 3370 cm^{-1} (curve 'c') is assigned to N-H stretching vibrations of glycerine-1,3-dimethacrylaturethane-triethoxysilane. In addition, the FT-IR spectrum of the pure ORMOCER resin (curve 'd') exhibits peaks at 3370 cm^{-1}, 2950 cm^{-1} and 2860 cm^{-1}, 1720 cm^{-1} and 1638 cm^{-1} which are due to the N-H stretching vibrations, C-H stretching of methyl and methylene groups, C=O carbonyl groups and C=C of acrylate groups, respectively. Moreover, a closer look at the IR spectrum of the pure ORMOCER resin reveals a peak at 1020 cm^{-1}, which corresponds to the Si-O-Si vibrations. The appearance of Si-O-Si vibration at 1020 cm^{-1}, clearly suggests that the ORMOCER resin is inorganically condensed.

^{29}Si NMR spectroscopic measurement of ORMOCER resin was also carried out in order to study the nature of the silicon species present therein. The ^{29}Si NMR spectrum of ORMOCER resin (Fig. 3.4) exhibits only one broad signal at -66 to -70 ppm. The signal at -66 to -70 ppm is attributed to the T^3 [RSi(OSi)$_3$] units [43-45]. There were no signals corresponding to T^1 [RSi(OSi)(OH)$_2$] and T^2 [RSi(OSi)$_2$(OH)] units indicating that the glycerinedimethacrylaturethanetriethoxysilane (GUS)-based ORMOCER resin possesses a highly condensed inorganic network. The broad signal in the range of -80 ppm to -140 ppm is an artefact from the glass tube.

Before carrying out the preparation of free-standing ORMOCER thin films, the change in the chemical structure of ORMOCER resin during UV-curing over a period of time was monitored by FT-IR absorption spectroscopy. Fig. 3.5 shows the FT-IR spectra of pure ORMOCER resin (curve 'a') and UV-cured ORMOCER samples over a period of time, 30 sec (curve 'b'), 60 sec (curve 'c') and 180 sec (curve 'd'). The peaks at 1638 cm^{-1} and 810 cm^{-1} are attributed to the n(C=C) stretching vibrations of methacrylate groups and the alkene C-H stretching in the acrylate group of the ORMOCER resin, respectively. The intensity of the 1638 cm^{-1} peak is gradually decreased with increasing the UV exposure time, as depicted in Fig. 3.5 (curve 'b' to 'd'). The sharp decrease in the intensity of methacrylate n(C=C) peaks after UV curing over a period of time (30-180 sec) clearly suggests the maximum consumption of n(C=C) double bonds during the polymerisation process; while the integrated area of the n(C=O) peaks (1720 cm^{-1}) remains constant. Whereas, the alkene C-H stretching (810 cm^{-1}) in the acrylate group of ORMOCER resin became almost negligible after UV-

curing for 180 sec [38, 40-42]. The above mentioned results clearly suggest that the UV-curing process for a period of 180 sec is sufficient to fabricate highly polymerised free-standing ORMOCER thin films.

TG and DSC curves of the pure ORMOCER and the ORMOCER/zeolite Beta nanocomposites containing different amounts (20, 30, and 40 wt.%) of zeolite Beta crystallites (at a heating rate of 10 °C min^{-1}) are shown in Fig 3.6 and Fig 3.7, respectively. Note that the following conclusions on the specific degradation mechanisms of ORMOCER and ORMOCER-zeolite Beta nanocomposites were drawn by the combination of results from TG (weight loss) and DSC (enthalpy change). As the trends in the thermal decomposition of the pure ORMOCER and its nanocomposites are similar (Fig. 3.6), for simplicity, the discussion will be restricted to four different stages of weight losses at < 300 °C, 300-440 °C, 440-540 °C and 540-700 °C, respectively. All the samples exhibit a negligible weight loss (~ 7 wt.%) in the first stage (< 300 °C in Fig. 3.6 and a weak exothermic peak in Fig. 3.7) which might be due to the removal of residual solvent (ethyl acetate), water and C_2H_5OH molecules resulting from the polycondensation process of Si-OH and Si-OC$_2$H$_5$ groups from the ORMOCER matrix [46]. Such processes generally lead to the enhancement of Si-O-Si bonding within the ORMOCER matrix; and indeed it may lead to free volume (space) to a certain extent within the ORMOCER matrix (between organic and inorganic phase) which will be discussed in a subsequent paragraph. The second stage (300-440 °C in Fig. 3.6 and a broad exothermic peak in Fig. 3.7) exhibits a relatively high weight loss (~ 30-35 wt.%) which is attributed to the decomposition of random session of methacrylic groups (oxidative degradation of soft segments) of the ORMOCER backbone chains as described in the literature [47-48]. The release of CO_2 generally occurs during the thermal decomposition of methacrylic groups (oxidation of soft segments) of the ORMOCERs. However, the anhydride formation dominates the minor decarboxylation reaction. The third stage (440-540 °C in Fig. 3.6 and sharp exothermic peaks in Fig. 3.7) weight loss (~5-17 wt.%) may be due to the fragmentation of anhydride ring structures followed by release of CO_2, CO, propene, isobutylene etc [49]. The fourth stage (540-700 °C in Fig. 3.6 and a broad exothermic peak in Fig. 3.7) weight loss (~11-24 wt.%) can be attributed to the thermo-oxidative degradation of urethane groups (hard segments) of the ORMOCER matrix. As can be seen from Fig. 3.6 (curves 'a' to 'd') that the amount of inorganic residue increased with increasing the amount

of zeolite Beta (20 to 40 wt.%). The amounts of inorganic residue present in the pure ORMOCER and its nanocomposites are 15 wt.% (pure ORMOCER), 33 wt.% (20 wt.% zeolite Beta), 40 wt.% (30 wt.% zeolite Beta) and 45 wt.% (40 wt.% zeolite Beta), respectively. As expected, the ORMOCER-zeolite Beta nanocomposites (curves 'b', 'c' and 'd' in Fig. 3.6) exhibit higher thermal decomposition temperatures as compared to the pure ORMOCER (curve 'a' in Fig. 3.6). These results indicate that the introduction of zeolite Beta crystallites into the ORMOCER matrix enhances the thermal stability of the ORMOCER-zeolite Beta (20-40 wt.%) nanocomposites. A significant shift in the decomposition temperatures (especially in the range of 300-440 °C and 440-540 °C; Fig. 3.6 and Fig. 3.7) and the exothermic peaks of the nanocomposites to the high temperature regions clearly suggest that the zeolite Beta crystallites act as fillers or cross linking agents within the ORMOCER matrix. Nevertheless, the decrease in exothermicity at 440-540 °C (Fig. 3.7) may be correlated to increasing stiffness and toughness of the zeolite Beta incorporated nanocomposites and slow release of adsorbed gas, respectively. However, no clear trend can be observed in the decomposition temperature range of 540-700 °C (Fig. 3.6 and Fig. 3.7).

The peak decomposition temperatures (T_{1max}, T_{2max}, T_{3max} and T_{4max}) of pure ORMOCER and ORMOCER-zeolite Beta nanocomposites obtained from DSC curves (Fig. 3.7) are summarized in Table 3.1. It can be seen from Table 3.1 that the decomposition temperatures of pure ORMOCER exhibited a peak at 169 °C (T_{1max}), 391 °C (T_{2max}), 457 (T_{3max}) and 597 °C (T_{4max}), respectively. As the zeolite Beta content in the ORMOCER system increased from 20 to 30 wt.%, the peak decomposition temperatures increased gradually from 169 to 172 °C (T_{1max}), 391 to 427 °C (T_{2max}) and 457 to 493 °C (T_{3max}), respectively. These results indicate that zeolite Beta crystallites act as inorganic filler within the ORMOCER matrix. Most probably, the interaction between the zeolite Beta crystallites with the ORMOCER matrix might be higher for 30 wt.% zeolite Beta containing ORMOCER system. However, further increase of the zeolite Beta content (40 wt.%) in the ORMOCER system led, in turn, to a slight decrease in the peak decomposition temperatures [T_{1max} (170 °C), T_{2max} (413 °C) and T_{4max} (582 °C)]. This could be due to the less amount of ORMOCER matrix present in this system which contributes to the decrease in the peak decomposition temperatures. Further investigations are necessary (e.g., thermogravimetry coupled with mass

spectrometry; TG/MS) to understand the nature of decomposition of ORMOCER-zeolite Beta nanocomposites.

The N_2 adsorption-desorption isotherms of pure ORMOCER and the ORMOCER-zeolite Beta nanocomposites containing different amounts of zeolite Beta (20, 30 and 40 wt.%) are shown in Fig. 3.8. As can be seen from Fig. 3.8, there was no significant uptake of N_2 in pure ORMOCER and the nanocomposites containing 20 and 30 wt.% of zeolite Beta at low relative pressures (P/P_0 = 0.5-0.30). These results clearly indicate that the zeolitic pores of the nanocomposites are completely blocked by the ORMOCER matrices, and thereby rendering them inaccessible to N_2-molecules. However, the nanocomposite containing 40 wt.% of zeolite Beta exhibits higher N_2 uptake than the other nanocomposite samples, indicating the presence of zeolite pores/crystallites that are accessible for N_2-molecules. The BET plots (figure not shown) of the 20 and 30 wt.% zeolite loaded samples did not exhibit any linear regression lines within the P/P_0 range of 0.05 to 0.30. Therefore, the BET plots of 20 and 30 wt.% zeolite loaded samples were not considered for the calculation of their surface areas. Whereas, the BET plot (figure not shown) of 40 wt.% zeolite loaded sample exhibited a linear regression line in the above mentioned P/P_0 range. The BET surface area of the nanocomposite containing 40 wt.% zeolite Beta was calculated to

be 90 m^2g^{-1}. Thin films of ORMOCER-zeolite Beta nanocomposite membranes having 100 µm thickness were also prepared in order to evaluate their performance for gas separation applications. Note that the ORMOCER-zeolite Beta nanocomposite membranes are mechanically stable enough for handling and performing permeation studies.

Fig. 3.9 shows the SEM images of surface and polished cross-section views of pure ORMOCER and ORMOCER nanocomposites containing 20, 30 and 40 wt.% of zeolite Beta. The surface and cross-section of the pure ORMOCER membranes are very smooth and continuous, as is evident from Fig. 3.9 'a' and 'b'. As the zeolite loadings increased the surface roughness of the membranes increased to some extent

(Fig. 3.9 'c', 'e' and 'g'). Most importantly, the polished cross-sectional SEM images of the ORMOCER-zeolite Beta nanocomposite membranes (Fig. 3.9 'd', 'f' and 'h') show that the zeolite Beta crystallites are well dispersed throughout the ORMOCER matrix, even at high amount of zeolite Beta loading (40 wt.%). In order to examine the presence of visible voids or phase separation between the zeolite Beta crystallites and the ORMOCER matrix, high

magnification SEM images of the unpolished cross sectional views were taken and are shown in Fig. 3.10. Again, it can be seen that the pure ORMOCER membrane (Fig. 3.10 'a') is very smooth and continuous. It is very clear from Fig. 3.10 ('b', 'c' and'd') that no defects or voids between the zeolite crystallites and the ORMCOER matrix were observed. These results suggest that the zeolite crystallites are well-adhered to the ORMOCER matrix. In addition, the crystallites' negative footprints on the ORMOCER matrix reflect this fact. This could be due to the presence of strongest possible interaction between the zeolite Beta crystallites and the ORMOCER matrix via hydrogen bonding. The proposed mechanism for the formation of hydrogen bonds between the zeolite Beta crystallites and the ORMOCER matrix is shown in Fig. 3.11. It is pertinent to mention here that no primers or silane coupling agents were used for the fabrication of ORMOCER-zeolite Beta nanocomposites. Therefore, the above mentioned results indicate that the ORMOCER used in the present study is useful for the fabrication of continuous and defect free nanocomposite membranes with high zeolite crystallites dispersion. However, the average maximum crystallite size of zeolite Beta within the ORMOCER matrix is approximately 200 nm to 1 μm, indicating the homogeneous distribution of zeolite Beta crystallites within the ORMOCER matrix.

To evaluate the applicability of the resulting membranes for gas separation applications, single gas (H_2 and He) permeation measurements were carried out at room temperature on the ex-situ activated (pure ORMOCER) membranes at 120, 170, 200 and 250 °C. These results are summarized in Table 3.2. Note that the activation temperatures were chosen on the basis of the TG and DSC results obtained for the pure ORMOCER. The thicknesses of the membranes used in this permeation study were approximately 100 μm. The ORMOCER membrane activated at 120 °C showed lower permeability for H_2 and He gases than the membrane activated at 170 °C. Such an increase in the permeability of the pure ORMOCER membrane activated at 170 °C might be due to the movement of polymer groups/chain fractions within the ORMOCER matrix or enhancement in condensation of the Si-O-Si bonds followed by the removal of water molecules, leading to the creation of free space between the organic and inorganic network within the ORMOCER matrix. However, the ORMOCER membranes activated at high temperatures (200 and 250 °C) showed much lower permeability for H_2 and He gases, indicating reduction in free volume space by polymer chain rigidification of the ORMOCER matrix. It is important to mention that the pure

ORMOCER membranes undergo colour changes from colourless transparent (120 °C) to brown (170 °C) and then to dark-brown (200 and 250 °C) during the activation process. Therefore, 120 °C was chosen as the activation temperature for further studies.

The single gas (H_2, He and N_2) permeabilities and permselectivities for the pure ORMOCER and the ORMOCER-zeolite Beta nanocomposite membranes with different zeolite loadings are tabulated in Table 3.3. Prior to the room temperature single gas permeation measurements, all the membranes were activated at 120 °C for 24 h. The pure ORMOCER membrane (Table 3.3) showed negligible permeability for H_2, He and N_2 gases. These results suggest that the ORMOCER matrix possesses a highly condensed and/or cross-linked organic-inorganic network. It is evident from the Table 3.3 that increasing the zeolite loadings from 20 to 30 wt.% and eventually to 40 wt.% increased the H_2, He and N_2 permeabilities of the corresponding nanocomposite membranes. Most importantly, the ORMOCER nanocomposite membrane loaded with 40 wt.% of zeolite Beta showed higher permeability for H_2 (57.3 Barrer), He (69.3 Barrer) and N_2 (0.77 Barrer) in comparison to the pure ORMOCER membrane. Such a significant increase in permeability indicates that a percolation threshold is most probably reached and hence the existence of connected paths through zeolite crystallites in the ORMOCER-zeolite Beta (40 wt%) nanocomposite membrane. It is pertinent to recall here that the ORMOCER-zeolite Beta (40 wt.%) exhibited a higher BET surface area (90 m^2g^{-1}) than the other nanocomposites. Among the nanocomposite membranes, the ORMOCER nanocomposite membrane loaded with 20 wt.% of zeolite Beta showed the best performance in terms of both H_2/N_2 and He/N_2 permselectivities (Table 3.3). Nevertheless, the permselectivity (H_2/N_2 and He/N_2) decreased sharply with further increase in zeolite loadings from 30 to 40 wt%. Similar trends in permeability and permselectivity were reported for composite [polyimide-zeolite Beta and poly(ether sulfone)-zeolite Beta] membranes [39], where increasing the amount of zeolite loading was found to be coupled with increasing the gas peremeability and decreasing the permselectivity. It seems that the percolation threshold is most probably reached for the ORMOCER-zeolite Beta (40 wt.%) membrane and hence a decrease in permselectivity. This is in accordance with the fact that the kinetic diameters of H_2 (0.289 nm), He (0.26 nm) and N_2 (0.364) are smaller than the pore diameters of zeolite of Beta (0.66 x 0.67 nm and 0.56 x 0.56 nm). A detailed study concerning the separation of H_2 from H_2/N_2 and natural gases

using GUS-based ORMOCER-zeolite nanocomposite membranes is currently ongoing. The results will soon be published elsewhere.

3.5 Conclusions

We have successfully fabricated a series of free-standing ORMOCER-zeolite Beta (BEA) nanocomposite membranes by incorporating zeolite Beta crystallites into GUS-based ORMOCER systems. SEM images of ORMOCER-zeolite Beta nanocomposite membrane cross sections show that the zeolite Beta crystallites, ranging from 200 nm to 1 µm, are homogeneously distributed within the ORMOCER matrix. ORMOCER-zeolite Beta membranes are free of visible defects or voids and the zeolite Beta crystallites are well-adhered to the ORMOCER matrix as is evident from the high resolution SEM images. In particular, the ORMOCER-zeolite Beta nanocomposite membrane with 40 wt.% zeolite loading exhibited a nearly 16-times increase in H_2 and He permeabilities in comparison to the pure ORMOCER membrane. However, all the membranes showed negligible N_2 permeability, exemplifying the highly condensed and/or cross-linked nature of the GUS-based ORMOCER matrix. The addition of a sufficient amount of dimethyldiethoxysilane (DMDES), during the synthesis of GUS-based ORMOCER resin, might increase the free volume within the ORMOCER matrix, which may lead to the development of high-flux mixed matrix membranes for the separation of H_2 and He from $H_2/He/N_2$ gas mixtures and natural gases.

3.6 Acknowledgements

_____

3.7 Tables

Table 3.1 Degradation temperatures of pure ORMOCER and ORMOCER-zeolite Beta nanocomposites[a].

Zeolite Beta loading (wt.%)	T_{1max} °C	T_{2max} °C	T_{3max} °C	T_{4max} °C
0	169	391	457	597
20	172	415	495	600
30	172	427	493	585
40	170	413	-	582

[a]DSC analysis

_____

_____

Table 3.2 H_2 and He permeabilities of the pure ORMOCER membranes activated (ex-situ) at different temperatures under vacuum[a].

Pre-activation	Permeability (Barrer)[b]	
temperature (°C)	H_2	He
120	3.4	4.5
170	11.7	14.7
200	3.6	4.2
250	3.7	2.9

[a]Single gas permeation measurements were carried out at room temperature
[b]1 Barrer = 1×10^{-10} cm^3 (STP) cm/ cm^2 s cm Hg

_____

_____

Table 3.3 Single gas (H_2, He and N_2) permeabilities and permselectivities of the pure ORMOCER and the ORMOCER-zeolite Beta nancocomposite membranes[a].

Zeolite Beta loading	Permeability (Barrer)[b]			Permselectivity	
(wt%)	H_2	He	N_2	H_2/N_2	He/N_2
0	3.4	4.5	0,02	170	225
20	10.7	9.8	0.04	267	246
30	11.9	8.4	0.12	99	70
40	57.3	69.3	0.77	74	90

[a]Prior to the room temperature single gas (H_2, He and N_2) permeation measurements, all the membranes were activated (ex-situ) at 120 °C for 24 h.
[b]1 Barrer = 1×10^{-10} cm^3 (STP) cm/ cm^2 s cm Hg

_____

3.8 Figures
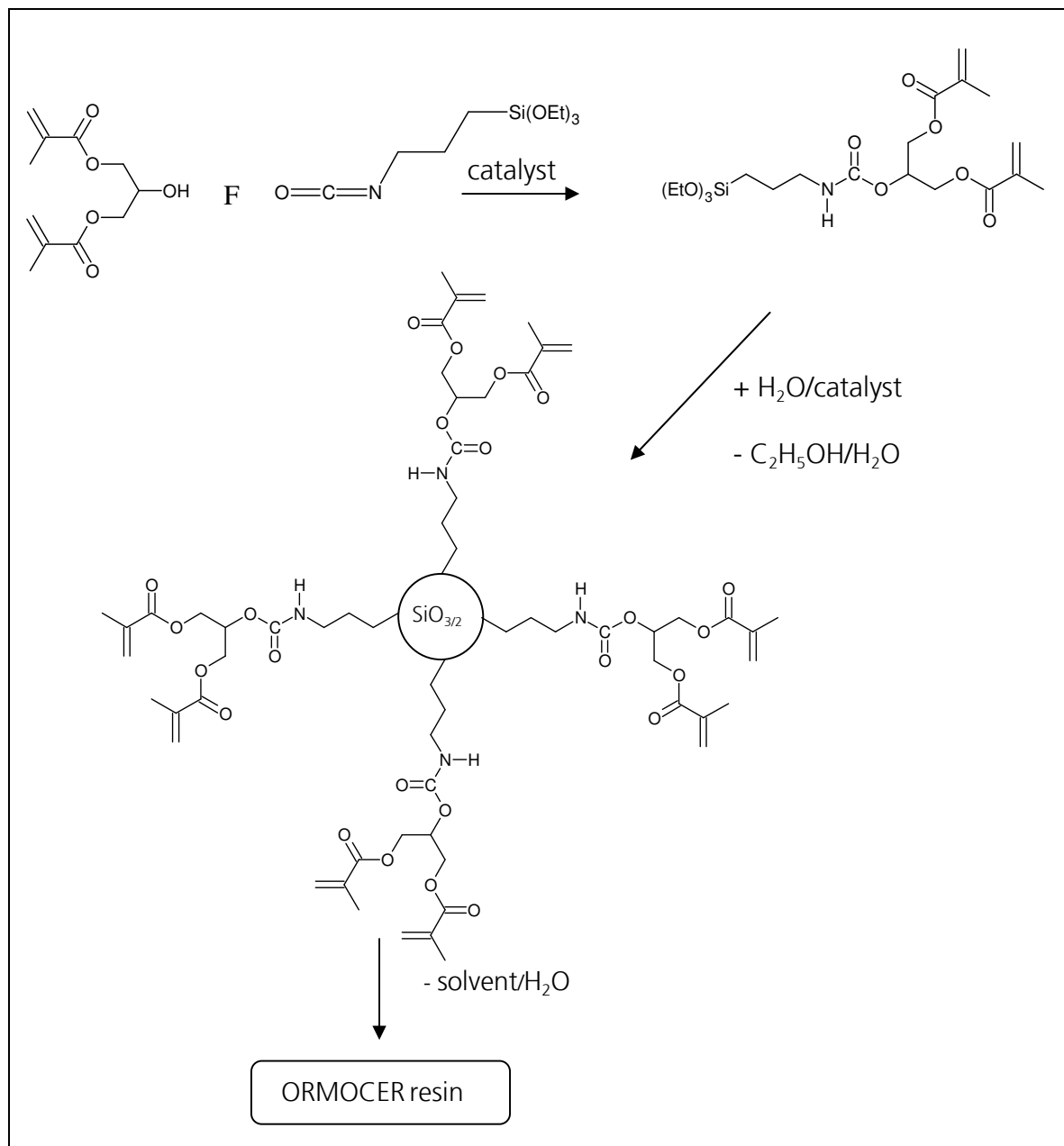
Figure 3.1: Synthesis scheme of ORMOCER resin.

_____

```
┌─────────────────────────────┐
│        ORMOCER resin        │
└─────────────────────────────┘
```

addition of solvent   ⇓   stirring for 5 min.

```
┌─────────────────────────────┐
│        ORMOCER resin        │
└─────────────────────────────┘
```

addition of Irgacure-184   ⇓

```
┌─────────────────────────────┐
│        ORMOCER resin        │
└─────────────────────────────┘
```

addition of zeolite Beta particles   ⇓   ultrasonication for 30 min.
at room temperature

```
┌─────────────────────────────┐
│    ORMOCER-zeolite Beta     │
│          mixture            │
└─────────────────────────────┘
```

Casting a solution on a glass   ⇓   UV-curing, 180 sec
plate

```
┌─────────────────────────────┐
│    ORMOCER-zeolite Beta     │
│   Free standing thin films  │
└─────────────────────────────┘
```

⇓   vacuum drying 120 $^{\circ}$C for 24 h

```
┌─────────────────────────────┐
│    ORMOCER-zeolite Beta     │
│   free standing thin films  │
└─────────────────────────────┘
```

Figure 3.2: Flow chart of the preparation methodology of ORMOCER-zeolite Beta nanocomposite membranes

_____
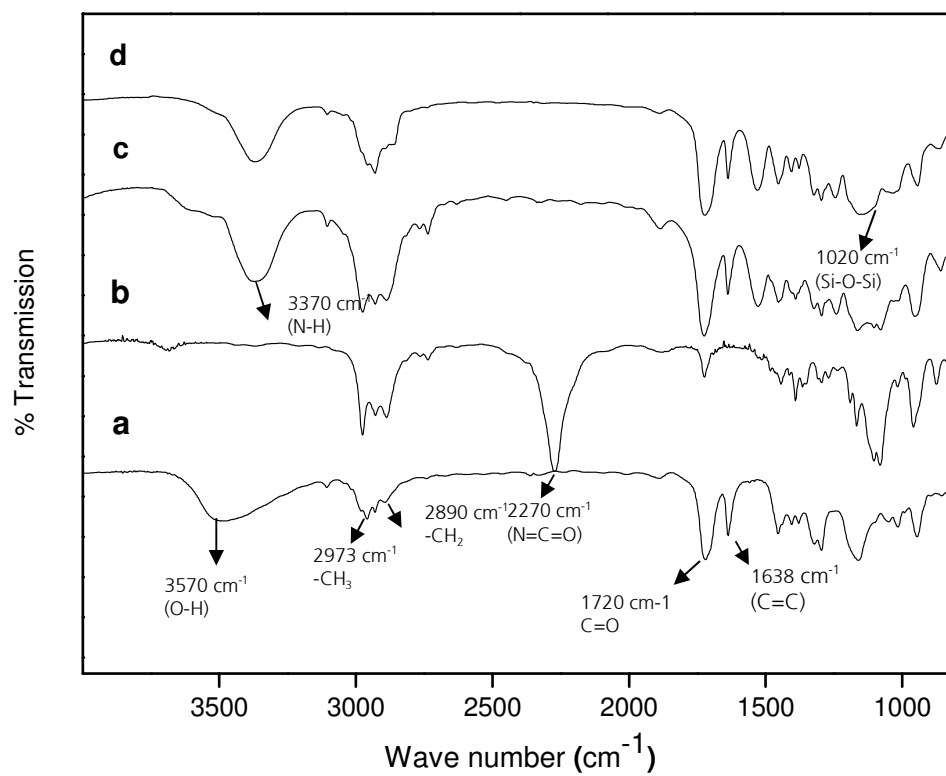
Figure 3.3: FTIR spectra of precursors used in the preparation of ORMOCER resin: (a) glycerine-1,3-dimethacrylate, (b) 3-isocynatopropyltriethoxysilane, (c) glycerine-1,3-dimethacrylaturethanetriethoxysilane and (d) ORMOCER resin
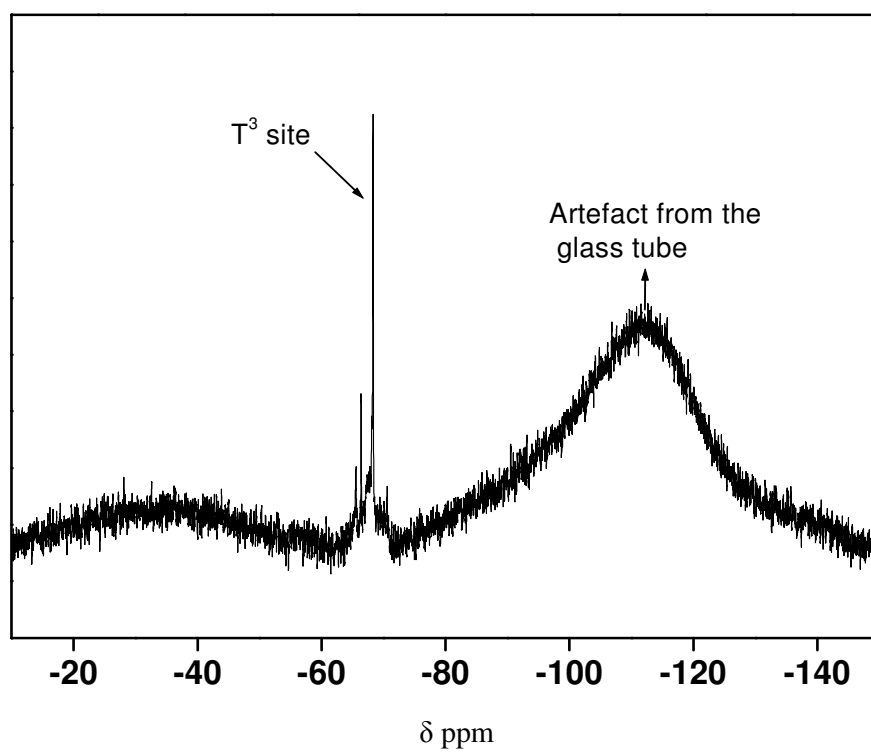
Figure 3.4: ^{29} Si NMR of pure ORMOCER resin.
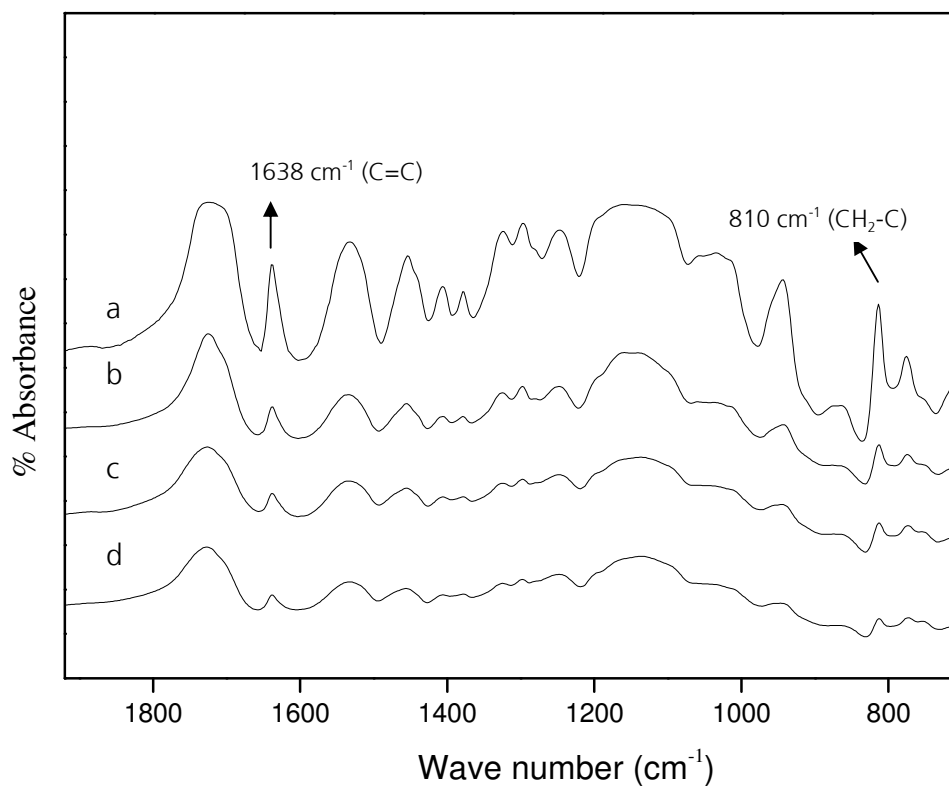
Figure 3.5: FTIR spectra of pure ORMOCER resin (a) and after UV curing over a period of time, (b) 30 sec, (c) 60 sec and (d) 180 sec. under N_2 atmosphere
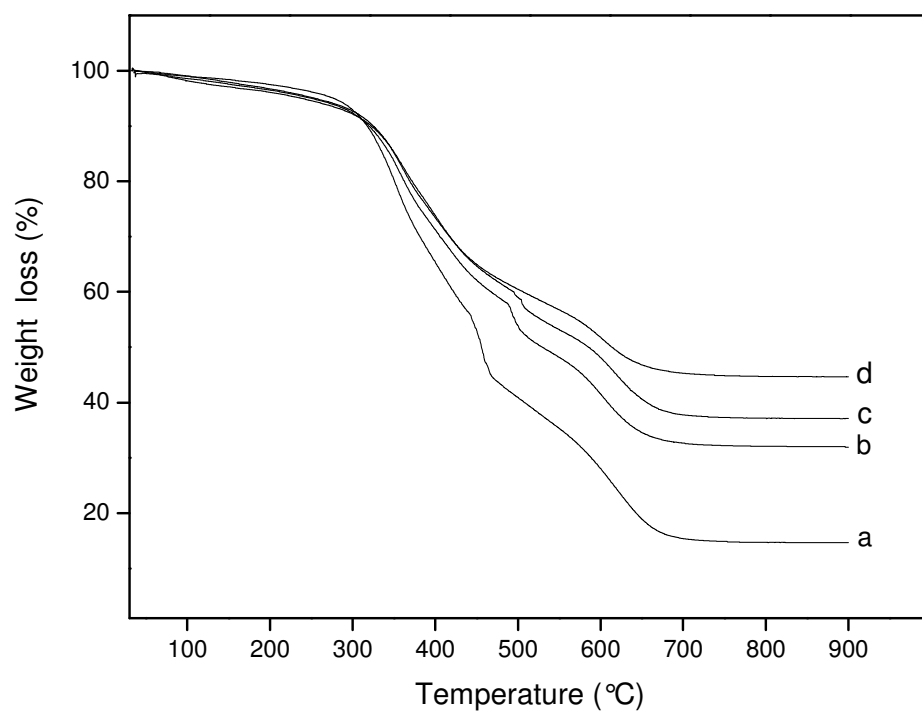
Figure 3.6: Thermo gravimetric analysis (TGA) curves of pure ORMOCER (a) and ORMOCER-zeolite Beta nanocomposites with different zeolite loadings, 20 wt.% (b), 30 wt.% (c) and 40 wt.% (d), at a heating rate of 10 °C min^{-1} under air atmosphere
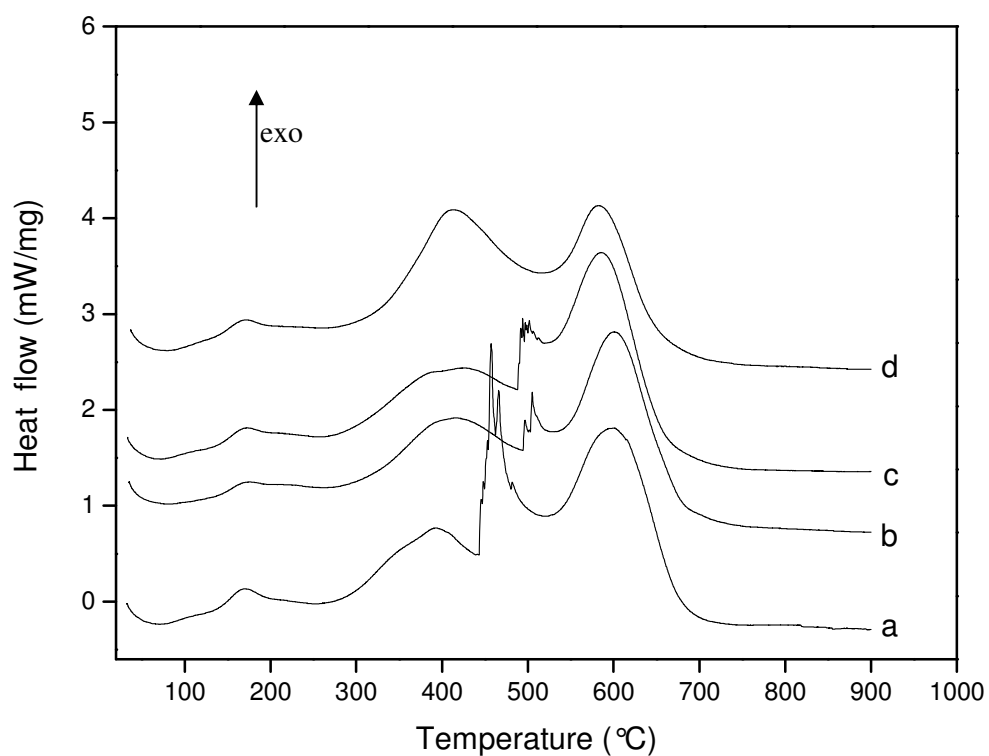
Figure 3.7: Differential scanning calorimetry (DSC) curves of pure ORMOCER (a) and ORMOCER-zeolite Beta nanocomposites with different zeolite loadings, 20 wt.% (b), 30 wt.% (c) and 40 wt.% (d), at a heating rate of 10 °C min^{-1} under air atmosphere .
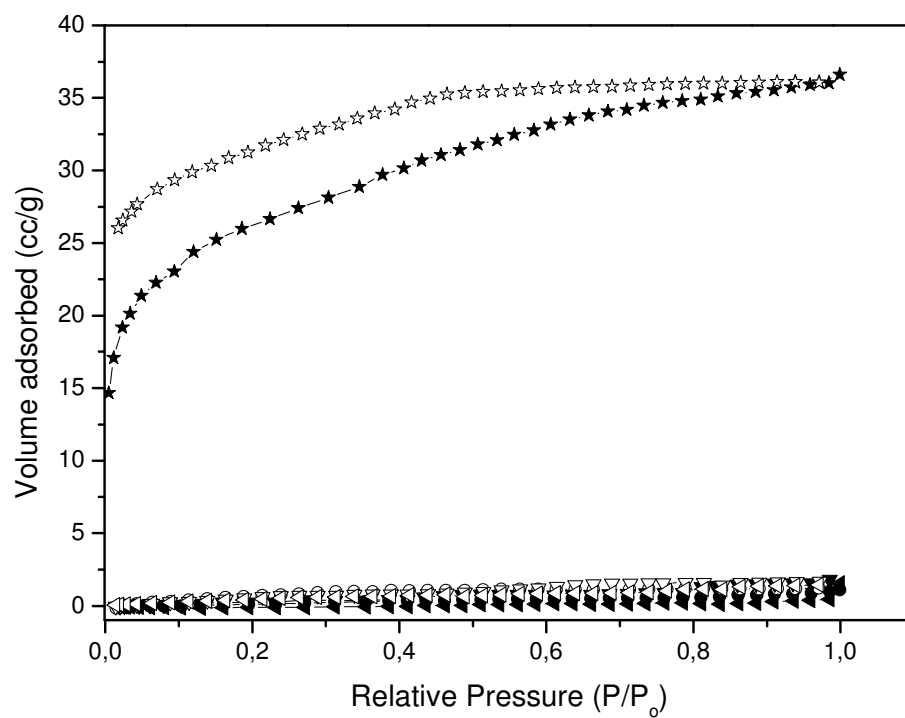
Figure 3.8: N_2 adsorption-desorption isotherms of pure ORMOCER ($\bullet$) and ORMOCER-zeolite Beta nanocomposites with different zeolite loadings, 20 wt.% ($\blacktriangledown$), 30 wt.% ($\blacktriangleleft$) and 40 wt.% ($\bigstar$) (Filled symbols: adsorption; Blank symbols: desorption).

_____
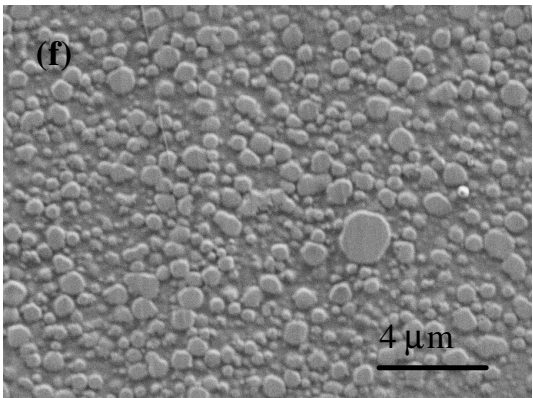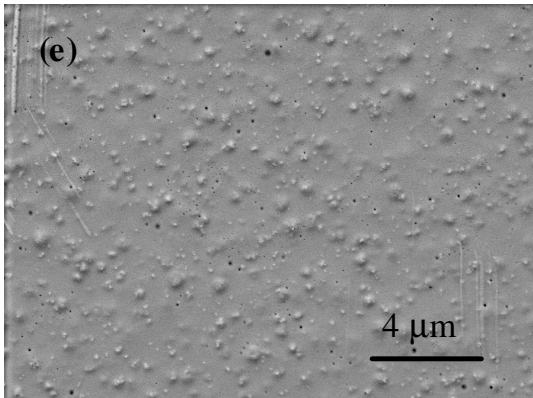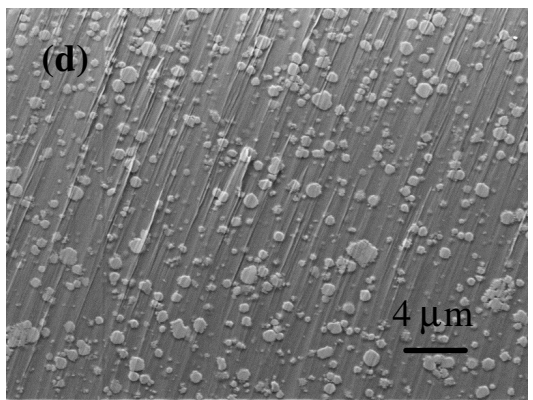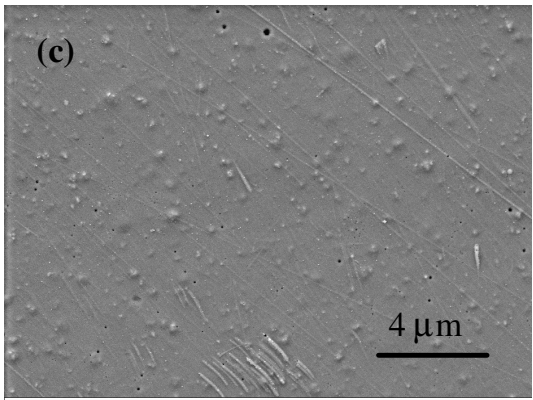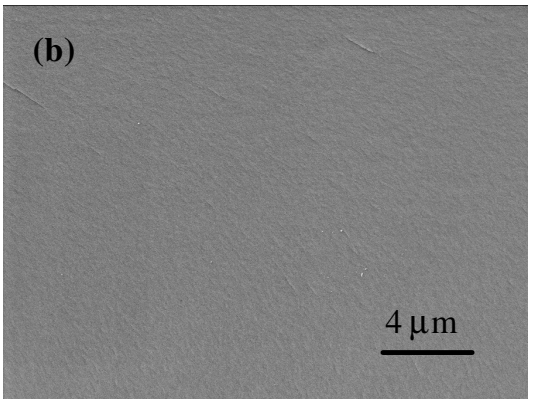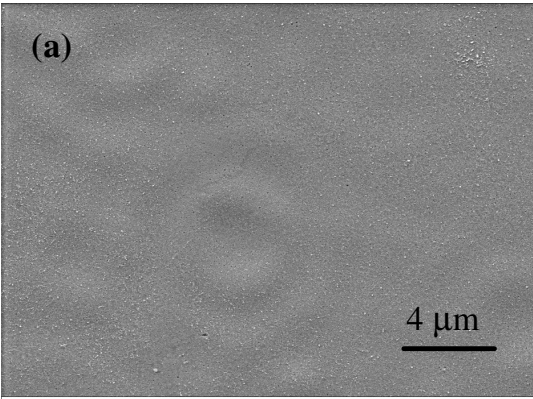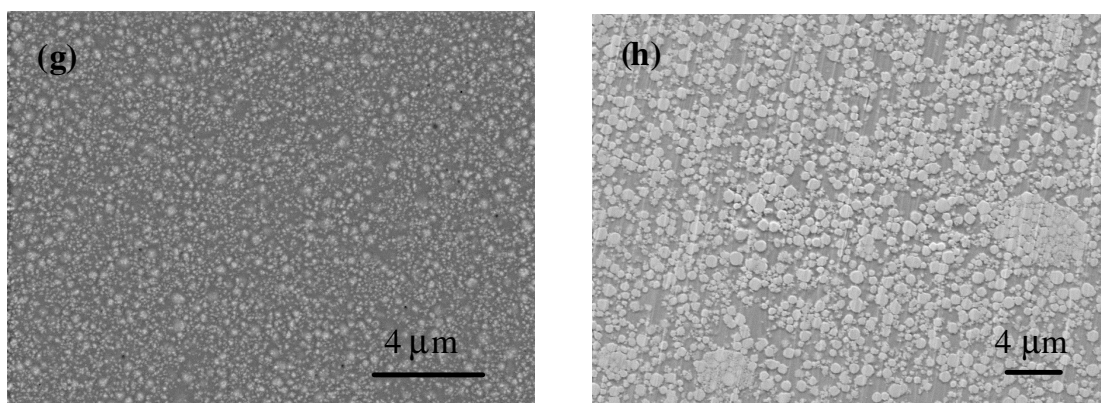
Figure 3.9: Surface and polished cross sectional views of the SEM images of the pure
ORMOCER membranes (a and b); and the ORMOCER-zeolite Beta nanocomposite membranes
with different zeolite loadings, 20 wt.% (c and d), 30 wt.% (e and f) and 40 wt.% (g and h).
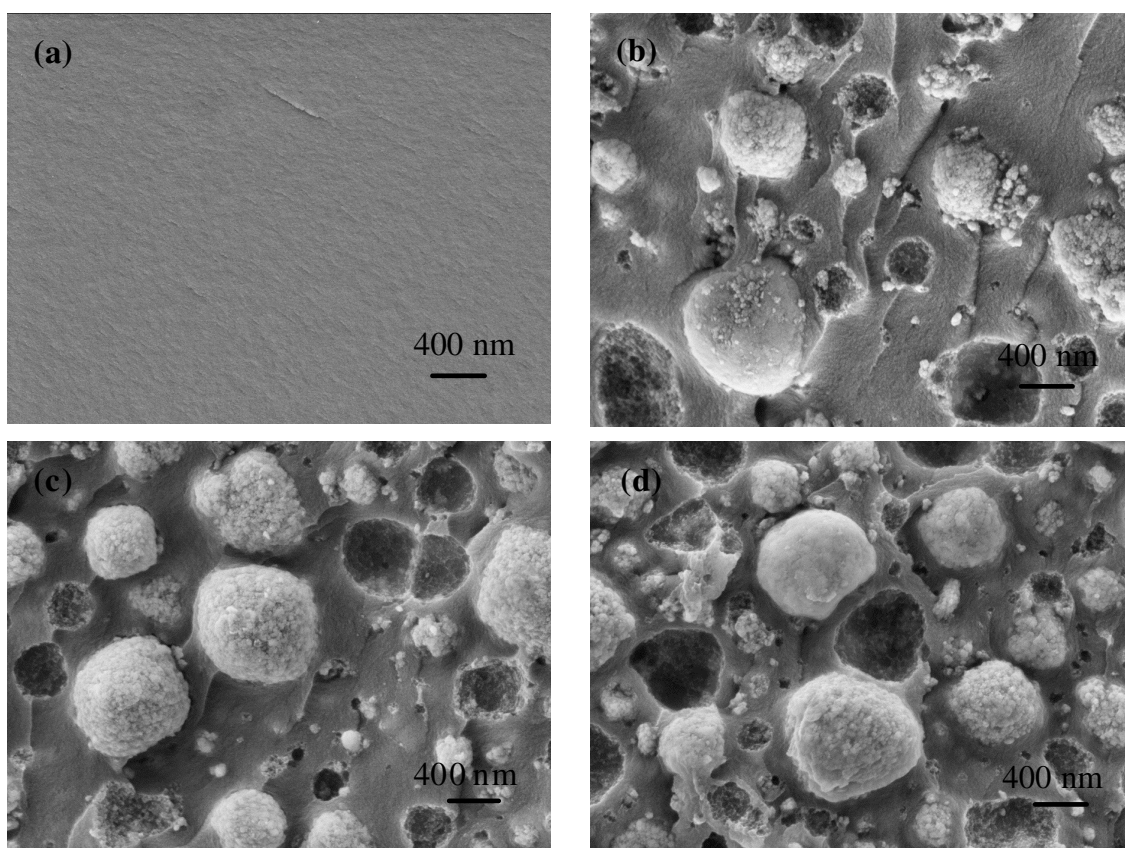
Figure 3.10: Scanning electron microscopy (SEM) images of unpolished cross-sectional views of pure ORMOCER membrane (a); and the ORMOCER-zeolite Beta nanocomposite membranes with different zeolite loadings, 20 wt.% (b), 30 wt.% (c) and 40 wt.% (d).

_____
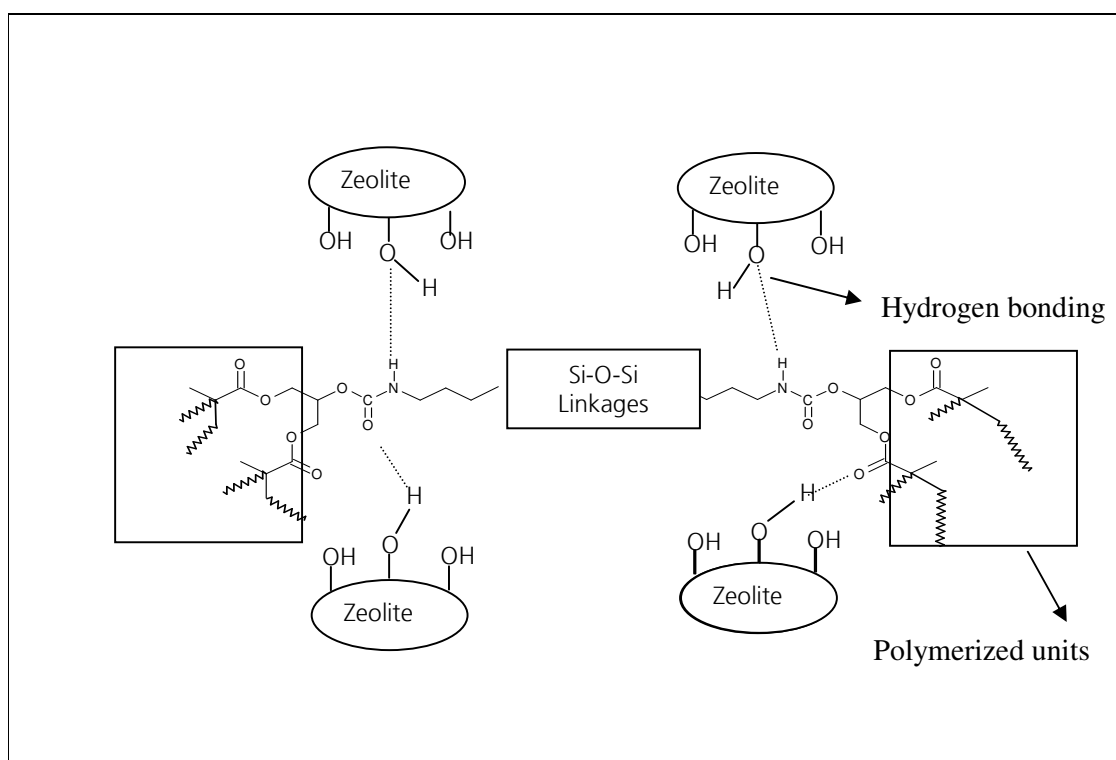
Figure 3.11: Proposed mechanism of interaction of the zeolite Beta crystallites with the ORMOCER matrix

_____

_____

References

[1]   R. Mahajan, D. Q. Vu, W. J. Koros, Mixed matrix membrane materials: an answer to the challenges faced by membrane based gas separations today?, J. Chinese Institute Chem. Eng., 33 (2002) 77-86.

[2]   A. F. Ismail, N. Ridzuan, S. A. Rahman, Latest development on the membrane formation for gas separation, Songklanakarin J. Sci. Technol., 24 (2002) 1025

[3]   T.-S. Chung, L. Y. Jiang, Y. Li, S. Kulprathipanja, Mixed matrix membranes (MMMs) comprising organic polymers with dispersed inorganic fillers for gas separation, Progr. Polym Sci., 32 (2007) 483.

[4]   S. P. Nunes, Organic-inorganic membranes for gas separation, Annales de Chimie, 32 (2007) 119.

[5]   S. Choi, J. Coronas, Z. Lai, D. Yust, F. Onorato, M. Tsapatsis, Fabrication and gas separation properties of polybenzimidazole (PBI)/nanoporous silicates hybrid membranes, J. Membr. Sci., 316 (2008) 145.

[6]   B. Liu, Y. Cao, T. Wang, Q. Yuan, Preparation of novel ZSM-5 zeolite–filled chitosan membranes for pervaporation separation of dimethyl carbonate/methanol mixtures, J. Appl. Polym. Sci., 106 (2007) 2117.

[7]   M. B. Patil, T. M. Aminabhavi, Pervaporation separation of toluene/alcohol mixtures using silicalite zeolite embedded chitosan mixed matrix membranes, Sep. Purificat. Technol., 62 (2008) 128.

[8]   L. M. Vane, V. V. Namboodiri, T. C. Bowen, Hydrophobic zeolite–silicone rubber mixed matrix membranes for ethanol-water separation: Effect of zeolite and silicone component selection on pervaporation performance, J. Membr. Sci., 308 (2008) 230.

[9]   D.-H. Son, R. K. Sharma, Y.-G. Shul, H. Kim, Preparation of Pt/ zeolite–Nafion composite membranes for self-humidifying polymer electrolyte fuel cells, J. Power Sources, 165 (2007) 733.

[10]   T. Sancho, J. Soler, M. P. Pina, Conductivity in zeolite–polymer composite membranes for PEMFCs, J. Power Sources, 169 (2007) 92.

[11]   B. Libby, W. H. Smyrl, E. L. Cussler, Polymer-zeolite composite membranes for direct methanol fuel cells, AIChE J., 49 (2003) 991.

_____

_____

[12]   W. Yuan, H. Wu, B. Zheng, X. Zheng, Z. Jiang, X. Hao, B. Wang, Sorbitol-plasticized chitosan/zeolite hybrid membrane for direct methanol fuel cell, J. Power Sources, 172 (2007) 604.

[13]   T. T. Moore, W. J. Koros, Non-ideal effects in organic–inorganic materials for gas separation membranes, J. Mol. Struct., 739 (2005) 87.

[14]   Y. Li, H-M. Guan, T-S. Chung, S. Kulprathipanja, Effects of novel silane modification of zeolite surface on polymer chain rigidification and partial pore blockage in polyethersulfone (PES)–zeolite A mixed matrix membranes, J. Membr. Sci., 275 (2006) 17.

[15]   H. Sun, L. Lu, X. Chen, Z. Jiang, Surface-modified zeolite filled chitosan membranes for pervaporation dehydration of ethanol, Appl. Surf. Sci., 254 (2008) 5367.

[16]   R. Mahajan, W. J. Koros, Mixed matrix membrane materials with glassy polymers. Part 2., Polym. Eng. Sci., 42 (2002) 1432.

[17]   A. M. W. Hillock, S. J. Miller, W. J. Koros, Crosslinked mixed matrix membranes for the purification of natural gas: Effects of sieve surface modification, J. Membr. Sci., 314 (2008) 193.

[18]   H. H. Yong, H. C. Park, Y. S. Kang, J. Won, W. N. Kim, Zeolite-filled polyimide membrane containing 2,4,6-triaminopyrimidine, J. Membr. Sci., 188 (2001) 151.

[19]   Q-L, Liu, J. Xiao, Silicalite-filled poly(siloxane imide) membranes for removal of VOCs from water by pervaporation, J. Membr. Sci., 230 (2004) 121.

[20]   S. Maheshwari, E. Jordan, S. Kumar, F. S. Bates, R. L. Penn, D. F. Shantz, M. Tsapatsis, Layer Structure Preservation during Swelling, Pillaring, and Exfoliation of a Zeolite Precursor, J. Am. Chem. Soc., 130 (2008) 1507.

[21]   S. Choi, J. Coronas, E. Jordan, W. Oh, S. Nair, F. Onorato, D. F. Shantz, M. Tsapatsis, Layered silicates by swelling of AMH-3 and nanocomposite membranes, Angew. Chem. Int. Ed., 47 (2008) 552.

[22]   S. Choi, J. Coronas, Z. Lai, D. Yust, F. Onorato, M. Tsapatsis, Fabrication and gas separation properties of polybenzimidazole (PBI)/nanoporous silicates hybrid membranes, J. Membr. Sci., 316 (1+2) (2008) 145.

_____

_____

[23]   C. V. Funk, D. R. Lloyd, Zeolite-filled microporous mixed matrix (ZeoTIPS) membranes: Prediction of gas separation performance, J. Membr. Sci., 313 (2008) 224.

[24]   Y. Li, T-S. Chung, Z. Huang, S. Kulprathipanja, Dual-layer polyethersulfone (PES)/BTDA-TDI/MDI co-polyimide (P84) hollow fiber membranes with a submicron PES-zeolite beta mixed matrix dense-selective layer for gas separation, J. Membr. Sci., 277 (2006) 28.

[25]   L. Y. Jiang, T. S. Chung, S. Kulprathipanja, An investigation to revitalize the separation performance of hollow fibers with a thin mixed matrix composite skin for gas separation, J. Membr. Sci., 276 (2006) 113.

[26]   S. Husain, W. J. Koros, Mixed matrix hollow fiber membranes made with modified H-SSZ-13 zeolite in polyetherimide polymer matrix for gas separation, J. Membr. Sci., 288 (2007) 195.

[27]   K-H. Haas, K. Rose, Hybrid inorganic/organic polymers with nanoscale building blocks: precursors, processing, properties and applications, Rev. Adv. Mater. Sci., 5 (2003) 47.

[28]   G. Schottner, Hybrid Sol-Gel-Derived Polymers: Applications of Multifunctional Materials, Chem. Mater., 13 (2001) 3422.

[29]   K-H. Haas, Hybrid inorganic-organic polymers based on organically modified Si-alkoxides, Adv. Eng. Mater., 2 (2000) 571.

[30]   S. Jacob, S. Cochet, C. Poinsignon, M. Popall, Proton conducting inorganic-organic matrices based on sulfonyl- and styrene derivatives functionalized polycondensates via sol-gel processing, Electrochim. Acta, 48 (2003) 2181.

[31]   S. Jacob, C. Poinsignon, M. Popall, Inorganic-organic hybrid protonic polymeric materials for fuel cells based on polycondensed and organically cross-linked sulfonyl- and styrene-functionalized alkoxysilanes, Electrochim. Acta, 50 (2005) 4022.

[32]   K-H. Haas, S. Amberg-Schwab, T. Ballweg, Synthesis and properties of hybrid inorganic-organic polymers based on organically modified Si-alkoxides and their use for permeation control, Advances in Science and Technology (Faenza, Italy) 31(10th International Ceramics Congress, 2002, Part B (2003) 581.

[33]   H. Wolter, T. Ballweg, W. Storch, Membrane for oxygenator, Eur. Patent, (2000) EP 0985442.

_____

_____

[34]   T. Ballweg, H. Wolter, W. Storch, Ormocer - and derived microporous inorganic hollow fibers, Keramische Zeitschrift, 53 (2001) 678.

[35]   T. Ballweg, H. Wolter, Hollow fibers from hybrid polymers, Gummi, Fasern, Kunststoffe, 53 (2000) 277.

[36]   R. W. Thompson, B. E. Libby, M. B. Berry, K. Rose, K.-H. Haas, Incorporation of zeolites into hybrid polymer matrices, US Patent, (2001) US 6, 248, 682.

[37]   M. B. Berry, B. E. Libby, K. Rose, K.-H. Haas, R. W. Thompson, Incorporation of zeolites into composite matrices, Micropor. Mesopor. Mater., 39 (2000) 205.

[38]   H. Wolter, and W. Storch, Urethane (meth)acrylate alkoxysilane, a new type of reactive polymers for the preparation of inorganic-orgnaic copolymers (ORMOCER®s), Polymer & Materials Research Symposium, Bayreuth, (1993), 14.

[39]   Z. Huang, J-F. Su, X-Q. Su, Y-H. Guo, L-J. Teng, C. M. Yang, Preparation and permeation characterization of β-zeolite-incorporated composite membranes, J. Appl. Polym. Sci., 112 (2009) 9.

[40]   H. Wolter, and W. Storch, C. Gellermann, Novel carboxy funtionalized sol-gel precurors, Mat. Res. Soc. Symp. Proc 435, (1996) 67.

[41]   L. Armelao, C. Eisenmenger-Sittner, M. Groenewolt, S. Gross, C. Sada, U. Schubert, E. Tondello, A. Zattin, Zirconium and hafnium oxoclusters as molecular building blocks for highly dispersed ZrO_2 or HfO_2 nanoparticles in silica thin films, J. Mater. Chem., 15 (2005) 1838.

[42]   R. Houbertz, G. Domann, J. Schulz, B. Olsowski, L. Fröhlich, Impact of photoinitiators on the photopolymerization and the optical properties of inorganic–organic hybrid polymers, Appl. Phys. Lett., 84 (2004) 1105.

[43]   Y. Kaneka, N. Iyi, T. Mastsumoto, K. Fujii, K. Kurashima, T. Fujita, Synthesis of ion-exchangeable layered polysiloxane by sol-gel method reaction of aminoalkytri-alkoxysilane: a new preparation method for layered polysiloxane materials, J. Mater. Chem., 13 (2003) 2058.

[44]   N. Moszner, T. Völkel, S. Cramer von Clausbruch, E. Geiter, N. Batliner, V. Rheinberger, Macromol. Mater. Eng., 287 (2002) 339.

[45]   F. Brunet, Polymerization reactions in methyltriethoxysilane studied through ^{29}Si NMR with polarization transfer, J. Non-Crystal. Solids, 231 (1998) 58.

_____

_____

[46]   C. K. Chan, I. M. Chu, W. Lee, W.-K. Chin, Preparation and Properties of Organic-Inorganic Hybrid Materials Based on Poly{(butyl methacrylate)-*co*- [(3-methacryloxy-propyl)trimethoxysilane]}, Macromol. Chem. Phys. 202 (2001) 911.

[47]   C. Ma, Y. Du, F. Wang, Thermal degradation behaviors of poly(dimethylsiloxane)-urethane-graft-poly(methylmethacrylate) copolymers based on various diisocyanates. J. Mater. Sci., 37 (2002) 1247.

[48]   J. Zhang, A. Li, A. Wang, Synthesis and characterization of multifunctional poly(acrylicacid-co-acrylamide)/sodium humate superabsorbent composite, React. Funct. Polym., 66 (2006) 747.

[49]   H. G. Schild, Thermal degradation of poly(methacrylic acid): Further studies applying TGA/FTIR, J. Polym. Sci. Part A: Polym. Chem., 31 (1993) 2403.

_____

_____

Chapter 4

Fabrication of ORMOCER®-zeolite Beta mixed matrix membranes using dimethyldiethoxysilane (DMDES) as a siloxane modifier of networks

4.1 Abstract

Permeable, silicone-modified ORMOCER®-zeolite Beta (10-40 wt.%) mixed matrix membranes (MMMs) were fabricated, using a glycerine-1,3-dimethacrylate-urethanetriethoxysilane (GUS)-ORMOCER® resin and dimethyldiethoxysilane (DMDES) as a siloxane modifier of ORMOCER® networks, by solution casting followed by UV-curing. All the MMMs were characterized by SEM and single gas (O_2, N_2 and CO_2) permeation measurements. SEM images revealed that the zeolite Beta crystallites were uniformly distributed within the ORMOCER® matrix, and the MMMs were virtually free of interfacial voids, as indicated by high resolution SEM images. Among the MMMs studied, ORMOCER®-zeolite Beta (30 wt.%) MMM exhibited an increase in permeability of about 8, 7 and 12 times for O_2, N_2 and CO_2, respectively, and high permselectivities ($O_2/N_2 = 4.8$ and $CO_2/N_2 = 29.8$) compared to the polyimide-zeolite Beta (30 wt.%) composite membrane reported in the literature. In addition, ORMOCER®-zeolite A (3Å, 4Å and 5Å; 30 wt.%) MMMs were prepared and their permeation properties tested under similar conditions for comparison purposes.

4.2 Introduction

Mixed Matrix Membranes (MMMs) have recently emerged as an attractive technology for a variety of liquid and gas separation applications [1-4]. Such MMMs combine the advantages of both polymeric (low capital investment and easy processing capabilities) and inorganic (excellent diffusivity and molecular sieving capabilities)

_____

membranes. MMMs are generally composed of continuous polymeric and discrete organic or inorganic matrices as fillers. The incorporation of inorganic matrices into polymeric matrices has a remarkable effect on the resulting MMMs. Significant improvement, for instance in separation efficiency, high flux and durability, has been achieved for the MMMs in comparison to their pristine counterparts. Several reports have recently appeared on the fabrication of MMMs using various types of porous inorganic matrices, such as nanoporous fumed silica [5], layered silicates [6], zeolites (A, L, KFI, H-ZK-5, MFI and SSZ-13) [7-10], aluminophosphates (AlPO-5 and AlPO-14) [11, 12], silicoaluminophosphates (SAPO-5 and SAPO-34) [13, 14], and mesoporous silica (MCM-41 and MCM-48) [15, 16], zirconium phosphate [17] and titanium phosphate [17] materials. Very recently, Metal-Organic-Frameworks (MOFs) have also been used as fillers for the development of high performance MMMs [18, 19].

Among the zeolite-based MMMs, zeolite Beta (BEA)-containing MMM is of considerable interest due to its applicability in pervaporation [20], direct methanol fuel cells (DMFC) [21], proton exchange membrane fuel cells (PEMFC) [22] and gas (He/N_2, O_2/N_2 and CO_2/CH_4) separation [23-28]. Recently, Huang et al. [29] synthesized a series of thin film poly(ether sulfone) (PES)- and polyimide (PI)-based MMMs having different zeolite Beta loadings (10-30 wt.%) by solution-casting. A finding of special interest was that the zeolite Beta-PES membranes exhibited a significant increase in gas permeability as well as in permselectivity.

ORMOCER®s-based membranes [30-35] have received significant attention due to their excellent mechanical, thermal, chemical and gas permeation characteristics. In particular, the incorporation of zeolites, such as KNaA (LTA) and NaX (FAU), into ORMOCER® matrices resulted in a significant increase in the N_2 sorption capacity [36, 37]. Recently, we have reported the fabrication of void-free and free-standing GUS-based ORMOCER®-zeolite Beta (BEA) nanocomposite membranes with 10-40 wt.% of zeolite Beta loadings [38]. These nanocomposite membranes showed permeability especially for small gas molecules (kinetic diameter < 0.289 nm), such as He and H_2, but were nearly impermeable for N_2 (0.364 nm). The relative impermeability of these membranes for N_2 is mainly due to the highly condensed and/or cross-linked nature of the GUS-based ORMOCER® matrix. It should be possible to overcome this limitation and improve the membrane permeation performance especially for large gas molecules

(kinetic diameter > 0.289 nm), such as e.g. N_2, O_2, and CO_2, by systematically tailoring the GUS-based ORMOCER$^®$ siloxane network.

Organosilanes and siloxanes, such as dimethyldimethoxysilane (DMDMS), dimethyldiethoxysilane (DMDES), oligomeric dimethylsiloxane (ODMS) and polydimethylsiloxane (PDMS) have been used as polymer network modifiers in the preparation of various hybrid membranes [39-42]. It was demonstrated that the incorporation of DMDMS and DMDES in the polyurethane (PU)-based films enables a significant increase in O_2 permeability due to the creation of flexible siloxane linkages (free volume) [39]. In addition, Zhang et al. [40] studied the effect of varying concentrations of DMDES to triethoxyfluorosilane (TEFS)-film.

It was found that the incorporation of DMDES favours the formation of four-membered cyclic structures within TEFS and thereby increases the porosity. Park et al [41, 42] attempted to improve the gas (N_2, O_2 and CO_2) permeabilities of poly(amideimide)siloxane and polyimide/silica membranes by adding ODMS and PDMS, respectively.

In the present work, we have fabricated silicone-modified ORMOCER$^®$ (denoted as S-ORMOCER$^®$)-zeolite Beta (10-40 wt.%) MMMs using GUS-ORMOCER$^®$ resin and DMDES as a siloxane modifier of ORMOCER$^®$ networks. Further, we have studied their gas permeation performances especially for large gas molecules (O_2, N_2 and CO_2) and compared with S-ORMOCER$^®$-zeolite A (3Å, 4Å and 5Å; 30 wt.%) MMMs.

4.3 Experimental

4.3.1 Materials

3-isocyanatopropyltriethoxysilane (IPTES, 99%) and glycerine-1,3-dimethacrylate (GDMA, 98%) were obtained from Momentive Performance Materials. Dibutyl tin dilaurate (DBTL, 95%), dimethydiethoxysilane (DMDES) and ethyl acetate

---

$^®$ Registered trademark of Fraunhofer Gesellschaft zur Förderung der angewandten Forschung e.V., Germany

(97%) were purchased from Sigma-Aldrich. Irgacure 184 (1-hydroxy-cyclohexyl-phenyl-ketone) was obtained from CIBA Specialty Chemicals. All chemicals were used as obtained without further purification. High-silica zeolite Beta ($SiO_2/Al_2O_3 = 350$) and LTA-type zeolites (3A, 4A and 5A) were purchased from Zeolyst International and Zeochem AG, respectively. Before using, all the zeolite samples were activated at 250 °C for 4 h and stored under dry conditions.

4.3.2 Preparation of dimethyldiethoxysilane (DMDES)-modified GUS-ORMOCER® and corresponding MMMs

At first, a series of DMDES-modified GUS-ORMOCER® resins was prepared according to a known method [43] by keeping the glycerine-1,3-dimethacrylate-urethanetriethoxysilane (GUS) concentration constant (1 M) and varying the concentration of DMDES (0.0, 3.0 and 6.0 M). The proposed scheme for the formation of DMDES-modified GUS-ORMOCER resins is shown in Fig. 4.1. The GUS-ORMOCER® resins modified with DMDES (0, 3 and 6 M) are hereafter referred to as GUS-ORMOCER®, GUS-**3**DMDES-ORMOCER® and GUS-**6**DMDES-ORMOCER® resins, respectively. Their corresponding membranes were prepared by the solution casting method followed by UV-curing as described previously [38], and their single-gas permeability was tested for O_2, N_2 and CO_2. It was found from the permeability data that the GUS-**6**DMDES-ORMOCER® membrane showed a higher permeability. Therefore, the GUS-**6**DMDES-ORMOCER® resin was used for further study.

MMMs composed of zeolite Beta (10-40 wt.%) and LTA-type zeolites (3A, 4A and 5A; 30 wt.%) were prepared using GUS-**6**DMDES-ORMOCER® resin under similar conditions [38]. All the membranes were annealed at 120 °C (heating rate 5 °C/min) under vacuum, dwelled (at 120 °C) for 24 h, cooled to room temperature and stored under moisture free conditions. The resulting dried MMMs had an approximate thickness of about 190 to 210 µm.

4.3.3 Characterization

An FT-IR spectrometer, Nicolet Magna-IR 760, was used to identify the functional groups present in the GUS-ORMOCER® and DMDES-modified GUS-ORMOCER® resins. The FT-IR spectra were recorded in the range of 400 to 4000 cm^{-1}

_____

using solution cast thin films of those resins on KBr pellets. The spectra were scanned for 32 s with a resolution of 4 cm^{-1}. Liquid-state ^{29}Si-NMR measurements of GUS-ORMOCER$^{®}$ and DMDES-modified GUS-ORMOCER$^{®}$ resins were carried out on a Bruker Avance DPX 400 NMR spectrometer at a resonance frequency of 79.49 MHz (^{29}Si) in an external magnetic field of 9.4 Tesla. Measurements were carried out using CDCl$_3$ as solvent and tetramethylsilane (TMS) as the internal standard. The morphology of the MMMs was examined using a Zeiss-supra model 25 variable pressure field emission scanning electron microscope at an acceleration voltage of 10 kV.

4.3.4 Permeation measurements

Single gas (O$_2$, N$_2$, and CO$_2$) permeabilities were measured at room temperature using a home-made constant volume-variable pressure gas permeation setup shown in Fig. 4.2. It relies on maintaining a constant pressure of a gas permeant on the upstream face of the membrane and measuring the flux across the membrane of known thickness and area on the downstream (or permeate) face of the membrane. The membrane was fixed in a stainless-steel permeation cell and was sealed by flat O-rings (Viton). The effective permeation area of each membrane was about 0.65 mm. The purity of the gases (O$_2$, N$_2$ and CO$_2$; Linde AG) used in the present study was 99.999%. Prior to each measurement, the entire system was vacuum-degassed overnight (pressure: 1 x 10^{-8} mbar) using a turbo molecular vacuum pump. The vacuum connection was then closed and respective gases were dosed using mass flow controllers and argon was used as a sweep gas in the permeate side. The gas pressure in the feed side was varied from 0.3 to 1.3 bar. The pressures at both sides (feed and permeate) could be monitored by pressure transducers (MKS Instruments Deutschland GmbH) which were linked to a computer. The PC program was set in such a way as to collect permeation data after 3 min at each pressure. The gas permeation measurement of each single gas was repeated four times and the average permeability results are reported in Barrer [1 Barrer = 10^{-10} cm^3 cm / cm^2 s cm Hg]. The permeability coefficient (P) of a given gas in a membrane was calculated by using the equation (4.1)

$$P = \frac{273.15}{T} \quad \frac{V\,L}{A\,P_0} \quad \left[\frac{dp}{dt} \right] \qquad \text{eq. (4.1)}$$

_____

_____

V is the volume of the downstream chamber (cm^3), (dp/dt) is the rate of the pressure increase in the down stream chamber (cm Hg/s), A is the effective area of the membrane (cm^2), L is the thickness of the membrane (cm), P$_0$ is the pressure in the upstream chamber and T is the absolute temperature of the gas (K), respectively. The permselectivity of the membrane was calculated using the equation (2).

$$\alpha = \frac{P_A}{P_B} \qquad\qquad \text{eq. (4.2)}$$

where P$_A$ and P$_B$ are the permeability of membrane to a gas A and gas B.

4.4   Results and discussion

The FT-IR spectra of GUS-ORMOCER®, GUS-**3**DMDES-ORMOCER® and GUS-**6**DMDES-ORMOCER® resins are shown in Fig. 4.3. The FT-IR spectrum of GUS-ORMOCER® (curve a) shows the presence of stretching vibrations of N-H (3367 cm^{-1}), C-H of methyl (2932 cm^{-1}), carbonyl (1723 cm^{-1}), vinyl of methacrylates (1638 cm^{-1}) and bending vibrations of the N-H (1530 cm^{-1}) groups [38]. The other spectral features in the region 1200-1000 cm^{-1} arise primarily from the Si-O-Si asymmetric vibrations. In addition, the absorption band at 942 cm^{-1} is attributed to the presence of Si-OH groups due to incomplete condensation. The FTIR spectra of both GUS-**3**DMDES-ORMOCER® (curve b) and GUS-**6**DMDES-ORMOCER® (curve c) resins show similar features to that of GUS-ORMOCER® but with two significant bands at around 1262 cm^{-1} and 812 cm^{-1}. These two bands are assigned to symmetric bending and rocking vibrations of C-H groups in Si-CH$_3$ [39]. Furthermore, the increase in intensity of the absorption band at 2932 cm^{-1} (C-H stretching of the methyl groups) provides additional evidence for the successful incorporation of DMDES into the ORMOCER® networks. The above mentioned results agree well with the FTIR spectra reported for DMDES-modified poylurethane ionomer [39]. The broadening of bands (1200-1000 cm^{-1}) in the FTIR spectra of GUS-**3**DMDES-ORMOCER® (curve b) and GUS-**6**DMDES-ORMOCER® (curve c) may arise from the presence of cyclic/linear polysiloxanes and included a decreased number of hydrogen bonds between N-H group and silanols or carbonyl group in urethane moieties, respectively. These results are in accordance with the proposed scheme for the formation of DMDES-modified GUS-ORMOCER® resins, as illustrated in Fig. 4.1.

_____

Liquid-state ^{29}Si NMR spectroscopy was used to assess the nature of hydrolyzed/condensed Si species present in GUS-ORMOCER®, GUS-**3**DMDES-ORMOCER® and GUS-**6**DMDES-ORMOCER® resins; and their corresponding ^{29}Si NMR spectra are presented in Fig. 4.4. The ^{29}Si NMR spectrum of the GUS-ORMOCER® resin exhibits signals in the −66 to −70 ppm (curve a) range, corresponding to T^3 Si species [RSi(OSi)$_3$] [38]. No signals corresponding to the T^1 [RSi(OSi)(OH)$_2$] and T^2 [RSi(OSi$_2$)(OH)] Si species were observed in the region of −45 to −60 ppm. The absence of T^1 and T^2 signals clearly indicates that the GUS-ORMOCER® resin possesses a highly condensed inorganic network. On the other hand, in addition to the very weak T^3 signals, the ^{29}Si NMR spectra of both GUS-**3**DMDES-ORMOCER® (curve b) and GUS-**6**DMDES-ORMOCER® (curve c) resins exhibit sharp signals in the range of −18.3 to −22.2 ppm and low intensity signals at around −10 to −14 ppm. These signals are attributed to D_1 and D_2 species [44], indicating the formation of polydimethylsiloxane networks [D_x, (CH$_3$)$_2$Si(OSi)$_x$(OH)$_{2-x}$] within the DMDES-modified GUS-ORMOCER®s (curves b and c). The absence of D_0 signals around −4 ppm (in curves b and c) further suggests the complete polymerization of DMDES under the conditions employed in the present study.

In order to assess the influence of DMDES on GUS-ORMOCER®s, single gas (O$_2$, N$_2$ and CO$_2$) permeation measurements were carried out on GUS-ORMOCER®, GUS-**3**DMDES-ORMOCER® and GUS-**6**DMDES-ORMOCER® membranes, and their results are summarized in Table. 4.1. It can be seen from Table 4.1 that the GUS-ORMOCER® membrane was nearly impermeable for all the gases (O$_2$, N$_2$ and CO$_2$) owing to its highly condensed and/or cross-linked nature. As expected, the GUS-**3**DMDES-ORMOCER® membrane showed measurable permeabilities for O$_2$ (8.7 Barrer), N$_2$ (1.5 Barrer) and CO$_2$ (39.9 Barrer) with reasonable O$_2$/N$_2$ (5.8) and CO$_2$/N$_2$ (26.6) permselectivities. Indeed, the GUS-**6**DMDES-ORMOCER® membrane showed substantial improvement in O$_2$ (34.3 Barrer), N$_2$ (13.7 Barrer) and CO$_2$ (219.0 Barrer) permeabilities with low O$_2$/N$_2$ (2.5) and CO$_2$/N$_2$ (15.9) permselectivities. The above mentioned results reveal the presence of intrinsic free volume within the DMDES-modified GUS-ORMOCER® membranes. Essentially the same behavior resulted with the bis(γ-aminopropyl)-polydimethylsiloxane-modified polyimide (PI) membranes [45]. Note that further increase in the amount of DMDES (9.0 M) in GUS-ORMOCER® led to mechanically unstable membranes (GUS-**9**DMDES-ORMOCER®). Therefore, the GUS-**6**DMDES-ORMOCER® resin was chosen as the standard resin for the fabrication

_____

of zeolite-based MMMs with improved permeation and permselectivity characteristics. For reasons of simplicity, the GUS-**6**DMDES-ORMOCER® resin will hereafter be referred to as silicone-modified ORMOCER® (S-ORMOCER®) resin. MMMs composed of zeolite Beta (10-40 wt.%) and LTA-type zeolites (3Å, 4Å and 5Å; 30 wt.%) were prepared under similar conditions using S-ORMOCER® resin, and their SEM and permeation results are discussed in the subsequent paragraphs.

Fig. 4.5 shows the unpolished cross-sectional SEM images of the pure S-ORMOCER® membrane (a and b) and its corresponding MMMs containing 10 wt.% (c and d), 20 wt.% (e and f), 30 wt.% (g and h), and 40 wt.% (i and j) zeolite Beta loadings at different magnifications. As seen in Fig. 4.5a and b, the S-ORMOCER® membrane exhibits the fairly smooth surface characteristic of polymeric membranes, whereas, the S-ORMOCER®-zeolite Beta (10-40 wt.%) MMMs (Fig. 4.5c to j) show internal surface roughness with bumps and pits. It is observed in Fig. 4.5d, f, h and j that the internal surface roughness becomes more and more pronounced as the zeolite Beta content increases from 10 to 40 wt.%. It can be seen that the zeolite Beta crystallites are homogeneously distributed within the S-ORMOCER® matrix. The mean diameter of the zeolite Beta crystallites is in the range of 200 to 800 nm, and no agglomeration was observed under the incorporation conditions used even at a high amount of zeolite Beta loading (40 wt.%). High magnification SEM images (Fig. 4.5d, f, h and j) did not reveal the presence of voids between the zeolite Beta crystallites and the S-ORMOCER® matrix. It is well known that the performance of MMMs generally depends on how the zeolite crystallites are distributed and adhered to the matrix. Note that, as reported for our previous study [38], no primer or silane-coupling agent was used for the fabrication of S-ORMOCER®-zeolite Beta MMMs.

Unpolished cross-sectional SEM images of S-ORMOCER®-zeolite A (3Å, 4Å and 5Å) MMMs containing 30 wt.% zeolite loadings were done at different magnifications and are displayed in Fig. 4.6. As can be seen from Fig. 4.6 (a, c, and e), the zeolite A crystallites (~ 3-4 µm) are not as uniformly distributed as zeolite Beta crystallites (Fig. 4.5c to j) within the S-ORMOCER® matrix. In addition, high magnification SEM images (Fig. 4.6b, d and f) reveal the presence of voids in some regions between the zeolite A crystallites and the S-ORMOCER® matrix. This could be due either to the incompatibility between the hydrophilic zeolite A ($SiO_2/Al_2O_3 = 2$) and the hydrophobic S-ORMOCER® matrix resulting in a bad wetting or to the large size (~

_____

_____

3-4 μm) and irregular morphology of the zeolite A crystallites employed in the present study. However, at the moment one cannot exclude that the formation of such voids could also be due to stress formation within the curing steps, i.e. induced shrinkage of the S-ORMOCER® matrix. Nevertheless, these voids can be eliminated by chemical modification of the surface of zeolite A crystals using silanes. Li et al [7] demonstrated that the surface modification of zeolite A crystals using (3-aminopropyl)-diethoxymethyl silane (APDEMS) provides void-free polyethersulfone (PES)-zeolite A MMMs with significant improvement in permeability and permselectivity. It must be emphasized that the zeolite Beta crystallites employed in the present study are relatively hydrophobic (SiO_2/Al_2O_3 = 350), smaller in size (200-800 nm) and possess favorable spherical morphology – hence the formation of void-free S-ORMOCER®-zeolite Beta MMMs (Fig. 4.5c to j).

The effect of zeolite Beta (10-40 wt.%) loading and zeolitic (LTA-types; 3Å, 4Å and 5Å; 30 wt.%) structures on single gas permeation properties of S-ORMOCER®-based MMMs was systematically investigated at 25 °C, and the results are summarized in Table 4.2. It shows that the O_2, N_2 and CO_2 permeabilities of S-ORMOCER®-zeolite Beta MMMs decreased as the loading of zeolite Beta increased (from 10-30 wt.%). Interestingly, the O_2, N_2 and CO_2 permeabilities of the S-ORMOCER®-zeolite Beta (30 wt.%) MMM are about 8-, 7- and 12-times higher, respectively, than that of the polyimide-zeolite Beta (30 wt.%) composite membrane prepared by Huang et al [29]. Moreover, the O_2/N_2 and CO_2/N_2 permselectivities of S-ORMOCER®-zeolite Beta (10-30 wt.%) MMMs are relatively higher than that of the S-ORMOCER® membrane. Notably,

S-ORMOCER®-zeolite Beta (30 wt.%) exhibits two-times higher permselectivities (O_2/N_2 = 4.8 and CO_2/N_2 = 29.8) than the S-ORMOCER® membrane (O_2/N_2 = 2.5 and CO_2/N_2 = 15.9). Such an enhancement of permselectivity could be either due to the intrinsic molecular sieving effect of zeolite Beta or to the polymer chain rigidification followed by pore blockage within the S-ORMOCER®-zeolite Beta MMMs. Table 4.2 also shows that the O_2, N_2 and CO_2 permeabilities of the S-ORMOCER®-zeolite Beta (40 wt.%) MMM are significantly higher than for the S-ORMOCER® membrane, albeit with lower O_2/N_2 (3.6) and CO_2/N_2 (17.7) permselectivities. This is most probably due to the fact that the percolation threshold is reached for the S-ORMOCER®-zeolite Beta (40 wt.%) MMM.

_____

It is well known that the pore size of the zeolites greatly influences the gas permeabilities and permselectivities of MMMs. Although the SEM studies indicated the presence of voids (100-200 nm) in some regions between the zeolite A (3Å, 4Å and 5Å) crystallites and the S-ORMOCER® matrix (Fig. 4.6b, d and f), as desired, the overall O_2 and CO_2 permeabilities of LTA-types of S-ORMOCER® (3Å, 4Å and 5Å; 30 wt.%) membranes are significantly lower than in the S-ORMOCER® and S-ORMOCER®-zeolite Beta (10-40 wt.%) MMMs (Table 4.2). Most importantly, the O_2/N_2 and CO_2/N_2 permselectivities of S-ORMOCER®-zeolite A (3Å, 4Å and 5Å; 30 wt.%) MMMs are nearly comparable to those of the S-ORMOCER® membrane. These results suggest that the voids (100-200 nm) present between the zeolite A crystallites and the S-ORMOCER® matrix play a negligible role in gas permeation in comparison to the intrinsic molecular sieving effect of S-ORMOCER®-zeolite A (3A, 4A and 5A; 30 wt.%) MMMs. As expected, LTA-types of S-ORMOCER® (3Å, 4Å and 5Å; 30 wt.%) MMMs exhibit an increase in O_2, N_2 and CO_2 permeabilities as the pore size of zeolite A increased (from 3Å to 5Å). As shown in Table 4.2, N_2 permeabilities of LTA-types of S-ORMOCER® (3A, 4A and 5A; 30 wt.%) MMMs are slightly higher than in the S-ORMOCER®-zeolite Beta (30 wt.%) MMM. This could be due to the fact that both O_2 and CO_2 have stronger affinity to the cations (K, Na and Ca) present in the LTA-type zeolites [46] and hence result in an increase in N_2 permeabilities. Again, the gas permeabilities (O_2 = 27.7, N_2 = 10.6 and CO_2 = 151.7 Barrer) of the S-ORMOCER®-zeolite 4A (30 wt.%) membrane are significantly higher but with lower permselectivities (O_2/N_2 = 2.6 and CO_2/N_2 = 14.3) than those of the poly(ether sulfone)-zeolite 4A (20 wt.%) composite membrane (permeabilities: O_2 = 0.58, N_2 = 0.09 and CO_2 = 2.32 Barrer; permselectivities: O_2/N_2 = 6.4 and CO_2/N_2 = 25.5) prepared by Huang et al [47].

4.5 Conclusions

Permeable, silicone-modified, S-ORMOCER®-zeolite Beta (10-40 wt.%) and S-ORMOCER®-zeolite A (3A, 4A and 5A; 30 wt.%) MMMs were fabricated, using GUS-ORMOCER® resin and DMDES as a siloxane modifier of ORMOCER® networks, by the solution casting method followed by UV-curing. Cross-sectional SEM images of S-ORMOCER®-zeolite Beta (10-40 wt.%) MMMs show that the zeolite Beta crystallites are homogeneously distributed throughout the S-ORMOCER® matrix, and the MMMs are completely free from visible voids. However, SEM images of S-ORMOCER®-

_____

zeolite A (3A, 4A and 5A; 30 wt.%) MMMs reveal the presence of voids (100-200 nm) in some regions between the zeolite A (3A, 4A and 5A) crystallites and the S-ORMOCER$^{®}$ matrix. In particular, the S-ORMOCER$^{®}$-zeolite Beta (30 wt.%) MMM exhibits high permeabilities (in Barrer) for O_2 (34.1), N_2 (7.1) and CO_2 (212.1) and high permselectivities (O_2/N_2 = 4.8 and CO_2/N_2 = 29.8), whereas, S-ORMOCER$^{®}$-zeolite A (3A, 4A and 5A; 30 wt.%) MMMs exhibit an overall decrease in O_2, N_2 and CO_2 permeabilities and O_2/N_2 and CO_2/N_2 permselectivities.

4.6   Acknowledgements

_____

_____

4.7 Tables

Table 4.1

Single gas permeation properties of the GUS-ORMOCER$^®$ and DMDES modified

GUS-ORMOCER$^®$ membranes at 25 °C.

Membranes	Permeability (Barrer)[a]			Permselectivity	
	O_2	N_2	CO_2	O_2/N_2	CO_2/N_2
GUS-ORMOCER$^®$	-[b]	-[b]	-[b]	-	-
GUS-**3**DMDES-ORMOCER$^{®c}$	8.7	1.5	39.9	5.8	26.6
GUS-**6**DMDES-ORMOCER$^{®d}$	34.3	13.7	219.0	2.5	15.9

[a] Barrer = 1×10^{-10} cm^3 (STP) cm/cm^2 s cm Hg.
[b] GUS-ORMOCER$^®$ was nearly impermeable to gases under the present conditions.
[c] GUS-ORMOCER$^®$ modified with 3 moles of DMDES.
[d] GUS-ORMOCER$^®$ modified with 6 moles of DMDES.

_____

Table 4.2

Single gas permeation properties of the S-ORMOCER[®][a] and its corresponding MMMs at 25 °C.

Membranes	Permeability (Barrer)[b]			Permselectivity	
	O_2	N_2	CO_2	O_2/N_2	CO_2/N_2
S-ORMOCER[®]	34.3	13.7	219.0	2.5	15.9
S-ORMOCER[®]-zeolite Beta (10 wt.%)	28.9	9.9	193.4	2.9	19.5
S-ORMOCER[®]-zeolite Beta (20 wt.%)	24.8	6.2	173.6	4.0	28.0
S-ORMOCER[®]-zeolite Beta (30 wt.%)	34.1	7.1	212.1	4.8	29.8
S-ORMOCER[®]-zeolite Beta (40 wt.%)	56.3	15.6	277.2	3.6	17.7
S-ORMOCER[®]-zeolite 3A (30 wt.%)	26.6	9.5	140.0	2.8	14.3
S-ORMOCER[®]-zeolite 4A (30 wt.%)	27.7	10.6	151.7	2.6	14.3
S-ORMOCER[®]-zeolite 5A (30 wt.%)	25.7	11.2	159.0	2.3	14.2

[a] GUS-ORMOCER[®] modified with 6 moles of DMDES
[b] 1Barrer = 1×10^{-10} cm^3 (STP) cm/cm^2 s cm Hg

4.8 Figures
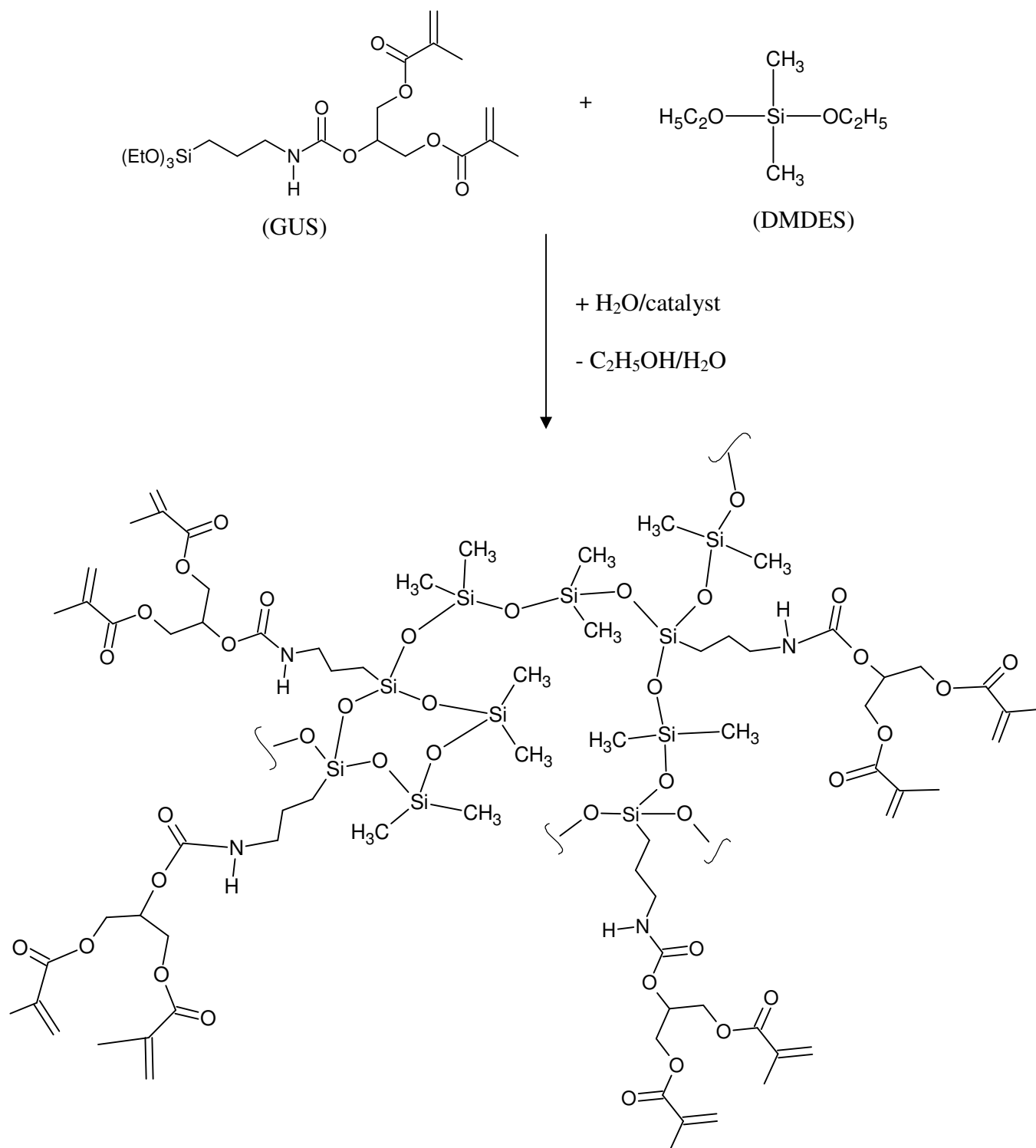
Figure 4.1: Schematic reaction route for the formation of DMDES-modified GUS-ORMOCER® resin.
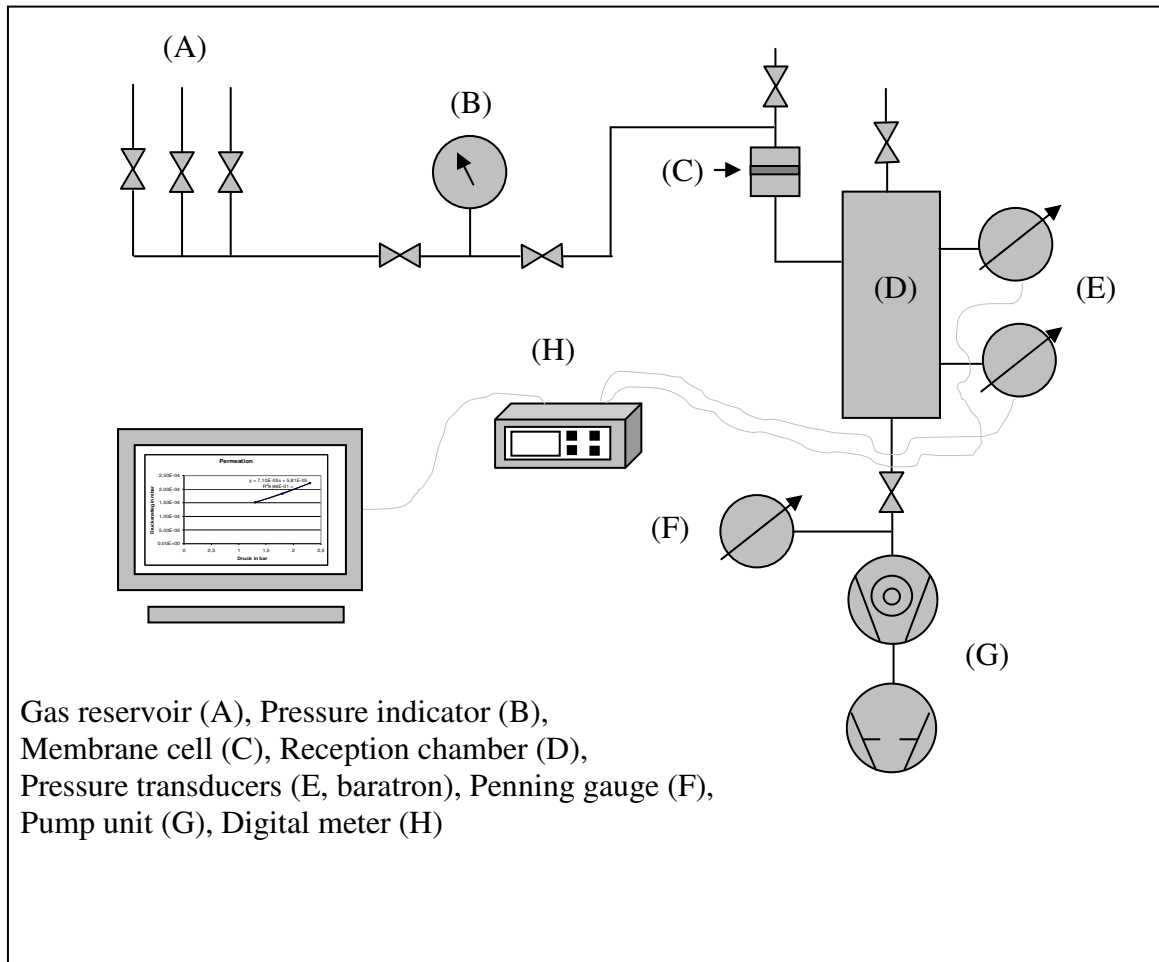
Figure 4.2: Schematic diagram of the single gas permeation experimental set-up for the flat-sheet membranes.
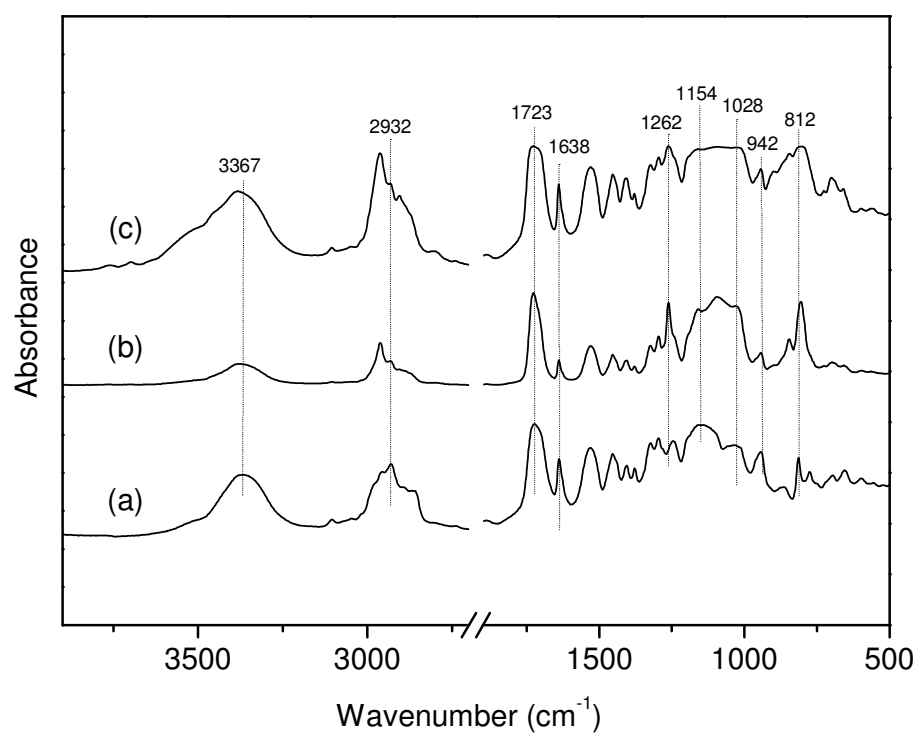
Figure 4.3: FT-IR spectra of: (a) pure GUS-ORMOCER®, (b) GUS-3DMDES-ORMOCER® and (c) GUS-6DMDES-ORMOCER® resins.
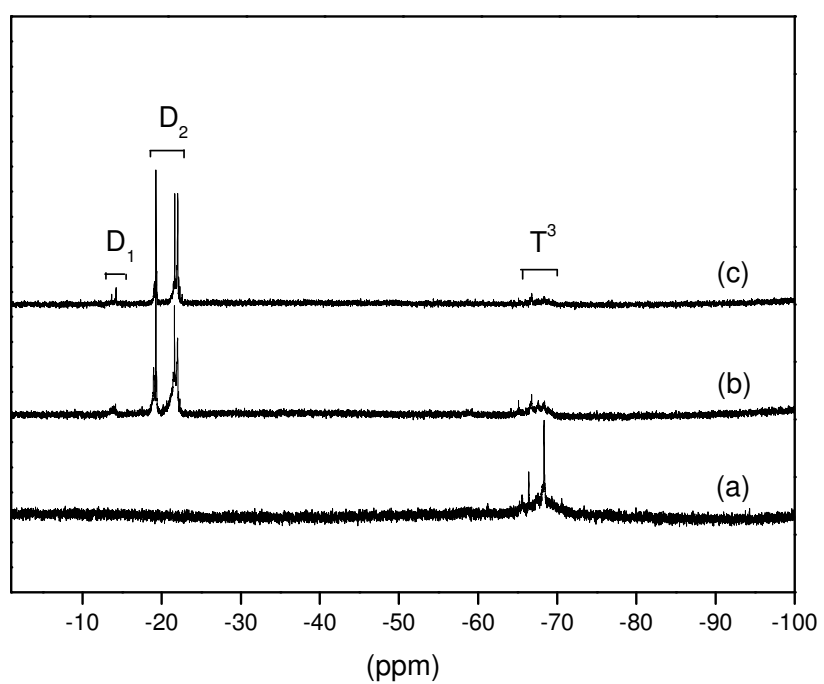
Figure 4.4: Liquid ^{29}Si NMR spectra of: (a) pure GUS-ORMOCER$^®$, (b) GUS-3DMDES-ORMOCER$^®$ and (c) GUS-6DMDES-ORMOCER$^®$ resins.
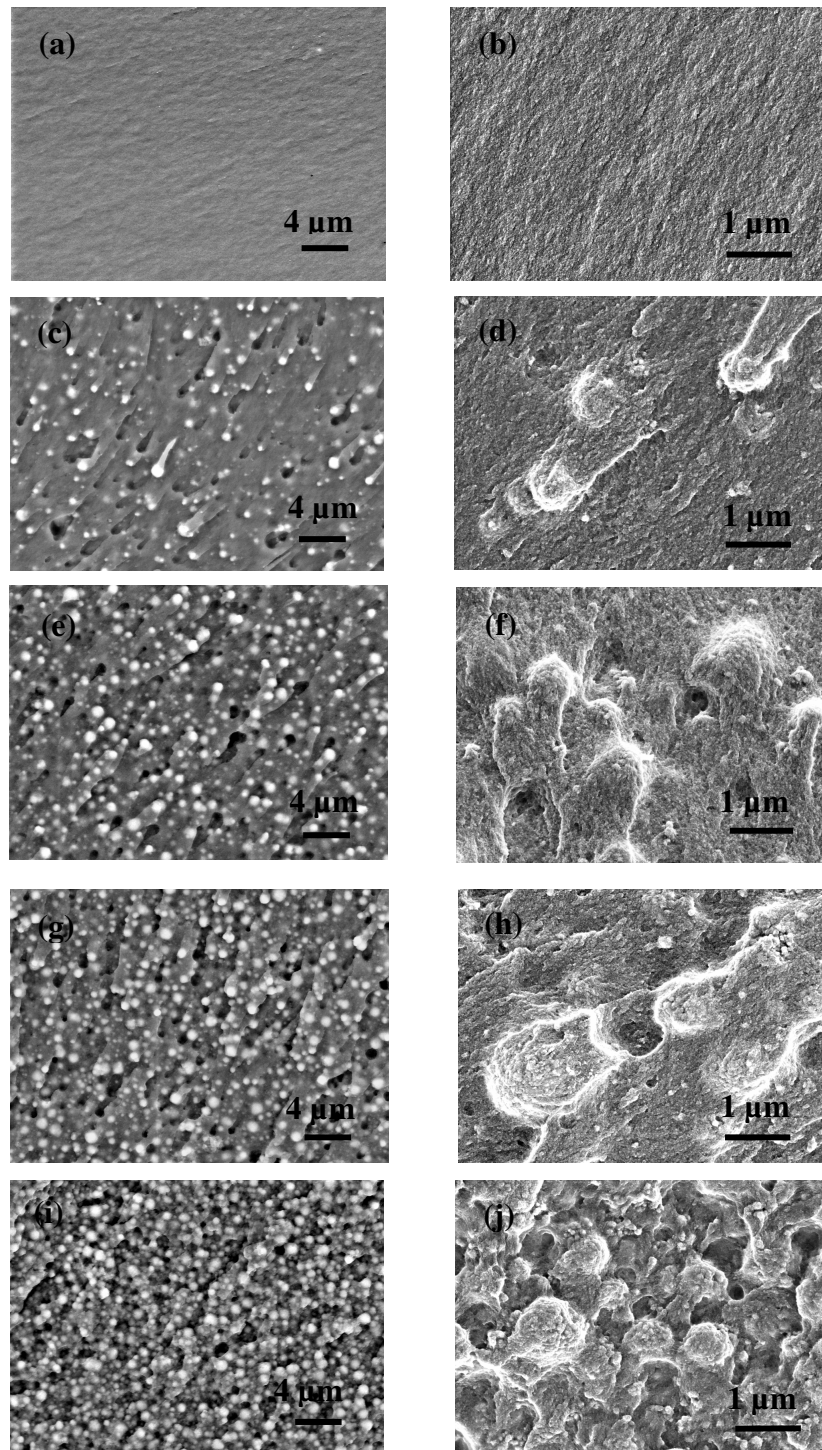
Figure 4.5: Unpolished cross–sectional SEM images of the S-ORMOCER® (a and b) and its corresponding MMMs containing 10 wt.% (c and d), 20 wt.% (e and f), 30 wt.% (g and h), and 40 wt.% (i and j) of zeolite Beta at different magnifications.
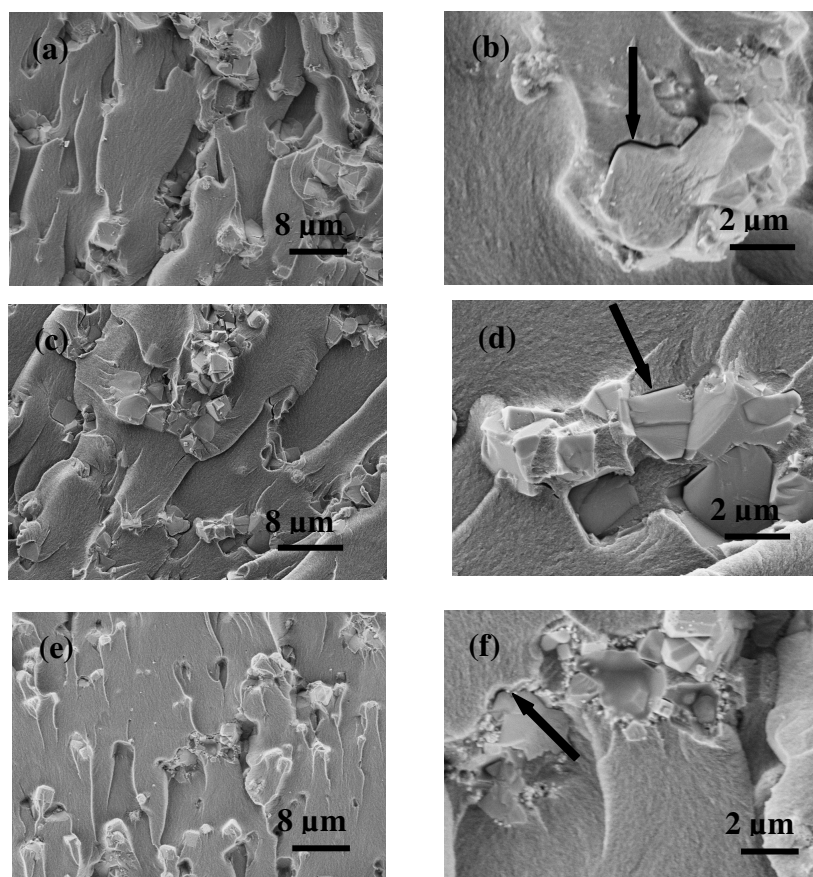
Figure 4.6: Unpolished cross-sectional SEM images of the S-ORMOCER®-zeolite 3Å (a and b), S-ORMOCER®-zeolite 4Å (c and d) and S-ORMOCER®-zeolite 5Å (e and f) MMMs at different magnifications. All the membranes were prepared with 30 wt.% of their respective zeolites.

References

[1]   R. Mahajan, D. Q. Vu, W. J. Koros, Mixed matrix membrane materials: an answer to the challenges faced by membrane based gas separations today?, J. Chin. Inst. Chem. Eng., 33 (2002) 77.

[2]   T. S. Chung, L. Y. Jiang, Y. Li, S. Kulprathipanja, Mixed matrix membranes (MMMs) comprising organic polymers with dispersed inorganic fillers for gas separation, Progr. Polym Sci., 32 (2007) 483.

[3]   S. P. Pereira Nunes, Organic-inorganic membranes for gas separation, Ann. Chim., 32 (2007) 119.

[4]   P. Bernardo, E. Drioli, G. Golemme, Membrane Gas Separation: A Review/State of the Art, Ind. Eng. Chem. Res., 48 (2009) 4638.

[5]   J. Ahn, W-J. Chung, I. Pinnau, M. D. Guiver, Polysulfone/silica nanoparticle mixed – matrix membranes for gas separation, J. Membr. Sci., 314 (2008) 123.

[6]   S. Choi, J. Coronas, Z. Lai, D. Yust, F. Onorato, M. Tsapatsis, Fabrication and gas separation properties of polybenzimidazole (PBI)/nanoporous silicates hybrid membranes, J. Membr. Sci., 316 (2008) 145.

[7]   Y. Li, H. M. Guan, T. S. Chung, S. Kulprathipanja, Effect of novel silane modification of zeolite surface on polymer chain rigidification and pore blockage in polyethersulphone (PES)-zeolite A mixed matrix membrane, J. Membr., Sci. 275 (2006) 17.

[8]   T. W. Pechar, S. Kim, B. Vaughan, E. Marand, M. Tsapatsis, H. K. Jeong, C. J. Cornelius, Fabrication and characterization of polyimide–zeolite L mixed matrix membranes for gas separations, J. Membr. Sci., 277 (2006) 195.

[9]   C. A. Scholes, S. E. Kentish and G. W. Stevens, Carbon dioxide separation through polymeric membrane systems for flue gas applications, Recent Patents Chem. Eng., 1 (2008) 52.

[10]   T-H. Bae, J. Liu, J. S. Lee, W. J. Koros, C. W. Jones, S. Nair, Facile high-yield solvothermal deposition of inorganic nanostructures on zeolite crystals for mixed matrix membrane fabrication, J. Am. Chem. Soc., 131 (2009) 14662.

[11]   S. D. Bhat, N. N. Mallikarjuna, T. M. Aminabhavi, Microporous alumino-phosphate (AlPO4-5) molecular sieve-loaded novel sodium alginate composite membranes for pervaporation dehydration of aqueous–organic mixtures near their azeotropic

compositions, J. Membr. Sci., 282 (2006) 473.

[12]   C. Liu, S. T. Wilson, S. C. Houdek, D. A. Lesch, Method for making high performance mixed matrix membranes incorporating molecular sieve for separation of liquids, gases and vapors, U.S. Pat. Appl. Publ., (2009) US 2009149565.

[13]   G. Ciobanu, G. Carja, O. Ciobanu, Structure of mixed matrix membranes made with SAPO-5 zeolite in polyurethane matrix, Microporous Mesoporous Mater., 115 (2008) 61.

[14]   P. Jha, J. D. Way, Carbon dioxide selective mixed – matrix membranes formulation and characterization using rubbery substituted polyphosphazene, J. Membr. Sci., 324 (2008) 151.

[15]   S. Kim, E. Marand, High permeability nano-composite membranes based on mesoporous MCM–41 nanoparticles in a polysulfone matrix, Microporous Mesoporous Mater., 114 (2008) 129.

[16]   S. Kim, E. Marand, J. Ida, V. V. Guliants, Polysulfone and mesoporous molecular sieve MCM-48 mixed matrix membranes for gas separation, Chem. Mater., 18 (2006) 1149.

[17]   A. K. Sahu, S. D. Bhat, S. Pitchumani, P. Sridhar, V. Vimalan, C. George, N. Chandrakumar, A. K. Shukla, Novel organic-inorganic composite polymer-electrolyte membranes for DMFCs, J. Membr. Sci., 345 (2009) 305.

[18]   E. V. Perez, K. J. Balkus Jr., J. P. Ferraris, I. H. Musselman, Mixed-matrix membranes containing MOF-5 for gas separations, J. Membr. Sci., 328 (2009) 165.

[19]   S. Basu, M. Maes, A. Cano-Odena, L. Alaerts, D. E. De Vos, I. F. J. Vankelecom, Solvent resistant nanofiltration (SRNF) membranes based on metal-organic frameworks, J. Membr. Sci., 344 (2009) 190.

[20]   S. G. Adoor, L. S. Manjeshwar, S. D. Bhat, T. M. Aminabhavi, Aluminum-rich zeolite beta incorporated sodium alginate mixed matrix membranes for pervaporation dehydration and esterification of ethanol and acetic acid, J. Membr. Sci., 318 (2008) 233.

[21]   Y. Wang, D. Yang, X. Zheng, Z. Jiang, J. Li., Zeolite beta–filled chitosan membrane with low methanol permeability for direct methanol fuel cell, J. Power Sources, 183 (2008) 454.

[22]   S. Erce, H. Erdener, R. G. Akay, H. Yuecel, N. Bac, I. Eroglu, Effects of sulfonated polyether-etherketone (SPEEK) and composite membranes on the proton exchange membrane fuel cell (PEMFC) performance, Inter. J. Hydrogen Energy, 34 (2009) 4645.

[23]   L. Y. Jiang, T. S. Chung, C. Cao, Z. Huang, S. Kulprathipanja, Fundamental understanding of nano-sized zeolite distribution in the formation of the mixed matrix single- and dual-layer asymmetric hollow fiber membranes, J. Membr. Sci., 252 (2005) 89.

[24]   L. Y. Jiang, T. S. Chung, S. Kulprathipanja, An investigation to revitalize the separation performance of hollow fibers with a thin mixed matrix composite skin for gas separation, J. Membr. Sci., 276 (2006) 113.

[25]   Y. Li, T. S. Chung, Z. Huang, S. Kulprathipanja, Dual-layer polyethersulfone (PES)/BTDA-TDI/MDI co-polyimide (P84) hollow fiber membranes with a submicron PES–zeolite beta mixed matrix dense-selective layer for gas separation, J. Membr. Sci., 277 (2006) 28.

[26]   L. Y. Jiang, T. S. Chung, S. Kulprathipanja, Fabrication of mixed matrix hollow fibers with intimate polymer-zeolite interface for gas separation, AIChE J., 52 (2006) 2898.

[27]   D. Sirikittikul, A. Fuongfuchat, W. Booncharoen, Chemical modification of zeolite beta surface and its effect on gas permeation of mixed matrix membrane, Polym. Adv. Technol., 20 (2009) 802.

[28]   Z. Huang, J-F. Su, Y-H. Guo, X-Q. Su, L-J. Teng, Synthesis of well-crystallized zeolite beta at large scale and its incorporation into polysulfone matrix for gas separation, Chem. Eng. Commun., 196 (2009) 969.

[29]   Z. Huang, J-F. Su, X-Q. Su, Y-H. Guo, L. J. Teng, C. M. Yang, Preparation and Permeation Characterization of β-Zeolite-Incorporated Composite Membranes J. Appl. Polym. Sci., 112 (2009) 9.

[30]   S. Jacob, S. Cochet, C. Poinsignon, M. Popall, Proton conducting inorganic-organic matrices based on sulfonyl- and styrene derivatives functionalized polycondensates via sol-gel processing, Electrochim. Acta, 48 (2003) 2181.

[31]   S. Jacob, C. Poinsignon, M. Popall, Inorganic-organic hybrid protonic polymeric materials for fuel cells based on polycondensed and organically cross-linked sulfonyl- and styrene-functionalized alkoxysilanes, Electrochim. Acta, 50 (2005) 4022.

[32]   H. Wolter, T. Ballweg, W. Storch, Membrane for oxygenator, Eur. Patent, (2000) EP 0985442.

[33]   K. H. Haas, S. Amberg-Schwab, T. Ballweg, Synthesis and properties of hybrid inorganic-organic polymers based on organically modified Si-alkoxides and their use for permeation control, Adv. Sci. Technol. 31 (2003) 581..

_____

[34]   T. Ballweg, H. Wolter, Hollow fibers from hybrid polymers, Gummi, Fasern, Kunststoffe, 53 (2000) 277.

[35]   T. Ballweg, H. Wolter, W. Storch, Ormocer– and derived microporous inorganic hollow fibers, Keramische Zeitschrift, 53 (2001) 678.

[36]   R. W. Thompson, B. E. Libby, M. B. Berry, K. Rose, K.-H. Haas, Incorporation of zeolites into hybrid polymer matrices, US Patent, (2001) US 6, 248, 682.

[37]   M. B. Berry, B. E. Libby, K. Rose, K. H. Haas, R. W. Thompson, Incorporation of zeolites into composite matrices, Micropor. Mesopor. Mater. 39 (2000) 205.

[38]   S. M. Kumbar, T. Selvam, C. Gellermann, W. Storch, T. Ballweg, J. Breu, G. Sextl, ORMOCERs (organic-inorganic hybrid copolymers)-zeolite Beta (BEA) nanocomposite membranes for gas separation applications, J. Membr. Sci., 347 (2010) 132.

[39]   C. L. Wang, D. Y. Chao, Study of oxygen-permeable polyurethane ionomer. II, J. Appl. Polym. Sci., 78 (2000) 1932.

[40]   Z. Zhang, B. P. Gorman, D. W. Mueller and R. Reidy, Processing and Characterization of DMDES-TEFS Hybrid Thin Films, 202nd ECS Meeting – Salt Lake City, UT October 20-25 (2002).

[41]   H. B. Park, S. Y. Ha and Y. M. Lee, Percolation behavior of gas permeability in rigid-flexible block copolymer membranes, J. Membr. Sci., 177 (2000) 143.

[42]   H. B. Park, J. K. Kim, S. Y. Nam and Y. M. Lee, Imide-siloxane block copolymer/silica hybrid membranes: preparation, characterization and gas separation properties, J. Membr. Sci., 220 (2003) 59.

[43]   H. Wolter. W. Storch, T. Ballweg, PCT Int. Appl. (2001) WO 2001068961.

[44]   S. Monredon-Senani, C. Bonhomme, F. Ribot and F Bobanneau, Covalent grafting of organoalkoxysilane on silica surfaces in water rich medium as evidenced by ^{29}Si NMR, J. Sol-Gel Sci. Technol., 50 (2009) 152.

[45]   Y. Yamada, N. Furukawa, Y. Tujita, Structures and gas separation properties of silicone-containing polyimides, High Perform. Polym., 9 (1997) 145.

[46]   F. Laeri, F. Schüth, U. Simon and M Wark, Host-Guest Systems Based on Nanoporous Crystals, Wiley-VCH Verlag GmbH & Co. KGaA, (2003).

[47]   Z. Huang, Y. Li, R. Wen, M. M. Teoh, S. Kulprathipanja, Enhanced gas separation properties by using nanostructured PES-Zeolite 4A mixed matrix membranes, J. Appl. Polym. Sci., 101 (2006) 3800.

_____

Chapter 5

Influence of technological processing parameters on the photopolymerization of glycerine-1,3-dimethacrylateurethanetriethoxysilane (GUS)-based ORMOCER®s

5.1 Abstract

Inorganic-organic hybrid polymers (ORMOCER®s) were prepared via the sol-gel process followed by UV-curing using specially designed innovative photo-curable organoalkoxysilanes. When processing an ORMOCER® system, the resulting material properties are significantly influenced by the technological processing parameters such as photoinitiator concentration, duration of irradiation and UV light intensity. In order to investigate this relationship, the glycerine-1,3-dimethacrylateurethanetriethoxysilane (GUS)-based ORMOCER® material was chosen as model system. The effect of the photoinitiator concentration on the extent of C=C bond conversion and its correlation towards the optical properties of GUS-based ORMOCER® was studied in detail. The conversion of C=C bond was increased from 52 % to 82 % by increasing the photoinitiator concentration from 0.25 to 2.0 wt.-%. These observations are in good agreement with the results obtained from the refractive indices of the GUS-based ORMOCER® materials at selected wavelengths.

5.2   Introduction

ORMOCER[®]s are hybrid polymers consisting of inorganic oxidic (Si, Al, Ti, and Zi, etc.) components and polymerized organic components (polyethylene oxides, polymethacrylates, polyethylene, etc.). They are prepared via sol-gel processing [1] in combination with organic cross-linking reactions for example from reactive functionalized organosilanes. A wide range of inherent properties can be achieved, including glass-like ones (transparency, chemical, mechanical and thermal behaviour) and polymer-like ones (toughness, functionalization ability, and low processing temperature) [2-4], leading to various applications, such as functional coatings [5-7], dental composites [8, 9], electrolytes for fuel cells/Li-batteries [10, 11], and optical/photonic/microelectronic devices [12-14]. ORMOCER[®] materials are very attractive for several reasons: They allow combinations of various inorganic precursors with special silanes bearing functional groups so that application adapted material properties can be obtained; and most importantly, they can be processed either by thermal- or photo-curing at ambient conditions. In general, photo-curing offers various advantages over traditional thermal curing, including high polymerization rates and low energy requirements. Therefore, there has been a growing demand for photo-curable ORMOCER[®] systems [15]. Among the photo-curable ORMOCER[®] systems, glycerine-1,3-dimethacrylateurethanepropyltriethoxysilane (GUS)-based ORMOCER[®] systems are of great interest due to their facile photopolymerization, excellent film transparency, and highly cross-linked network structure. These copolymers have found successful application as dental composites with valuable properties (low shrinkage, high flexural strength, and high abrasion resistance) [16]. Furthermore, there has been considerable work on the applications of GUS-based ORMOCER[®] systems as semipermeable [17], blood oxygenator [18] and hollow fiber membranes [19, 20]. In view of the effectiveness of these systems, void-free and free-standing GUS-based ORMOCER[®]-zeolite nanocomposite membranes with 20 - 40 wt.-% of zeolite Beta loadings($\Phi = 200 - 800$ nm) have been recently fabricated [21]. These nanocomposite membranes have

_____

[®] Registered trademark of Fraunhofer Gesellschaft zur Förderung der angewandten Forschung e.V., Germany

been found to possess improved gas permeation characteristics. For instance, a nanocomposite membrane with 40 wt.-% zeolite Beta loading exhibits a nearly 16-times increase in H_2 and He permeability in comparison to the pure GUS-based ORMOCER® membrane.

The photoinitiator concentration is one of the most important processing parameters, which can influence the chemical and physical properties of the resulting hybrid materials. In particular, there has been ongoing interest to study the effects of technological processing parameters (photoinitiator concentration, duration of irradiation, and UV light intensity, etc.) on the optical and electrical properties of ORMOCER® systems [22-23]. Thus, it is highly desirable to understand the effects of these parameters on the structure (cross-linking behaviour) of hybrid materials. Although the application of GUS-based ORMOCER®s has been studied in detail [16-20], the influence of the photoinitiator concentration on its photopolymerization was not systematically investigated so far. The incentive of the present study was to assess the influence of the photoinitiator concentration on the degree of conversion of C=C bonds of the methacrylic groups of GUS-based ORMOCER® coatings and their corresponding optical properties.

5.3 Experimental

5.3.1 Materials

Glycerine-1,3-dimethacrylate (GDMA, 98 %) and 3-isocyanatopropyltriethoxysilane (IPTES, 99 %) were obtained from Momentive Performance Materials. Dibutyltindilaurate (DBTDL, 95 %), ethylacetate (97 %) and propylacetate (99 %) were purchased from Aldrich. Dodecanediol-1,12-dimethacrylate (DDDMA, 97 %) and the photoinitiator, Irgacure 184 (1-hydroxy-cyclohexyl-phenyl-ketone) were purchased from Rohm & Haas and CIBA Specialty Chemicals, respectively. All chemicals were used as received without further purification.

5.3.2 Synthesis of GUS-based ORMOCER® resin

The GUS-based ORMOCER® resin was synthesized via the sol-gel process in combination with organic cross-linkers having UV polymerizable organic functionalities according to previous literature [24]. In a typical procedure, the 3-isocyanatopropyltriethoxysilane (IPTES) was covalently linked to glycerine-1,3-dimethacrylate (GDMA) in presence of dibutyltindilaurate (DBTL) as catalyst followed by hydrolysis and condensation reactions. Dodecanediol-1,12-dimethacrylate (DDDMA) was added as diluent. Note that the role of dodecanediol-1,12-dimethacrylate was mainly to maintain the spin-ability properties of the GUS-based ORMOCER® resin. The resultant transparent GUS-based ORMOCER® resin was dissolved in a mixture of solvent (ethylacetate) and water in order to remove the catalyst (ammonium fluoride). Therefore, both water and solvent were removed by solvent extraction and distillation methods under reduced pressure at maximum temperature of 35 to 40 °C, respectively. The molar composition of the GUS-based ORMOCER® resin used in the present study was IPTES: GDMA : DBTL: DDDMA = 1 : 1 : 0.2 : 0.0016. The reaction mechanism for the formation of the resin is shown in Fig. 5.1. The specific inorganic structure is not completely known.

5.3.3 Preparation of GUS-based ORMOCER® coatings

Fig. 5.2 shows the flow chart for the preparation methodology of cured GUS-based ORMOCER® coatings for refractive index measurements. These coatings were prepared by spinning a lacquer solution of GUS-based ORMOCER® on a glass substrate using CONVAC ST 146 spin-coater. Before spin coating, the resin was diluted with solvent (propylacetate) into 1:1 ratio, and then the resulting solution mixture was filtered through a 0.2 µm hydrophobic polypropylene (PTFE, Advantec MFS) filter in order to ensure the highest optical quality of the materials. The solution mixtures were then spin-coated (3000 rpm, 15 s) on glass substrates and stored in an aluminium-foil covered plastic box in order to avoid sunlight. To harden the coatings, they were irradiated homogeneously by UV Hg lamp (UV intensity 2000-11000 mW/cm^2, 110-230 V) under

nitrogen atmosphere for up to 3 min. The distance between sample and UV light source was adjusted to give an intensity of 65 mW/cm^2. A similar procedure was followed for all other samples containing different concentrations of photoinitiator. The proposed UV curing structural model of GUS-based ORMOCER$^®$ material is shown in Fig. 5.3. Before determining the refractive index, these samples were dried at 40 °C for about 2 h in order to remove the solvent. The thickness of the samples used in this study was about 5 to 6 µm.

5.3.4 Characterization

The infrared spectra of GUS-based ORMOCER$^®$ resins and their precursors were recorded on a Nicolet Magna-IR 760 FT-IR spectrometer in the range of 400 to 4000 cm^{-1} (resolution of 4 cm^{-1}, 32 scans per spectrum). The resin was blended on a KBr pellet and cured under UV light (UV intensity 64-65 mW/cm^2, nitrogen atmosphere) and then it was removed from the UV chamber sequentially over a period of time and analyzed immediately by FT-IR spectrometer. The chemical conversion of the methacrylate groups was determined by monitoring the decrease of C=C bands after UV irradiation. The ^{29}Si-NMR measurements of the GUS-based ORMOCER$^®$ resins were carried out on a Bruker Avance DPX 400 NMR spectrometer with a 9.4 T magnetic field, equipped with a quaternary nuclear probe head. The spectrum was obtained with CDCl$_3$ as solvent and tetramethylsilane as internal standard. The refractive index of the material was determined using a homebuilt prism-coupling method at wavelength λ = 635 nm, as described in the literature [25].

5.4 Results and discussion

FTIR is an effective analytical instrument for detecting functional groups and characterizing materials. The FT-IR spectra of 3-isocyanotopropyltriethoxysilane (spectrum 'a'), glycerine-1,3-dimethacrylate (spectrum 'b'), glycerine-1,3-dimethacrylaturethane-triethoxysilane (spectrum 'c') and GUS-based ORMOCER$^®$ resin (spectrum 'd') are shown in Fig. 5.4. Spectrum 'a' shows the absorption bands at 3000-2837, 2269 and 1082 cm^{-1}, which are assigned to the stretching vibrations of C-H

(methyl, methylene groups), N=C=O, and $\equiv$Si-OC$_2$H$_5$ groups. Spectrum 'b' shows absorption bands at 3507 (broad), 1720 and 1638 cm^{-1}, which are assigned to the stretching vibrations of O-H, carbonyl and C=C bonds of methacrylate groups, respectively. The intensity of the N=C=O band at 2269 cm^{-1} and the intensity of the broad O-H band at 3507 cm^{-1} gradually decreased during the reaction of 3-isocyanatopropyltriethoxysilane with glycerine-1,3-dimethacrylate, and the appearance of new vibration bands at 1527 and 3370 cm^{-1} (spectrum 'c') clearly suggests that the reaction of glycerine-1,3-dimethacrylate with 3-isocyanatopropyltriethoxysilane is completed. The characteristic bands at 1527 and 3370 cm^{-1} are assigned to $\nu_{(C-N, urethane)}$ and $\nu_{(N-H, urethane)}$ of glycerine-1,3-dimethacrylateurethanetriethoxysilane. In addition, the FT-IR spectrum of GUS-based ORMOCER® resin (spectrum 'd') shows similar characteristic features as that of glycerine-1,3-dimethacrylateurethanetriethoxysilane (spectrum 'c') except for an intense broad band in the region of 1000-1200 cm^{-1}, which corresponds to the Si-O-Si vibrations, respectively. The appearance of the Si-O-Si vibration band clearly suggests that the GUS-based ORMOCER® resin is inorganically condensed.

Characterisation of the silicate network of the hybrid sol is of crucial importance to understand the mechanism involved in the photopolymerization process. Moreover, it is believed that the condensation state of the silicate network could significantly influence the photopolymerization process by restricting the mobility of the polymerizable groups. Therefore, the ^{29}Si NMR spectroscopic measurement of GUS-based ORMOCER® resin was carried out in order to investigate the nature of the silicon species present therein. The ^{29}Si NMR spectrum of the GUS-based ORMOCER® resin is shown in Fig. 5.5. The spectrum exhibits only one broad signal at -63 to -70 ppm, which is attributed to the T^3 [RSi(OSi)$_3$] units [26]. The T^n notation is well know in silicon chemistry, where T denotes a silicon atom and superscript 'n' denotes the number of Si-O-Si bonds attached to silicon. There were no signals corresponding to T^1 [RSi(OSi)(OH)$_2$] and T^2 [RSi(OSi)$_2$(OH)] units also indicating that the GUS-based ORMOCER® resin possesses a highly condensed inorganic network. The broad signal in the range of -80 to -140 ppm is an artefact from the glass tube.

The effect of the curing condition on the conversion of the C=C bonds of the GUS-based ORMOCER® resin was also studied in detail. The change in the chemical structure after UV-curing over a period of time at ambient temperature was monitored by FT-IR spectroscopy. Fig. 5.6 shows the FT-IR spectra of GUS-based ORMOCER®

resin (spectrum 'a') and UV-cured GUS-based ORMOCER® samples over a period of time, 30 sec (spectrum 'b'), 60 sec (spectrum 'c') and 180 sec (spectrum 'd'). The absorption band at 1638 cm^{-1} is attributed to the $\nu_{(C=C)}$ of the methacrylate groups. The intensity of this band is gradually decreased by increasing the UV exposure time, indicating a progressing of photopolymerization [see Fig. 5.6 (spectrum 'b' to spectrum 'd')]. The maximum decrease in the intensity of this band was observed at 180 sec (see Fig. 5.6 spectrum 'd'), which clearly suggests maximum amount of C=C bonds of the methacrylate groups are consumed by photopolymerization. The above-mentioned results indicate that a UV-curing process for a period of 180 sec is sufficient to fabricate highly polymerized GUS-based ORMOCER® thin coatings , which yielded a non-sticky coating.

The influence of the photoinitiator concentration on the degree of conversion of C=C bonds (which is also called the degree of photopolymerization) before and after photo-curing of GUS-based ORMOCER® resins was calculated using eq. 5.1 [23]

$$ DP\,(\%) = 100 \times \left\{ 1 - \left[\frac{P^{I}_{C=C}}{P^{I}_{C=O}} \middle/ \frac{P_{C=C}}{P_{C=O}} \right] \right\} \tag{5.1} $$

where $P^{I}_{C=C}$ and $P^{I}_{C=O}$ are the integrated band areas of C=C and C=O bonds of the cured coatings, while $P_{C=C}$ and $P_{C=O}$ are the integrated band areas of uncured coatings.

Fig. 5.7 shows the calculated degree of conversion of C=C bonds at 25 °C as a function of a photoinitiator concentration with light intensity of 64 mW/cm^2 in nitrogen atmosphere. The photoinitiator concentration was varied from 0.25 to 3.0 wt.-%. As can be seen in Fig. 5.7, the degree of conversion of C=C bond increased with increasing concentration of the photoinitiator. The degree of conversion of C=C bonds were 52 % at 0.25 wt.-% and it increased up to 82 % at 2.0 wt.-%. When further increasing the photoinitiator concentration, no significant change in the degree of conversion of C=C bonds was observed. This could be due to severe limitation on the segmental motion of the macroreactive radicals within the GUS-based ORMOCER® system (i.e. chain propagation is blocked within the polymeric system due to vitrification of the network [27]). Consequently, the termination rate of the polymerization reaction in extremely high viscous resin was slower. Therefore, the remaining reactive macroradicals have less chance to come closer to complete the reaction [28]. Moreover, the high cross-linking network of GUS-based ORMOCER® systems may also lead to the trapping of

reactive photoinitiator radicals. As the mobility of the reactive species slowly depletes, the polymerization reaction eventually stops. Therefore, it is assumed that the degree of conversion of C=C bonds remains nearly constant at a photoinitiator concentration of above 2.0 wt.-%. From these results it is confirmed that a 2.0 wt.-% photoinitiator concentration is sufficient to reach a nearly saturated degree of conversion of C=C bonds within the GUS-based ORMOCER® coatings. In order to gain better insight into the effects of the photoinitiator concentration on the degree of conversion of C=C bonds of inorganic-organic hybrid polymers (ORMOCER®s), the radical chain polymerization process will be considered [29]. It is assumed that the photoinitiator radicals are uniformly distributed throughout the GUS-based ORMOCER® resin. At a low concentration of photoinitiator, the photopolymerization begins where the radical is formed. In general, the free radical polymerization reaction includes initiation, propagation, and termination steps. In brief, these steps are contained in eqs. 5.2 to 5.6. The first step is initiator dissociation; [eq. (5.2), initiation] i.e., a reactive radical $A^\bullet$ is formed and hence the photopolymerization process begins [eq. (5.3)–(5.5), propagation…termination (5.6)].

$$A\text{-}A \xrightarrow{\ h\gamma\ } A^\bullet + A^\bullet \tag{5.2}$$

$$A^\bullet + B \longrightarrow AB^\bullet, \tag{5.3}$$

$$AB^\bullet + B \longrightarrow AB^\bullet_2, \tag{5.4}$$

$$AB^\bullet_{x\text{-}1} + B \longrightarrow AB^\bullet_x, \tag{5.5}$$

$$AB^\bullet_x + AB^\bullet_x \longrightarrow (AB)_{2x}, \tag{5.6}$$

$A^\bullet$ is a primary radical, $AB^\bullet$ and AB_{2x} represents growing radical and dead polymer molecule having 2x oligomeric units, respectively. At the onset of the polymerization reaction, a too-fast initiation produces a large number of radicals, which is generally referred to as autoacceleration. During this portion of the polymerization, the mobility of the macroradicals is slowly depleted due to vitrification of the polymer network and thus causes the reduction in the polymerization and termination rate. Thus it seems possible to assert that very low concentrations of photoinitiator within the GUS-based ORMOCER® resin lead to longer polymer chains while higher concentrations of photoinitiator lead to smaller polymeric structural units. It is known that the kinetic

chain length (v) of the radical chain polymerization is inversely proportional to the square root of the initiator radical concentration [eq. (5.7)]

$$v = \kappa \frac{[B]}{\{[A^{\bullet}]\}^{1/2}}$$ (5.7)

where B is the number of monomer molecules consumed by each radical and $A^{\bullet}$ is the initiator radical and k is the rate constant.

Therefore, we assume that the structural sizes generated at high concentrations of photoinitiator within GUS-based ORMOCER® systems are smaller in comparison to the larger sized structural units generated at low concentrations of photoinitiator during the photopolymerization process. The different sized structural units might cause a different packing density within the materials. This behaviour is a key feature, which directly influences the final polymer network structure and properties of GUS-based ORMOCER® materials and gives a structural insinuation. To support the above conclusion, we have investigated the refractive index of the GUS-based ORMOCER® system with various concentrations of photoinitiator during processing.

The refractive index as a function of the photoinitiator concentration of the final processed GUS-based ORMOCER® coatings at a selected wavelength at 635 nm is shown in Fig. 5.8. As can be seen from Fig. 5.8, there is a significant increase in the refractive index with varying photoinitiator concentrations from 0.25 to 2.0 wt.-%. This could be attributed to increased reactivity of methacrylic groups (i.e. polymerisation). The refractive index is 1.492 at 0.25 wt.-% and it increases up to 1.4985 at 2.0 wt.-%. When further increasing the photoinitiator concentration up to 4.0 wt.-%, there is no significant change in the refractive index. It seems that the refractive index has reached a steady value at a photoinitiator concentration of approximately 2.0 wt.-%. Overall, the refractive index of the GUS-based ORMOCER® resin is lower than that of polymerized GUS-based ORMOCER®s. These results are concurrent with the degree of conversion of C=C double bonds (see Fig. 5.7). Besides the photointiator concentration, other parameters (such as processing temperature, UV-light intensity, etc.,) are under consideration to correlate the FT-IR measurements data (degree of conversion of C=C bonds) with refractive index data of the GUS-based ORMOCER® system. These results will be published elsewhere.

5.5   Conclusions

The innovative GUS-based ORMOCER®s were prepared by using specially designed organoalkoxysilane via sol-gel process followed by UV-curing. The influences of the photoinitiator concentration on the degree of conversion of C=C bonds and its correlation towards the optical properties of the novel GUS-based ORMOCER® system have been investigated in detail. FT-IR results show that the degree of C=C bonds conversion of the methacrylic groups of the GUS-based ORMOCER® increased with increasing photoinitiator concentration. The maximum conversion of C=C bonds was obtained at a photoinitiator concentration of 2.0 wt.-%, whereas further increase in the photoinitiator concentration did not result in any significant change in the C=C bond conversion any more. The refractive indices of GUS-based ORMOCER® materials are in agreement with the degree of conversion of C=C bonds. These results provide a better understanding of the influences of technological processing parameters on the GUS-based ORMOCER® material properties

5.6 Acknowledgements

5.7   Figures

glycerine-1,3-dimethacrylate

3-isocyanatopropyltriethoxysilane

catalyst, 20 °C, 22 h

+ H_2O/catalyst

- C_2H_5OH/H_2O

- catalyst (extraction)

+ dodecanediol-1,12-dimethacrylate

GUS-based ORMOCER® resin
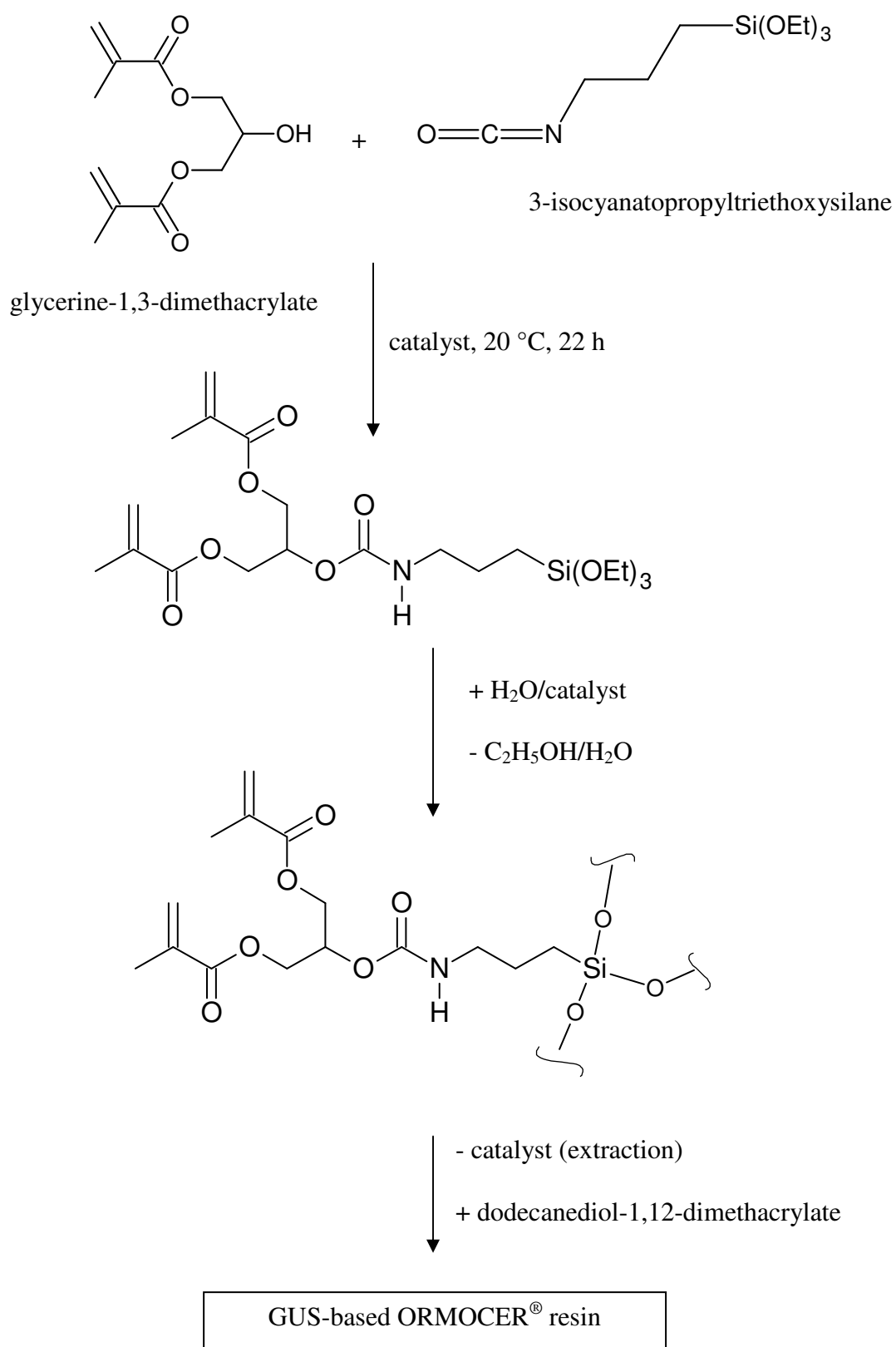
Figure 5.1: Reaction scheme for the preparation of GUS-based ORMOCER® resin.
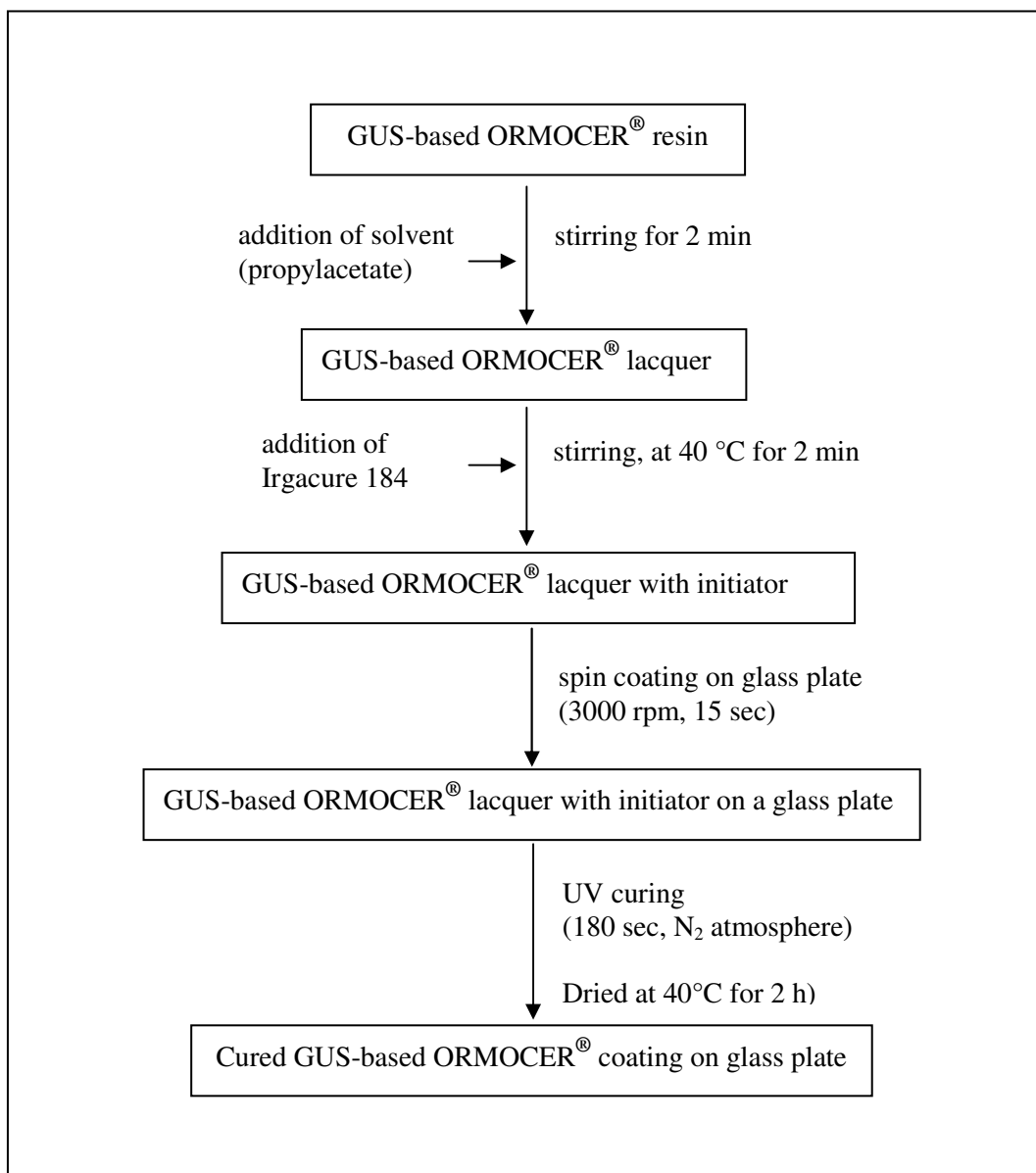
Figure 5.2: Flow chart for preparation of GUS-based ORMOCER® coating on glass substrate for measurement of the refractive index.
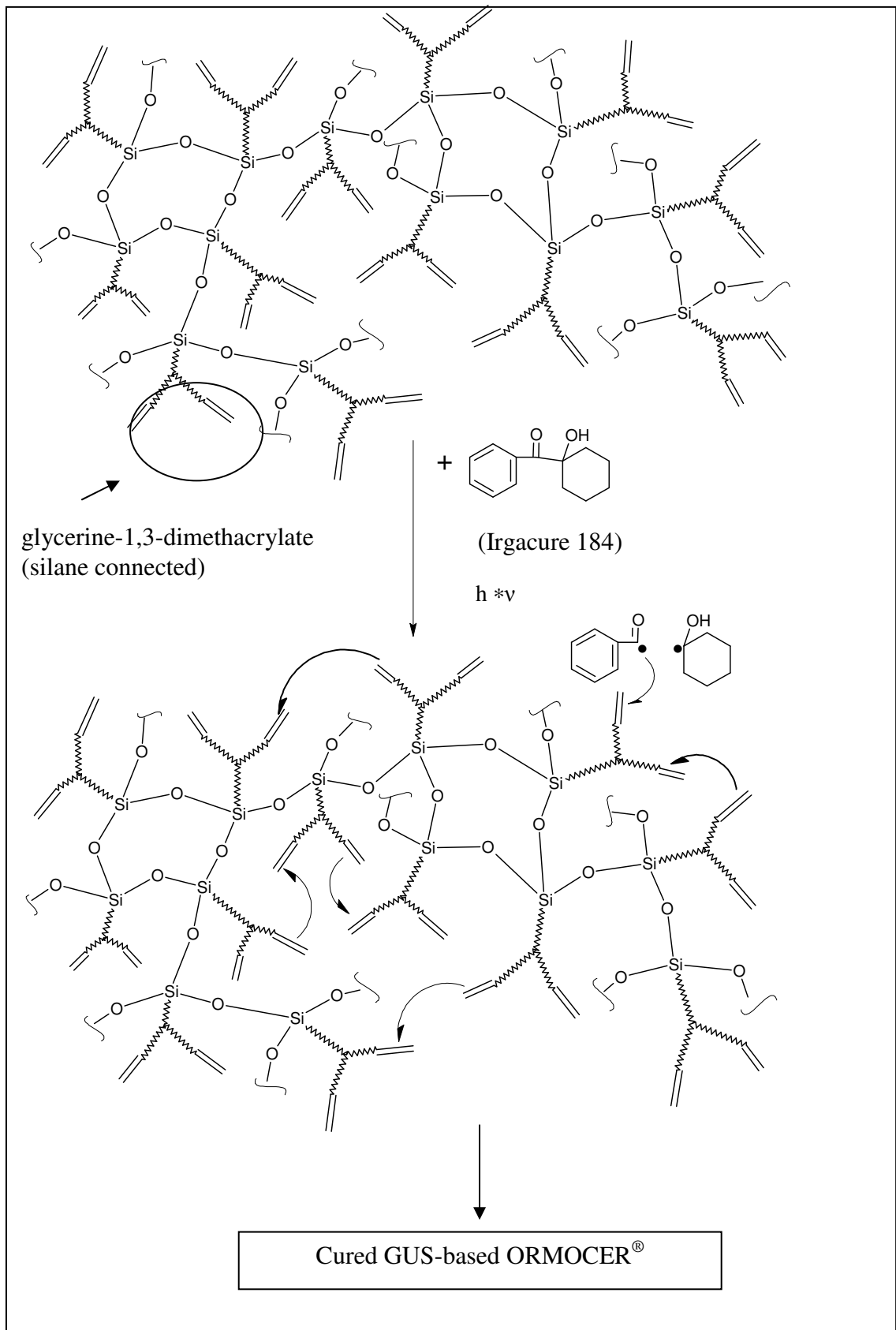
Figure 5.3: Proposed scheme for photopolymerization of GUS-based ORMOCER® resin.
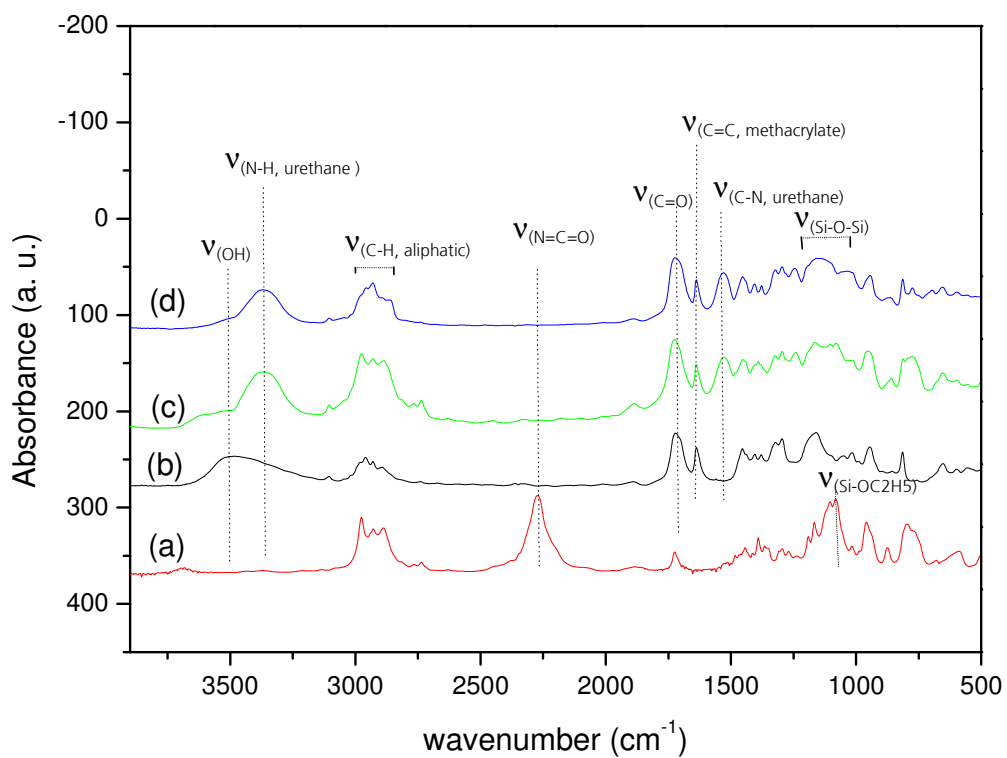
Figure 5.4: FTIR spectra of the precursors used for the preparation of GUS-based ORMOCER® resin: glycerine-1,3-dimethacrylate (a), 3-isocyanatopropyltriethoxysilane (b), glycerine-1,3-dimethacrylateurethanetriethoxysilane (c), and GUS-based ORMOCER® resin (d).
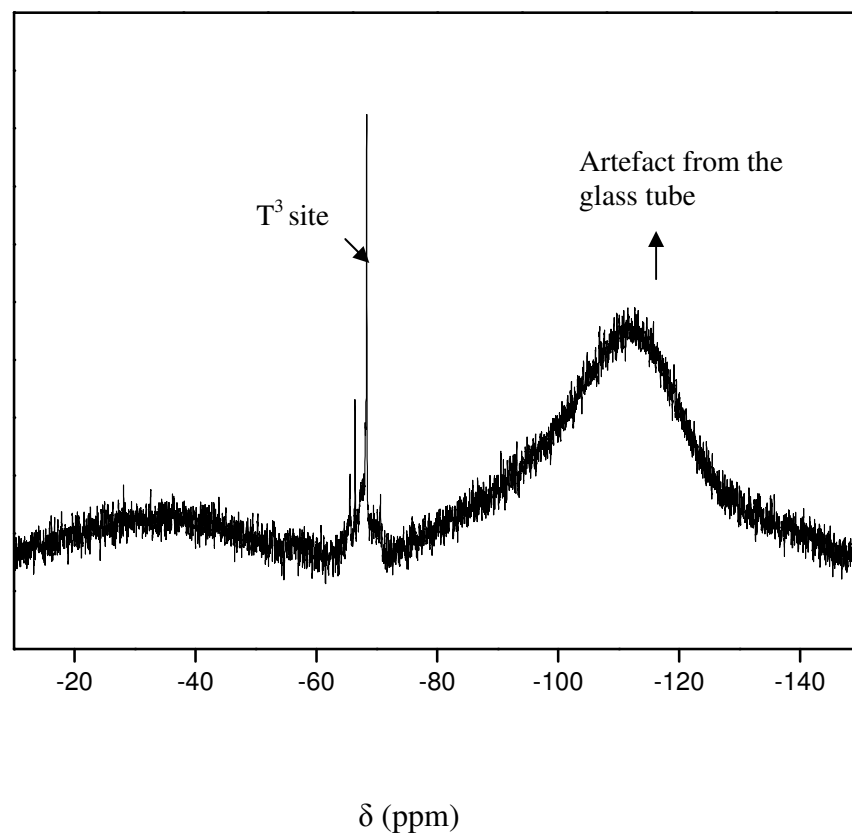
Figure 5.5: ^{29}Si NMR spectrum of GUS-based ORMOCER$^®$ resin.
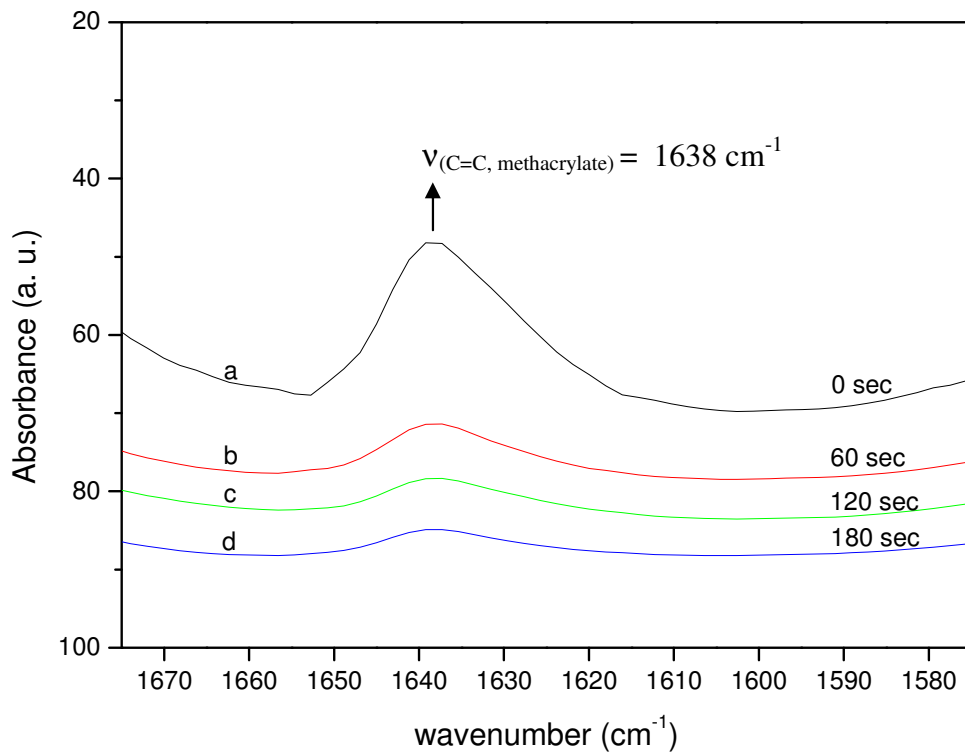
Figure 5.6: FTIR spectra of GUS-based ORMOCER® resin (a) and after UV curing at room temperature, 30 sec (b), 60 sec (c) and 180 sec (d).
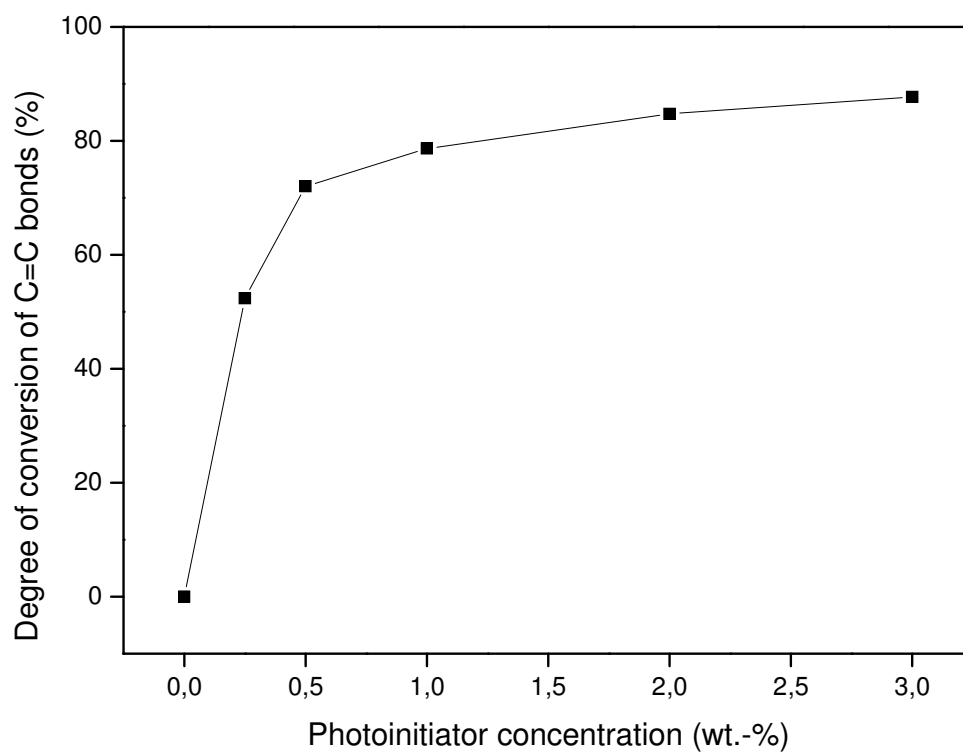
Figure 5.7: Calculated degree of conversion of C=C double bond of the methacrylic groups in GUS-based ORMOCER$^{®}$ system at 25 °C as a function of photoinitiator concentration.
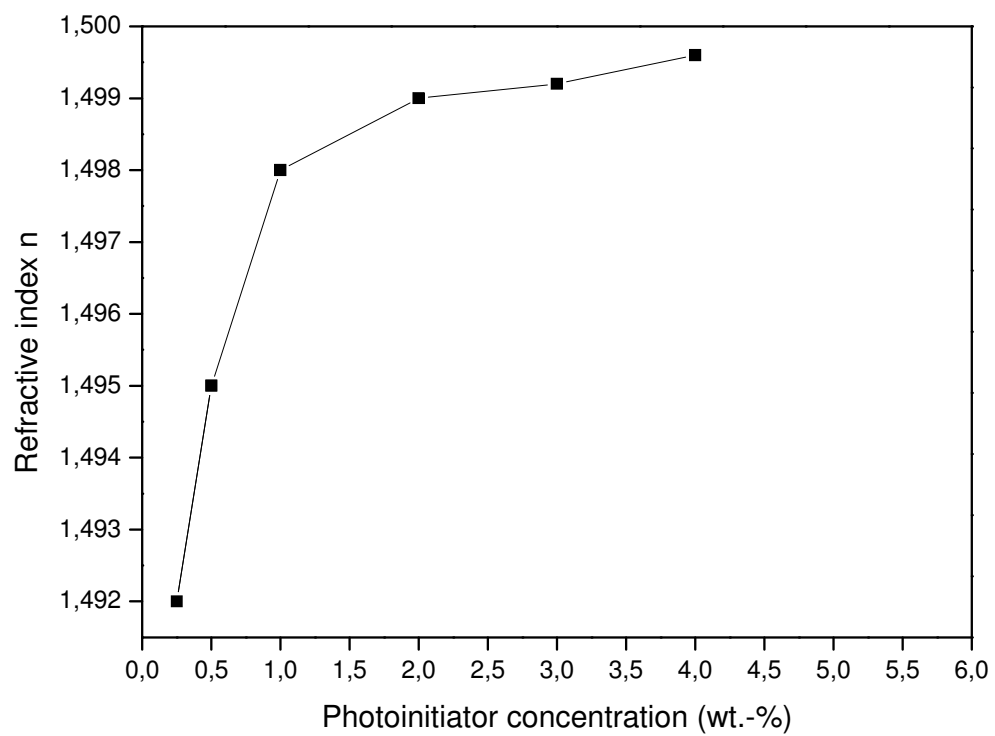
Figure 5.8: Variation of the refractive index of cured GUS-based ORMOCER® as a function of photoinitiator concentration determined at 635 nm.

References

[1] Brinker C. J., Scherrer G.W., Sol-Gel Sci., Academic Press, Inc., New York (1990).

[2] Hass K. H., Wolter H., Curr. Opin. Solid State Mater. Sci., 4 (1999) 571-580.

[3] Hass K. H., Adv. Eng. Mater., 2 (2000) 571-582.

[4] Hass K. H., Rose K., Rev. Adv. Mater. Sci., 5 (2003) 47-52.

[5] Schottner G., Kron J., Deichmann A., J. Sol-Gel Sci and Technol., 13 (1998) 183-187.

[6] Schottner G., Chem. Mater., 13 (2001) 3422-3435.

[7] Schottner G., Rose K., Posset U., J. Sol-Gel Sci. and Technol., 27 (2003) 71-79.

[8] Wolter H., Storch W., MACRO AKRON 94 35th IUPAC, International Symposium on Macromolecules, Ohio.

[9] Moszner N., Gianasmidis A., Klapdohr S., Fischer U. K., Rheinberger V., Dent. Mater., 24 (2008) 851-856.

[10] Jacob S., Poinsignon C., Popall M., Electrochim. Acta, 50 (2005) 4022-4028

[11] Popall M., Buestrich R., Semrau G.; Eichinger G., Andrei M., Parker W. O., Skaarup S., West K., Electrochim. Acta, 46 (2001) 1499-1508.

[12] Houbertz R., Domann G., Cronauer C., Schmitt A., Martin H., Park, J. U., Frohlich L., Buestrich R., Popall M., Streppel U.; Dannberg P., Wachter C., Brauer A., Thin Solid Films, 442, (2003) 194-200.

[13] Houbertz R., Declerck P., Passinger S., Ovsianikov A., Serbin J., Chichkov B. N., "Nanophotonic Materials: Photonic Crystals, Plasmonics, and Metamaterials" (R.W. Wehrspohn, H.S. Kitzerow, und K. Busch, Eds.), Wiley VCH, (2008) 97-114.

[14] Houbertz R., Wolter H., Dannberg P., Serbin J., and Uhlig S., Proc of SPIE 6126 (2006) 612605.

[15] Haas K. H.; Amberg-Schwab S., Rose K., Schottner G., Surf. Coat. Technol. 111 (1999) 72-79.

[16] Wolter H., Storch W., and Ott H., Mat. Res. Symp. Proc. 346 (1994) 143-149.

[17] Wolter H., Ballweg T., Storch W., Eur. Pat. Appl. (2000) EP 0985443.

[18] Wolter H., Ballweg T., Storch W., Eur. Pat. Appl. (2000) EP 0985442.

[19] Wolter H., Storch W., Ballweg T., PCT Int. Appl. (2001) WO 2001068961.

[20] Ballweg T., Wolter H., Storch W., Keramische Zeitschrift, 53 (2001) 678

[21] Kumbar S. M., Selvam T., Gellermann C., Storch W., Ballweg T., Breu J., Sextl G.,   J. Membr. Sci., accepted (2009)

[22] Popall M., Dabek A., Robertsson M. E., Gustafsson G., Hagel O. J., Olsowski B., Buestrich R., Cergel L., Lebby M., Kiely P., Joly J., Lambert D., Schaub M., Reichl H., Proceedings of the 48th Electronic Components & Technology Conference (1998) 1018-1025.

[23] Houbertz R., Domann G., Schulz J., Olsowski B., Frohlich L., Kim W. S., Appl. Phys. Lett., 84 (2004) 1105-1107.

[24] Wolter H., and Storch W,. Polymer & Materials Research Symposium, Bayreuth, 14 (1993).

[25] Fodermeyer V., Diploma Thesis, University of Würzburg (2009).

[26] Moszner N., Volkel T., Clausbruch, S. C., Geiter E., Batliner N., Rheinberger V., Macromol. Mater. Eng. 287 (2002) 339-347.

[27] Stevens M. P., Polymer chemistry: an introduction. Oxford University Press; New York: (1999) 167–204.

[28] Moad G.; Solomon D. H., Chemistry of Free-Radical Polymerization; Pergamon: New York, (1995) 210.

[29] Odian G., Principles of polymerization (Wiley, New York, 1981)

Curriculum Vitae

Personal details:

Name: Suresh M. Kumbar

Address: Kumbar Galli, Rabkavi 587314, Karnatak state, India
Cell no.: +919900853524
E-mail: kumbarsuresh@gmail.com
E-mail: kumbar_suresh@yahoo.co.in

Date of Birth: 5th september 1980

Nationality: Indian

Place of Birth: Sunadholi, India

Sex: Male

Marital status: Comitted

Education:

1999:   Pre-University courses in Physics, Mathematics, Chemistry and Biology
Commerce, BHS Arts & TGP Science Pre University College, Jamakhandi, India

2002:   Bachelor of Science Degree in Physics, Chemistry and Mathematics,
Commerce, BHS Arts & TGP Science College, Jamakhandi, India

2004:   Master of Science in Chemistry, Karnatak University, Dharwad, India

Scientific Background:

2004-2006:   Research Assistant at National Chemical Laboratory, Pune, India

2006-present: Doctorate in Natural Science at University of Bayreuth, Germany